Finite Element Modeling and Exploration of Double Hearing Protection Systems

By

Christian James

Thesis submitted to the Faculty of the
Virginia Polytechnic Institute and State University
in partial fulfillment of the requirements for the degree of
Masters of Science
In
Mechanical Engineering

Approved:

_____

Robert L. West, Advisor

_____

William R. Saunders, Committee Member

_____

Kenji Homma, Committee Member

February 10, 2006
Blacksburg, Virginia

Keywords: Finite element analysis, double hearing protection, earplug, viscoelastic

Report Documentation Page

Form Approved
OMB No. 0704-0188

1. REPORT DATE	2. REPORT TYPE	3. DATES COVERED
10 FEB 2006		**00-00-2006 to 00-00-2006**

4. TITLE AND SUBTITLE	5a. CONTRACT NUMBER
Finite Element Modeling and Exploration of Double Hearing Protection Systems	5b. GRANT NUMBER
	5c. PROGRAM ELEMENT NUMBER
6. AUTHOR(S)	5d. PROJECT NUMBER
	5e. TASK NUMBER
	5f. WORK UNIT NUMBER
7. PERFORMING ORGANIZATION NAME(S) AND ADDRESS(ES) **Virginia Polytechnic Institute and State University,Blacksburg,VA**	8. PERFORMING ORGANIZATION REPORT NUMBER
9. SPONSORING/MONITORING AGENCY NAME(S) AND ADDRESS(ES)	10. SPONSOR/MONITOR'S ACRONYM(S)
	11. SPONSOR/MONITOR'S REPORT NUMBER(S)

12. DISTRIBUTION/AVAILABILITY STATEMENT
Approved for public release; distribution unlimited

13. SUPPLEMENTARY NOTES

14. ABSTRACT

Noise levels in modern industrial and military environments are constantly increasing, requiring the improvement of current hearing protection devices. The improvement of passive hearing protection devices lies in examining the performance of major contributors to reduction of noise attenuation. The finite element method can be used to fully explore single hearing protection (SHP) and double hearing protection (DHP) systems, and the major performance mechanisms can be observed numerically as well as visually in modern postprocessing software. This thesis focuses on developing and evaluating double hearing protection finite element models, and exploring the behavior mechanisms responsible for reduced noise attenuation. The double hearing protection model studied consists of an earmuff preloaded to a barrier covered to simulate human flesh, and a foam earplug installed inside a rigid cylinder designed to simulate the human ear canal. Pressure readings are taken at the bottom of the simulated ear canal assembly. Advanced finite element models are used to reconcile differences between the experimental and finite element results, and to investigate the behavior of the modeled system. The foam earplug material properties for the finite element model are required in the same shear state of stress and boundary condition configuration as the experimental DHP setup, therefore a novel material extraction method is used to obtain this data. The effects of radial compression preload on the earplugs are considered, and the resulting foam earplug shear material properties are input into the finite element DHP model where the effects of the updated foam material properties are observed.

15. SUBJECT TERMS

16. SECURITY CLASSIFICATION OF:			17. LIMITATION OF ABSTRACT	18. NUMBER OF PAGES	19a. NAME OF RESPONSIBLE PERSON
a. REPORT	b. ABSTRACT	c. THIS PAGE			
unclassified	**unclassified**	**unclassified**	**Same as Report (SAR)**	**146**	

Finite Element Modeling and Exploration of Double Hearing Protection Systems

Christian James

(Abstract)

Noise levels in modern industrial and military environments are constantly increasing, requiring the improvement of current hearing protection devices. The improvement of passive hearing protection devices lies in examining the performance of major contributors to reduction of noise attenuation. The finite element method can be used to fully explore single hearing protection (SHP) and double hearing protection (DHP) systems, and the major performance mechanisms can be observed numerically as well as visually in modern postprocessing software.

This thesis focuses on developing and evaluating double hearing protection finite element models, and exploring the behavior mechanisms responsible for reduced noise attenuation. The double hearing protection model studied consists of an earmuff preloaded to a barrier covered to simulate human flesh, and a foam earplug installed inside a rigid cylinder designed to simulate the human ear canal. Pressure readings are taken at the bottom of the simulated ear canal assembly. Advanced finite element models are used to reconcile differences between the experimental and finite element results, and to investigate the behavior of the modeled system.

The foam earplug material properties for the finite element model are required in the same shear state of stress and boundary condition configuration as the experimental DHP setup, therefore a novel material extraction method is used to obtain this data. The effects of radial compression preload on the earplugs are considered, and the resulting foam earplug shear material properties are input into the finite element DHP model where the effects of the updated foam material properties are observed.

Acknowledgements

I would like to deeply thank Professor Robert West, my research advisor, for allowing me this great opportunity. His dedication and interest to this research helped me learn and prosper to the full extent possible. I appreciate the hundreds of hours of time and consideration he put forth, and his guidance has more than prepared me for my engineering career. I would like to thank Professor William Saunders for his support and valuable insight into the project. I greatly appreciate the experimental and supplemental finite element work done by Dr. Kenji Homma, as well as his professional guidance in the field of acoustics. I also thank all three individuals for serving on my thesis advisory committee. The research was funded by the NAVAIR SBIR Program, Contract No. N68335-03-C-0248, as a subcontract to Adaptive Technologies, Inc. I also appreciate the guidance and expertise of Dr. Larry Mitchell.

Many friends at Virginia Tech have provided their companionship and encouragement, which I deeply appreciate. I would like to thank my family for their constant support, from my undergraduate studies on through. Finally, I would like to thank Isabelle Melkonian for her unwavering support throughout my research.

Table of Contents

List of Figures

List of Tables

Chapter 1

Introduction

1.1 Overview and statement of need

The threat of hearing loss is a major concern for military applications and industrial environments alike. Dangerous noise levels can be found in numerous facets of American industry, from mining to manufacturing. American industry alone claims 7 to 10 million cases of noise induced hearing loss, with most of those being preventable. Nationwide hearing loss costs are currently unavailable, but estimates put the yearly economic costs of hearing loss in the hundreds of millions of dollars [1].

Noise levels in excess of 140 dB are commonly seen around modern weapons systems and support equipment. In 2002, the United States Veteran's Administration processed almost 65,000 claims for hearing loss, which cost the US government 441 million dollars. Some of the highest risks to hearing are present near modern aircraft, where ground crews and maintenance teams are exposed to high noise levels for extended periods of time. The latest aircraft under production is the F-35 Joint Strike Fighter, which offers versatility to all branches of the US military. The F-35 fighter jet is equipped with powerful, yet extremely loud jet engines. Sound levels from these engines can be in excess of 150 decibels [2], well over the 120 decibel threshold of pain for human hearing.

The Naval Air Systems Command (NAVAIR), the US Air Force and Navy commissioned a hearing protection Defense Technology Objective (DTO) for the evaluation of passive and active hearing protection devices in hopes of reducing future military related hearing loss cases. This proposal has stimulated research in proper fitting and comfort of hearing protection devices (HPDs), as well as on determining the operation and improvement of HPDs.

The improvement of passive HPDs lies in examining the performance of major contributors to reduction in noise attenuation. A final goal is altering components in the system to diminish the effects of these contributors. The frequency dependent contributions to reduction in noise attenuation are usually explored through experimental processes. Controlling boundary conditions and component parameters seeks to isolate the effect each component has in the complete HPD system. Unfortunately, the models

cannot be explored to the extent required for greater understanding needed to better design the HPD system. Due to recent advances in computational applications, a closer look at the HPD system response can be achieved.

One of the most important advances linked to improvement in computational capability is the finite element method. Advanced computing systems have allowed for the modeling and visual analysis of large-scale models with millions of degrees of freedom. Robust computing systems have also paved the way for coupled multi-physics systems capable of incorporating high frequency viscoelastic systems. Finite element models of single hearing protection (SHP) and double hearing protection (DHP) systems can be fully explored, and the major performance mechanisms can be observed numerically as well as visually in modern postprocessing software.

Research has been conducted by Adaptive Technologies Inc. (ATI) in conjunction with Virginia Tech to model and examine the performance of the David Clark AN/9 earmuff system, utilized by Navy aircraft carrier flight deck crews. The high noise levels produced by the upcoming Joint Strike Fighter require a closer look at evaluating and improving these hearing protection systems. ATI has undertaken the managerial and experimental aspects of the research as well as complimentary finite element modeling tasks. The research at Virginia Tech involved fundamental finite element modeling of the double hearing protection systems.

1.2 Hypothesis and goals

The double hearing protection system is defined as the combination of the described earmuff assembly, along with an installed earplug hearing protection device. The experimental setup involves a single polycarbonate earmuff and its corresponding viscoelastic seal, preloaded to the appropriate amount achieved by the headband of the earmuff system. The earplug in a human ear canal is simulated by installing the foam earplug into a machined acrylic sleeve whose dimensions are comparable to a human ear canal. For this research, the E-A-R Classic foam earplug will be analyzed, and hereafter referred to as the EAR foam earplug. In order to evaluate the DHP system, the behavior mechanisms that contribute to loss in noise reduction must be identified, such that further design changes can then be proposed. Experimental models alone cannot accomplish this

task. However, when combined with computational methods more insight can be obtained.

Noise reduction inhibiting mechanisms can be identified and evaluated through the use of finite element models reconciled with data from comparable experimental tests. Specifically, the utilization of advanced material models and coupled structural-acoustic finite element models can be used to accurately explore and characterize the experimental DHP system. In order to identify these behavioral characteristics, the finite element model must contain representative material properties and boundary conditions. This thesis develops and explores the finite element models which provide insight into the actual experimental response, as well as integrates a modern analytical material property extraction method to better characterize the EAR foam earplug and examine the changes these new properties have on the DHP system response.

It is believed more appropriate material properties for the EAR foam material will contribute to better correlation between the finite element and experimental results, as well as help quantitatively determine the contribution of the earplug response to the DHP system. Previous research in the hearing protection industry speculates that the EAR foam earplug vibration may contribute to DHP system response in the form of reduced noise attenuation levels at the material's resonance frequency. This phenomenon is minimally observed in previous finite element DHP results, as will be explained in Chapter 3. However, it is noted in Cremer, Heckl and Ungar [3] that deflections on the order of $1x10^{-8}$ meters attribute to large pressures in small enclosed acoustic cavities. This emphasizes the importance of correctly modeling the EAR foam earplug material, whose minute deflections may severely influence the pressure readings in the simulated ear canal. The EAR foam earplug material properties will be explored and its contribution to DHP system response will be evaluated.

1.3 Objectives

In order to identify the dominant behavioral mechanisms of the ABAQUS DHP model, certain key goals must be met. In general, the first step is modeling of the experimental system as closely as possible. The DHP test configuration system parameters must be modeled, including boundary conditions, loading and material

properties. Next, the finite element model results must be reconciled with experimental results. This allows for appropriate changes in system parameters, and helps understand the overall behavior of the finite element model response. Finally, the reconciled finite element model must be thoroughly explored, and the targeted mechanisms must be identified. Any further system parameters that do not model the physics of the system must be changed, and the process iterated. These broad goals can be broken down into specific objectives to help outline the process. The objectives are listed in the same order as the thesis is written:

Preliminary DHP model investigation

- The finite element DHP model is constructed to accurately represent the experimental test configuration.
- The preliminary finite element DHP model is to be reconciled with experimental results.
- The finite element DHP model is explored to identify the major contributing mechanisms of the system.
- The specific response of the EAR foam earplug is investigated, and its effect on the complete DHP system response evaluated.

Earplug material parameter extraction

- Experimental and analytical extraction methods are calibrated and verified with a simple axial deflection configuration. This determines if the chosen extraction method will appropriately model the EAR foam earplug material, as well as help form the overall extraction process.
- The experiment is conducted on the EAR foam earplug material in a comparable configuration to the actual experimental DHP test configuration, which is the preloaded shear configuration.
- The shear material properties are extracted and investigated.
- The valid frequency range of the properties are determined and applied.
- Determine an interpolation method to determine material properties for any preload value within the range of experiments.

Updated DHP model investigation

- Examine the effect of preload on the resonance of the EAR foam earplug.
- Update the finite element model with the shear material properties; prepare the material data for entry into the finite element software.
- Compare the updated DHP model results with the previous DHP model results, and determine the effect the new updated earplug material properties have played.
- Compare the updated DHP model results with the experimental DHP model results.
- Investigate and draw similarities in the updated and experimental DHP model results.
- Speculate on the major mechanisms in the experimental DHP model response from investigations of the finite element DHP model response.

To take full advantage of modern computational tools and finite element software, ABAQUS is chosen to be the finite element program used throughout the research. ABAQUS software contains state of the art solvers for nonlinear dynamic systems, and support capabilities for complex viscoelastic materials. It has excellent acoustic modeling properties and its solver and mesher algorithms are developed to handle large-scale models.

1.4 Scope of thesis

The scope of the thesis outlines components of the research that will be undertaken, and also what limits will be put in place. The research's scope will be divided into two sections, one for the finite element model of the DHP system and the other for the EAR foam earplug material extraction process.

Finite element DHP model scope

- Linear elastic material properties are used for the polycarbonate earcup.
- The EAR foam earplug material is modeled as a homogeneous, isotropic linear viscorlastic solid. Even though some material theories suggest that air pockets in the foam material may cause the foam to behave like a solid-fluid mixture, the high radial compressive strain seen by the foam material is assumed to reduce the amount of trapped interior air.
- Frequency dependent linear viscoelastic material models are used for the composite seal, flexlayer material, Siliclone RTV material and the EAR foam earplug.
- Complex contact conditions are not considered. It is assumed that any real relative motion between the earcup flap and the composite seal, between the composite seal and the flexlayer base, and between the Siliclone RTV and the EAR foam earplug is negligible.
- The baseline models constructed to validate the earcup geometry, correct composite seal behavior and correct DHP configuration are left out of the thesis to reduce its length.
- The final correlations drawn between the finite element and experimental DHP models are speculations; more experimental data is needed in the experimental configuration to make them facts.

Material extraction process

- The EAR foam earplug will be the only material analyzed.
- The structural response of the EAR foam earplug is considered to only be related to the amount of applied preload and the excitation frequency. All other parameters such as temperature, hysteresis, humidity and manufacturing material inconsistencies are neglected.
- A simple three-degree-of-freedom model will be used, even though some loading distribution in the accelerometer position may be present.
- The EAR foam earplug is considered modeled as completely attached to the polycarbonate sleeve's walls, even though some slipping may occur.

- Any loading or boundary conditions placed on the experimental extraction tests by the accelerometer lead are ignored.

1.5 Thesis outline

This thesis starts with framing the hypothesis, stating the goals and concept for solution, and finally outlining the objectives and scope of the work. Chapter 2 reviews relevant work in the field of SHP and DHP hearing protection devices, establishing the current basis for this research. Chapter 3 discusses the creation and exploration of the ABAQUS DHP model. The experimental system for the EAR foam earplug material is considered in Chapter 4, and the analytical material property extraction method is explored in Chapter 5. Chapter 6 discusses the updated ABAQUS DHP model using the extracted EAR foam material properties. Concluding arguments and suggestions for future work are placed in Chapter 7.

Chapter 2

Literature review

This thesis focuses on identifying the major contributors to degradation in hearing protection device performance, and in depth exploration of earplug vibration impact on the DHP system response. Several papers address the effects different earplugs have on noise attenuation, but do not speculate as to the specific reasons why. Here a brief history and explanation of hearing protection devices (HPDs) is provided, along with some insight provided by acoustic pioneers. Since accurate material properties are needed for finite element modeling, analytical material property extraction methods are presented, with justification for selection provided.

2.1 Hearing protection

Hearing protection devices

Many advances in the hearing protection industry have been made in the past 30 years. Research has been fueled by the steady increase in noise levels in military and industrial applications. Noise levels in excess of 120 decibels are common in modern workplaces. Limited exposure to noise in excess of 120 decibels causes pain and possible permanent damage to human hearing, while long term exposure to 80 decibels of sound may cause permanent damage over an extended period of time.

Many working environments cannot alter the sources responsible for the noise or construct costly sound barriers. The most cost effective solution is personal hearing protection devices. These devices can consist of earplugs, protective earmuffs, helmets or a combination of these components. Earplugs are inserted into the ear canal to prevent transmission of sound into the ear. Earplugs can be grouped into three major categories: custom molded, pre molded or user molded. Custom molded earplugs are created from professionally taken ear impressions, which result in a rigid earplug that fits well to the specific user. Pre molded earplugs are manufactured from soft materials with ridges and flaps that seal upon insertion into the ear. User molded earplugs are made from soft foam materials, and the user usually rolls and compresses the earplug before inserting it into the ear canal. Figure 2.1 shows a typical picture of each specific earplug category.

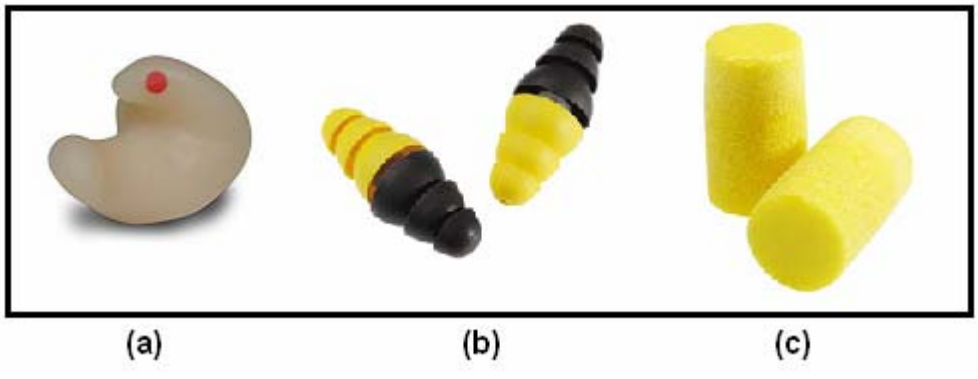

Figure 2.1 Comparing the custom molded (a), pre molded (b), and user molded (c) earplug types [24], [25], [26].

Earmuffs typically consist of a polycarbonate earcup with compressive seals that sit between the earcup and the user's head. A headband applies the pressure to hold the unit on the user's head and over their ears. Small leaks in the earcup-head seal can decrease the earmuff's efficiency, therefore an appropriate seal and headband force is required. Figure 2.2 shows the David Clark AN/9 earmuff unit under consideration in this work.

Figure 2.2 David Clark AN/9 earmuff system [4].

Helmets are worn over the user's head to reduce incident sound waves and help seal the earmuff system. It is believed that helmets are most important for high noise environments in the high frequency range to limit the bone conduction phenomenon. Sound is reflected by the helmet before it can be transmitted into the human skull, reducing the amount of vibration the skull experiences. A typical helmet unit combined with the David Clark DAV22589G-08 communication earmuff assembly can be seen in Figure 2.3.

Figure 2.3 Helmet and earmuff hearing protection unit [5].

Evaluating noise reduction

The effectiveness of earplugs has been studied for over 50 years, with most of the results being qualitative in nature. The lack of a universal standard for evaluating hearing protectors has reduced the effectiveness of quantitative hearing protection data. The most common evaluation method is real ear attenuation at threshold (REAT) method (ANSI 1957) [6]. A human subject is exposed to increased noise levels until pain is induced with and without the hearing protection. The difference in the pain threshold levels is considered the amount of noise the hearing protection device can attenuate. The other mainstream testing method is microphone in real ear (MIRE), where a small microphone

is placed in the inner ear canal and resulting pressure readings are taken. This method provides a definitive noise reading independent of the subject's audible perception, although any audible effects experienced by the human ear canal are obviously neglected. This provides for a pressure reading, but not necessarily the average perceived noise in the human ear canal. Berger's [7] experimental test results on 17 different subjects fitted with deep insertion EAR foam earplugs show a maximum discrepancy in 20 dB between subjects. This variation is most likely due to the different geometry of the subjects' ear canals. Figure 2.4 shows the plot of noise attenuation versus frequency.

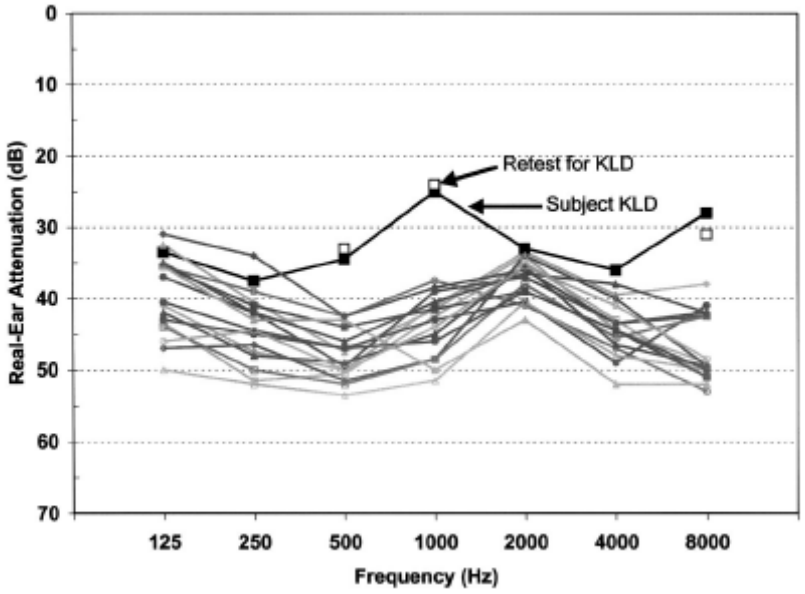

Figure 2.4 Noise attenuation values for 17 different subjects using EAR foam earplugs [7].

Notice the loss in real-ear attenuation in the 2 kHz octave band region. This was not referred to in Berger's work, but it is suspected in this thesis that this trend may be due to earplug material vibration. This assumption is made because almost all test subjects experienced a reduction in attenuation performance in this region, suggesting a similar mechanism for all subjects, although Berger [7] suggests this peak is due to the onset of bone conduction limits. Earplug vibration is speculated because this phenomenon is seen in experimental and finite element model DHP results in the 1-2 kHz

region. Since there is little information presented in this thesis on real human ear testing, this speculation is purely a simple observation and suggested for further investigation

.

Noise transmission mechanisms

Sound is perceived when acoustic energy vibrates the hair cells in the cochlea of the inner ear. Sound reaches the inner ear either by the air conduction path in the ear or through bone conduction vibration to the inner ear. Bone conduction is considered the limiting attenuation factor of the occluded ear, and one of the four noise transmission mechanisms. Berger [8] described the four methods of sound transmission in hearing protection devices (the occluded ear).

- Air leaks in the hearing protection devices (HPDs) provide a drop in noise attenuation, therefore proper sealing of the earmuff assembly and seating of installed earplugs is a necessity. The use of eyeglasses and excess hair may cause improper earmuff seating. Creasing in user molded earplugs is the main source of sound leaks in these HPDs.
- Transmission through the HPD material is the second established contributor. Sound piercing the earmuff and earplug material attributes for some loss in noise attenuation.
- The third method is bone conduction, which is currently believed to define the limit of all hearing protection devices. Skull vibration is transmitted down to the ear canal, and vibration of the ear canal walls produces noise in the ear canal.
- The fourth method is vibration of the HPD itself causes a loss in attenuation. Earplug vibration creates a piston like component in the closed ear canal, and large acoustic pressures are seen. Incredibly small deformation on the order of $1x10^{-8}$ meter has been shown to contribute rather large acoustic pressures inside enclosed volumes as described by Cremer et. al. [3]. The earmuff assembly can also vibrate, most likely due to the vibration of the assembly on the spring-like seal. This also creates a piston like behavior, and sound is created inside the occluded ear. The earcup also exhibits elastic deformation modes, causing large vibration amplitudes that excite the rest of the structural system.

As discussed in Chapter 1, the major mechanisms explored in this thesis are transmission through the HPDs, and actual vibration of the HPDs contributing to reduction in noise attenuation performance. Leak mechanisms on the earmuff system were previously explored by Anwar [9], and bone conduction will be neglected in this research. After identification of the DHP system behavior is established, the vibration of the earplug material will be thoroughly explored to determine if it in fact significantly contributes to HPD performance reduction.

Earplug behavior

The first indications that earplug behavior was more complicated than simply blocking incident sound waves was discovered by Zwislocki in 1953 [10]. He found that insertion of foam earplugs into the fleshy (cartilaginous) part of the ear canal increased the observed user sound, creating the “hollow voice” effect. This effect can be witnessed when the ear canal is blocked amplifying the low frequency noise created by the user. It has been termed the occlusion effect. Deep earplug insertion into the bony (osseous) section removed this occlusion effect. This work suggested that the unconstrained bone like ear canal walls vibrate and transmit sound, or the short earplug in combination with the fleshy ear canal walls vibrates and transmits sound, or a combination of the two mechanisms are present. A comparison of shallow and deep earplug insertion can be seen in Figure 2.5.

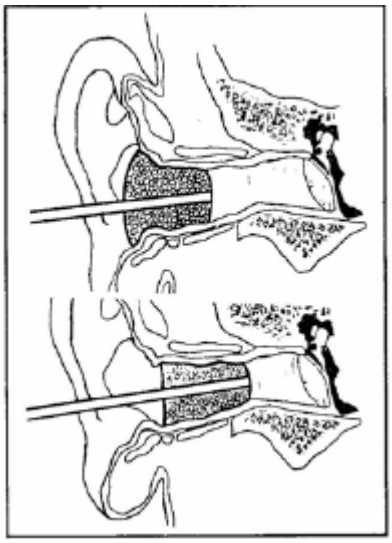

Figure 2.5 Shallow versus deep earplug insertion [11].

This assumption was investigated further by Khanna et. al. [12]. Their investigation involved making probe pressure measurements behind the installed earplug, and discovered larger pressure values than when no earplug was installed. They speculated this noise increase was due to the vibration of the fleshy ear canal section. Berger and Kerivan [13] investigated the placement of long EAR foam earplugs in the ear canal, and numerically confirmed the reduction in the occlusion effect with these deep seated earplugs. This observation points to the significance in the earplug boundary conditions in the ear canal and earplug vibration.

Earplug's effects on the occlusion phenomenon was further explored by Berger [13]. He utilized the EAR classic foam earplugs with several different insertion depths. The insertion depths were partial insertion (15-20% insertion), standard insertion (50-60% insertion) and deep insertion (80-100% insertion). Deep insertion was the maximum insertion distance before significant user pain was experienced. Figure 2.6 shows pictures of the three insertion cases.

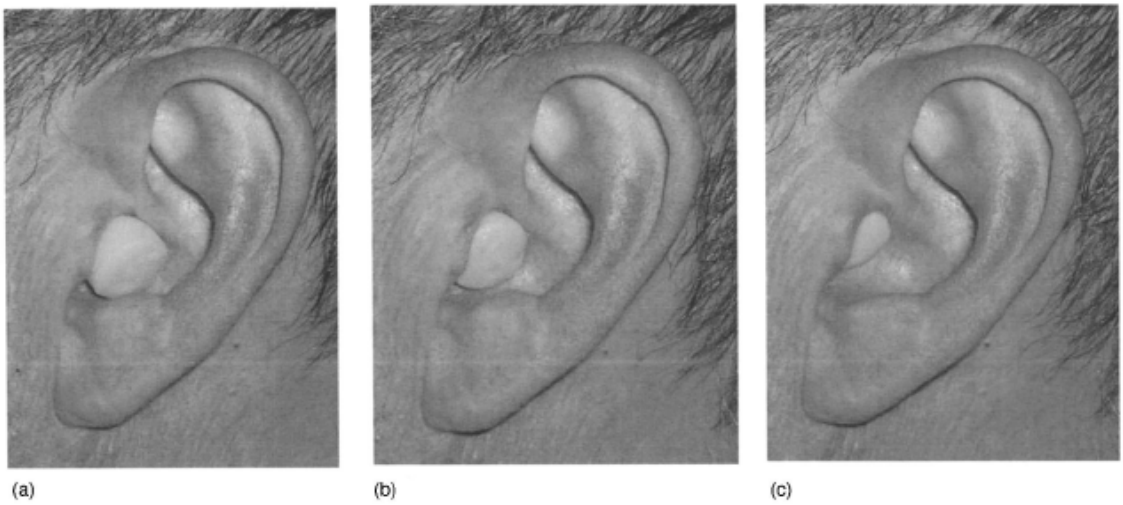

Figure 2.6 Partial insertion (a), standard insertion (b) and deep insertion (c) earplug cases [7].

Noise attenuation was found to vary with earplug insertion depth when combined with earmuff hearing protectors below 1 kHz. At and above 2 kHz the noise attenuation in the DHP system was found to be the same for all earplug configurations. This is thought to be due to bone conduction transmission effects overtaking the attenuation level the DHP system provides, although the possibility of a decrease in noise attenuation by a

resonance of the earplug is considered, and consequently motivates this thesis. The material properties of these earplugs are necessary in quantifying their behavior, and therefore a method for obtaining these properties in a configuration comparable to the experimental conditions is needed.

Modeling of the DHP system using the finite element method requires adequate knowledge of the material properties of the system components. Since the dominant deformation mode of the foam earplugs is shear, the material properties for this state of stress must be obtained (discussed in depth in Chapter 3). A simple, yet fruitful method is needed to easily extract a wide frequency band of viscoelastic material properties. Many methods are discussed in the following section, provided with arguments for the selected method.

2.2 Material property extraction

Several material extraction methods for simple vibration test situations have been proposed. Bierman et. al. [14] proposed the property extraction of a material cut into thin wafer specimens in shear. Property results over a broad frequency range were determined from this method. The elastomeric rubber material was cut into small wafers of 2 to 5mm thickness. A mass was mounted between the two wafers, and the resulting motion of the excited assembly was read by a miniature accelerometer mounted on the top of the mass. Figure 2.7 exhibits the experimental setup. The properties are extracted through the manipulation of a single degree of freedom spring–mass-damper system. A wide frequency range of material properties can be obtained by this method, although it is only derived from a one degree of freedom model, so contributions from higher order modes will not be taken into account. This method involves testing wafers of the material, and although shear material data is required, this method cannot be employed because it is suspected that this EAR foam material will not correctly scale from a smaller specimen size. Therefore, the entire earplug must be tested in its entirety in a setup as similar to the DHP experimental configuration as possible. This research did provide insight into analytical extraction methods, and helped form the path to the best method.

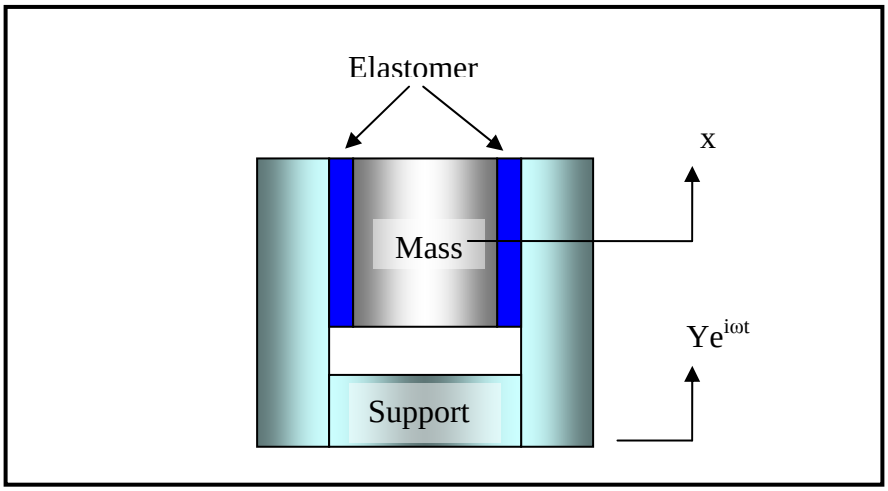

Figure 2.7 Experimental setup of the material shear wafer test configuration.

Nielson et. al. [15] proposed the material extraction method of placing the excitation force on top of the specimen and constraining the bottom of the specimen to a rigid surface. The shaker is suspended from soft springs, eliminating the static load due to the weight of the excitation system. Figure 2.8 shows the physical configuration of the test system. The material properties were extracted from the continuum mechanics derivation of system compliance. Low frequency results (40-1,000 Hz) could be easily obtained from this method, although the physical configuration of the experimental process is very difficult to obtain, and mid- to high-frequency results (1,000 – 6,000 Hz) leave much to be desired. Unfortunately, due to the observations of Berger [7] accurate material properties are needed in the 1,000 – 3,000 Hz frequency range.

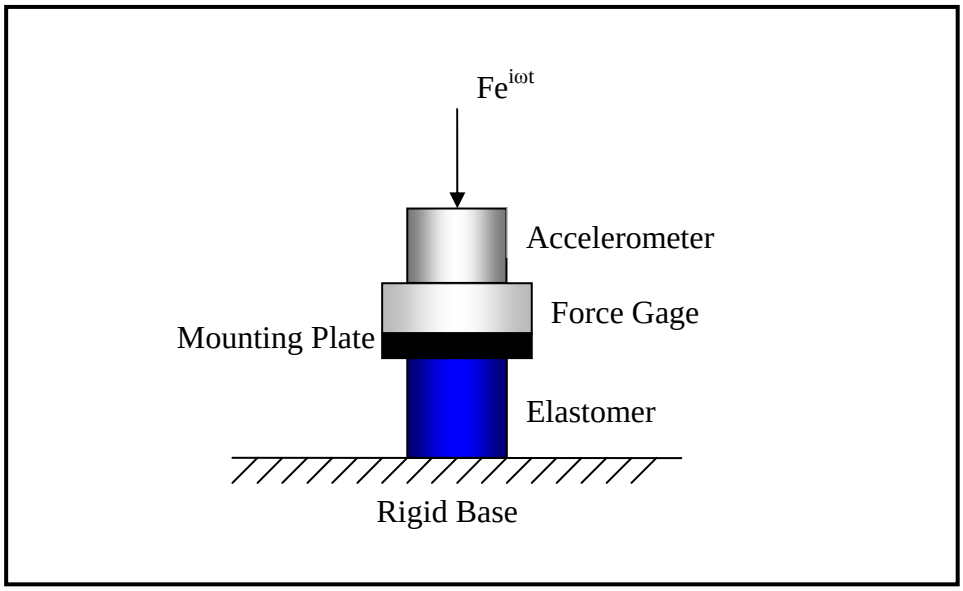

Figure 2.8 Experimental setup of the top excitation loading method.

The Inverse Nyquist Plane Parameter Method put forth by Mitchell [16], [17] utilizes a three degree of freedom spring–mass-damper system. The first degree of freedom represents the mass due to the impedance head, base assembly and a portion of the foam material. The second degree of freedom represents a portion of the foam material. The final node is a portion of the foam material and the miniature accelerometer attached to the foam specimen. This is discussed in more depth is chapter 4. The system matrices of the test configuration were constructed, using the transfer matrix method. The result of this formulation was an estimate of the effective mass expression between the force gage on the impedance head and the miniature accelerometer. This method provides valid material data for the mid- to high-frequency range, depending on the system resonances. The Inverse Nyquist Plane Parameter Method is the best available method to model the EAR foam material because it delivers excellent mid- to high-frequency results in the (1,000 – 6,000) Hz frequency range. This approach is test wise efficient, and offers hundreds of estimates in the frequency range of interest (an estimate for each spectral line). Also, this method provides accurate property estimates of highly damped materials and allows the specimen to be tested in the shear condition with applied preload.

2.3 Conclusion

It has been discovered through previous work that the major sound transmission mechanisms pertinent to this investigation are sound transmission through HPDs, and actual vibration of structural HPD components. Berger [8] speculated that the vibration of earplugs are a major contributor to HPD performance reduction. Through the work of Berger and others, it was shown that earplugs contribute different responses based on their installation, and points to the importance of boundary conditions and material properties in modeling these materials. The DHP system must be modeled as accurately as possible, and correct modeling of the earplug is no exception. To obtain preload and boundary condition specific material properties, an appropriate analytical material property extraction method must be utilized. After considering several modern methods, the Inverse Nyquist Plane Parameter Method is chosen for its accurate mid-frequency range results, its capability of modeling high-damping viscoelastic materials, and its ease of setup and execution. The two considered sound transmission methods in the finite element double hearing protection model are examined in the next Chapter.

Chapter 3

Double hearing protection model analysis

To understand how components of hearing protection devices contribute to the overall system's noise reduction, the DHP model is created. The test configuration and finite element models are constructed to isolate the noise reduction contributing effects for earmuff and earplug combinations by use of known geometry, materials and boundary conditions. The DHP ABAQUS model is constructed to match the experimental geometry, boundary conditions and loading as closely as possible to the experimental DHP setup. In order to fully capture the experimental system in the ABAQUS model, the behavior response of the DHP ABAQUS model must be explored and understood. The major mechanisms contributing to reduction in noise attenuation must be uncovered and evaluated.

3.1 DHP experimental configuration

The experimental process is designed to simply yet closely represent the real world configuration of a human wearing both earplug and earmuff hearing protection devices. A small particle board square box with a width of 89 cm, a height of 61 cm and a depth of 66 cm is covered with acoustic foam on its interior surfaces and placed on top of a solid wood table. This box provides an approximation to an anechoic environment for the acoustic tests, and limits the amount of reflected acoustic energy into the test structure. A speaker is hung from the inner top surface of the box, 20 cm above the tabletop. This speaker is the source of the acoustic excitation energy. A heavy aluminum base (MDF rigid base) is installed in the center of the wood table directly under the source speaker. The large mass of the MDF base is important to limit vibration in the base structure, therefore eliminating most extraneous causes of noise in the experiment. The flexlayer material is glued to the top of the MDF base. The flexlayer material is placed to represent a simplified version of human flesh on the face. The earcup and seal are placed on top of the flexlayer material, and preloaded with compression springs. The preload applied in the test approximates the average load applied by the earmuff's headband. A threaded rod is run through the brass guides glued to the earcup lugs. Springs are placed over the rods, on top of the attached lugs. A nut is tightened onto the

stud, and the amount of force applied to the structure is estimated from the deflection and spring constant of the compressed spring. Foam is placed around the springs to add damping and prevent the springs' resonance from influencing the experimental results. Figure 3.1 shows the actual setup of the preloaded earcup assembly built by Dr. Kenji Homma.

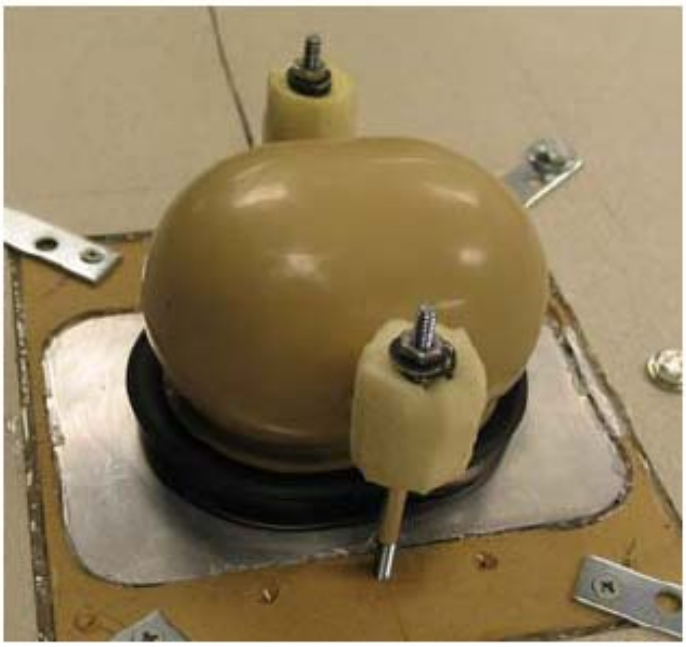

Figure 3.1 Preloaded earcup assembly mounted on the MDF base.

To simulate the human ear canal assembly, an acrylic tube is constructed with an inner diameter comparable to the human ear canal diameter (8mm diameter). The sleeve is pressed into the MDF base, and a PCB microphone is inserted into the bottom of the sleeve and sealed with clay. To simulate the fleshy portion of the ear canal walls, Siliclone RTV material is inserted inside the acrylic sleeve with the same inner diameter as the sleeve. The length of the Siliclone RTV material is 2 cm. The Siliclone RTV material is glued to the flexlayer material; an inner hole at the center of the flexlayer material is removed to attach to the Siliclone RTV material. Finally, the earplug is installed inside the simulated ear canal, contacting the Siliclone RTV material portion. The EAR foam earplug is rolled and inserted per the manufacturer's instructions. An illustration of the setup can be seen in Figure 3.2.

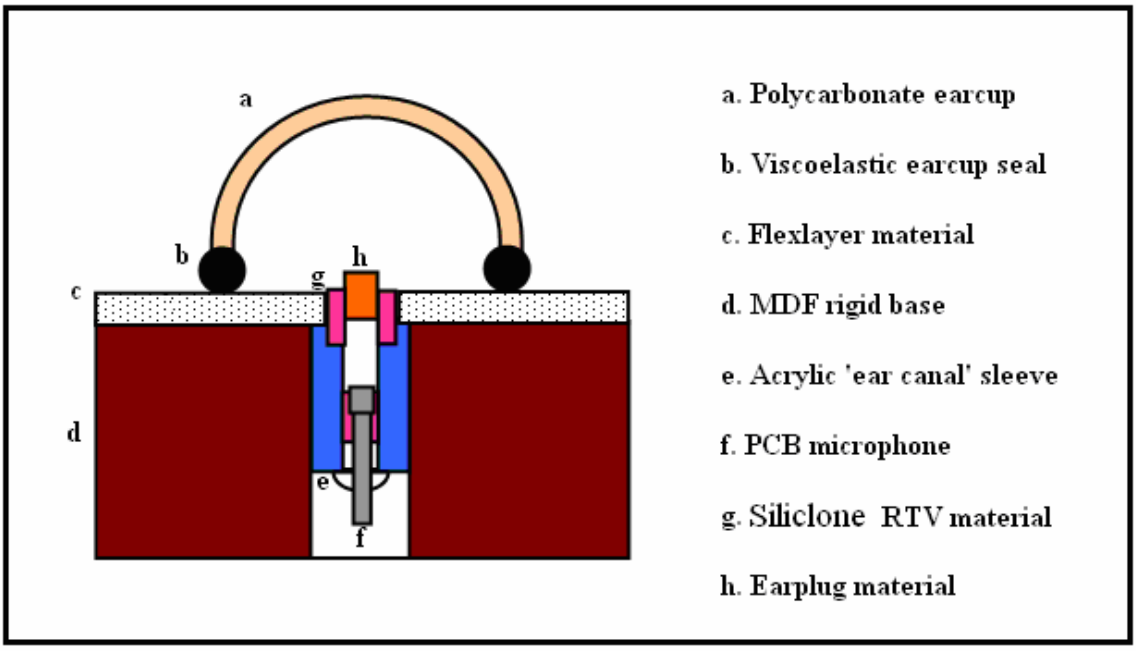

Figure 3.2 Experimental setup simulating the human head exhibiting DHP devices.

3.2 ABAQUS model

Model Geometry

The DHP ABAQUS model consists of a hemispherical boundary domain of quadratic acoustic elements 20 cm in radius. The bottom of the hemispherical domain consists of a rigid, purely reflective boundary condition, representing the rigid MDF and wood table. The radial surface is prescribed as an absorbing boundary condition to replicate the anechoic boundary condition that exists in the experimental process. A rigid cylinder is placed in the bottom surface to represent the acrylic sleeve utilized in the experiment. A monopole source is placed on top of the hemispherical domain in the same location as the speaker position in the experiment. The Siliclone RTV material is modeled inside the ear canal cylinder. The flexlayer material is modeled with the same geometry and location as the experimental configuration. The flexlayer is completely constrained on the bottom, and the inner cutout hole of the rigid cylinder is tied to the outer diameter surface of the Siliclone RTV material in the ear canal cylinder. The earmuff assembly consisting of the earcup model tied to the viscoelastic seal model is tied to the flexlayer material, covering up the ear canal cylinder. The polycarbonate

earcup contains mounting lugs on the sides, where the brass guides are attached as previously discussed. The earcup flap is considered the flanged piece at the bottom of the earcup which seats the earcup on the viscoelastic seal. The earmuff assembly is displayed in Figure 3.3, with labels clearly identifying the major components of the system. All structural and acoustic components are meshed with quadratic, fully integrated elements. Figure 3.4 displays the DHP ABAQUS model with a closer look at the ear canal assembly.

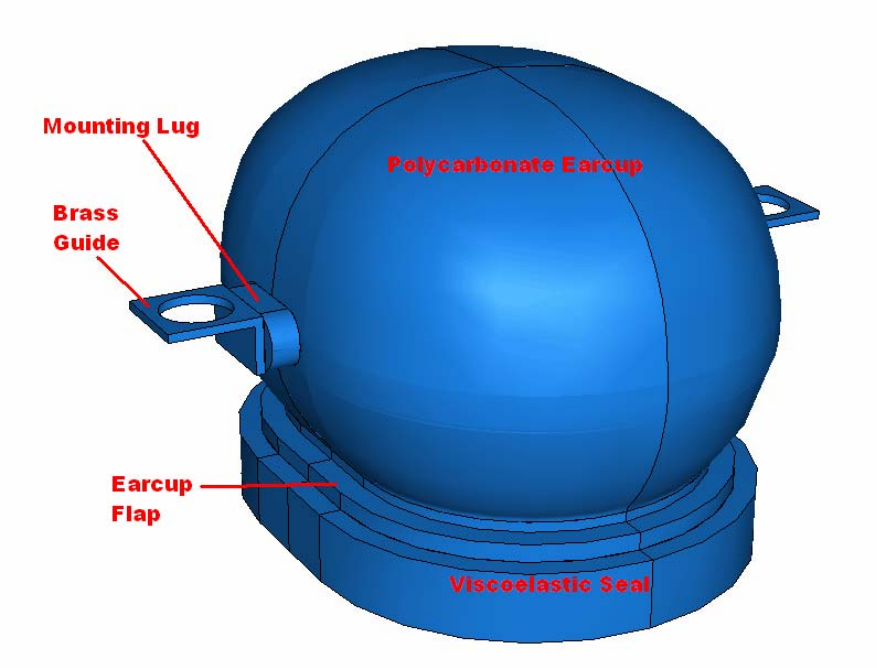

Figure 3.3 Labeled earmuff assembly.

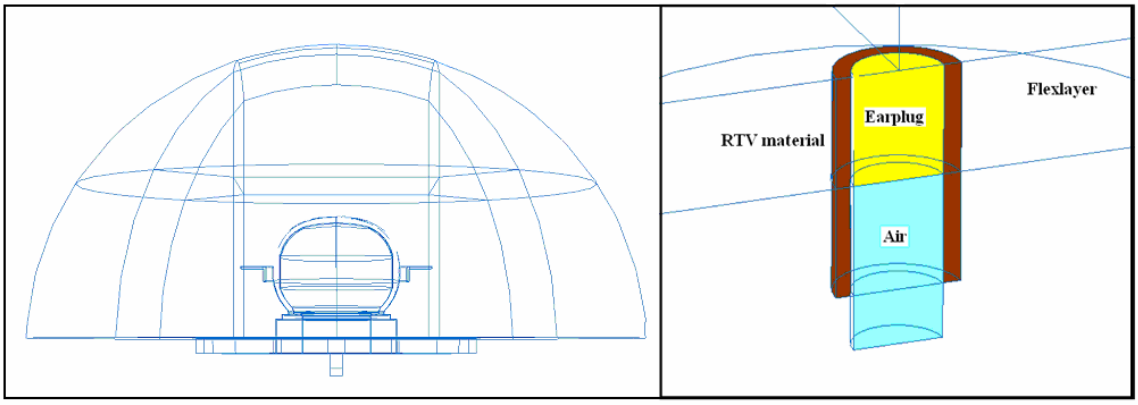

Figure 3.4 ABAQUS DHP model with a closer look at the ear canal assembly.

Material properties

The polycarbonate earcup is assumed to contain an elastic modulus of 2.2e9 Pa, a Poisson's ratio of 0.3 and a mass density of 970 kg/m^3. The acoustic domain is assumed to have a bulk modulus of 153,000 Pa, with no damping. The flexlayer, Siliclone RTV, composite seal and previous EAR foam earplug materials all contain frequency dependent viscoelastic material data that are documented in Appendix A.

The flexlayer, Siliclone RTV and EAR foam earplug material properties were all determined from tests on the Dynamic Mechanical Analysis (DMA) instrument, in the axial state. Two compression plates load the small material specimen, and a known displacement is provided to the material per frequency and temperature, and a reaction force of the material is registered. The DMA test is carried out by oscillating the specimen through a prescribed displacement while sweeping through a table of frequencies and temperatures. Temperature and frequency are inversely related, testing the material at lower temperatures is equivalent to testing the material at higher frequencies. Master curves for the material's storage and loss moduli are obtained for the entire frequency range of interest using the time-temperature-superposition technique. The reader is referred to Aklonis and MacKnight [18] for more information.

3.3 DHP model results

The ABAQUS DHP model is executed and solved for two hundred spectral lines, with linear frequency steps of 50 Hz. The noise attenuation rating is taken, which is the normalization of the output pressure at the bottom of the ear canal cylinder over the input monopole source pressure. This provides a quantitative estimate of the noise blocked by the DHP devices, in decibels, as a function of frequency. The same noise reduction (NR) metric is taken for the experimental DHP results and is defined in Eq. 3.1.

$$NR = 20\log_{10}\left(\frac{P_{ear\,canal}}{P_{source}}\right) \tag{3.1}$$

3.3.1 Comparing ABAQUS and experimental DHP results

The experimental and ABAQUS DHP model noise reduction plots are shown in Figure 3.5. The overall behavior of the experimental DHP system is captured in the ABAQUS DHP model, but there is a discrepancy between the two curves in the magnitude of noise reduction. The experimental DHP results also include ambient noise fields which are not present in the ABAQUS DHP finite element model. The difference in noise reduction magnitudes at the lower frequency bound (100 Hz) is partially due to the amount of damping in the composite seal, which dictates the resonance magnitude of the earmuff assembly. This topic along with model identification of the ABAQUS DHP results will be discussed in the following section.

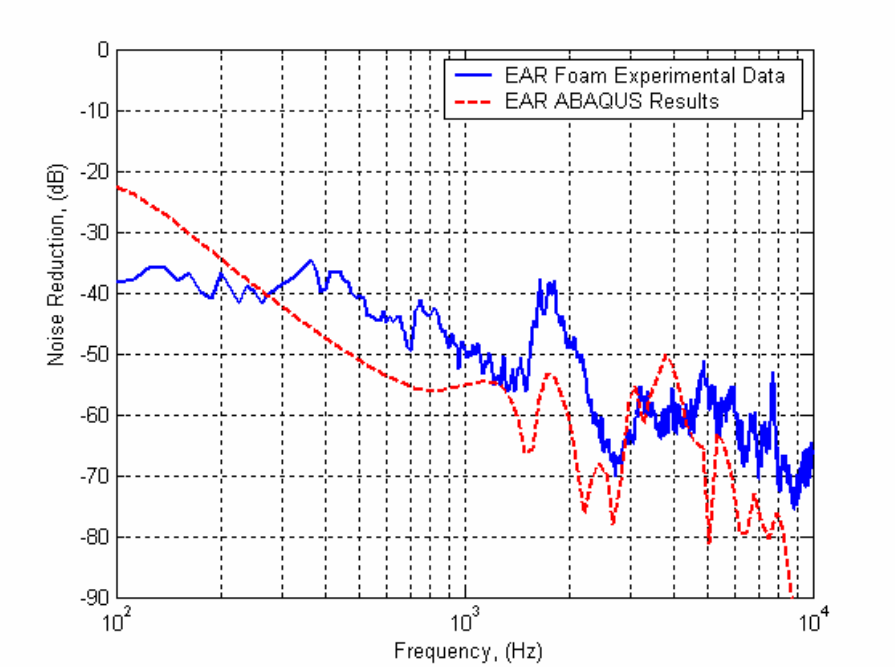

Figure 3.5 Comparing experimental and ABAQUS DHP results.

3.3.2 Model identification

To understand the behavior of the experimental DHP system, the ABAQUS DHP model was extensively explored. If the major mechanisms of the system can be clearly identified and matched to the response of the experimental DHP system, then insights can be gained into the actual behavior of the physical system. The ABAQUS DHP model is studied, and deformation modes and responses are compared between models. The

behavior of the finite element model can be divided into three major frequency regimes referred to in the divided response plot of Figure 3.6.

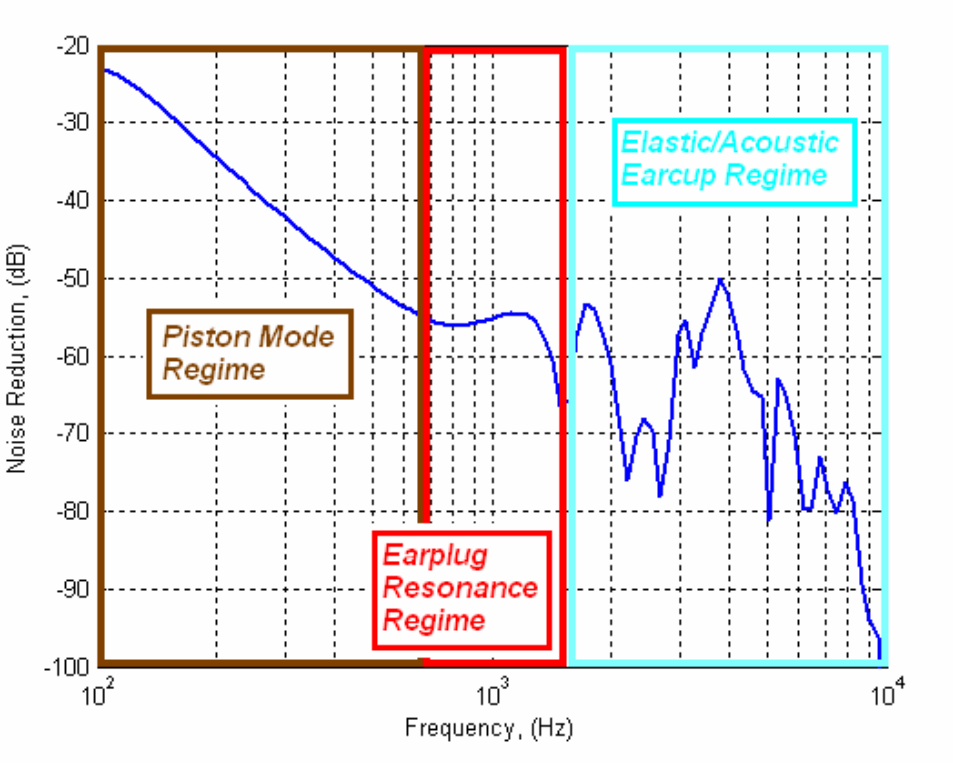

Figure 3.6 Displaying the three distinct labeled regimes.

3.3.2a Piston Mode regime

The first regime is the response due to the piston mode caused by exciting the natural frequency of the earcup seal; called the *Piston Mode* regime. It is defined from 100 to 700 Hz. This regime displays the lowest noise reduction of the entire frequency range, which increases exponentially as the excitation frequency is increased. This high ear canal cavity pressure results from the pumping mode of the earcup as a rigid body on an elastic earcup seal. The rigid body motion of the earcup on the elastic earcup seal creates large displacements in the earmuff assembly, which vibrates the flexlayer/Siliclone RTV/EAR foam earplug assembly (which will hereafter be referred to as the earplug assembly). This assembly can be seen in Figure 3.7. This regime was fully investigated by Anwar; the reader is directed to his thesis entitled “Low Frequency Finite Element Modeling of Passive Noise Attenuation in Hearing Defenders” [9].

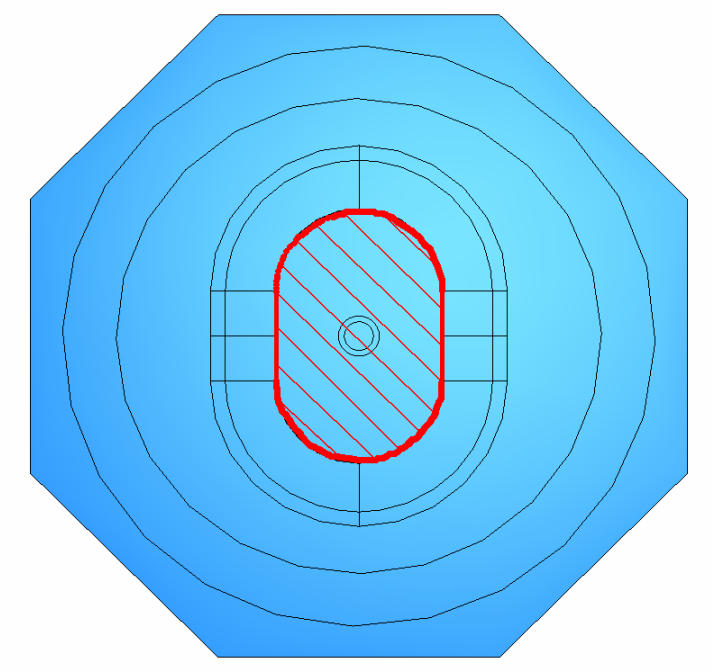

Figure 3.7 Bottom of ABAQUS DHP model, with cross-hatched earplug assembly section.

3.3.2b Earplug Resonance regime

The second regime is referred to as the *Earplug Resonance* regime (700 to 1,600 Hz). One major pressure peak distinguishes this section. This peak is caused by the resonant vibration of the earplug in the ear canal assembly. This response is due to the resonance of the earplug assembly in response to excitation of the first elastic earcup deformation mode. Even though this regime contains, and the earplug response is stimulated by, the first vibration mode of the elastic earcup its dominant mechanism is the earplug resonance. The specific frequency of this mode, however, is not only due to the geometry and material characteristics of the flexlayer, Siliclone RTV and EAR foam earplug but also the boundary conditions “applied” by the earcup seal. This results in an earcup assembly with an effective flexlayer area of the inner area of the earcup seal, shown as the cross-hatched region in Figure 3.7.

To justify that this regime is controlled by resonance of the earplug assembly, the noise reduction of the earmuff and earplug assemblies combined versus the earplug assembly alone is considered in Figure 3.8. This plot compares the noise reduction at the bottom of the ear canal (noise reduction of earmuff and earplug assemblies combined)

versus noise reduction levels at the bottom of the interior fluid domain, which is directly above the earplug (noise reduction of the earmuff assembly).

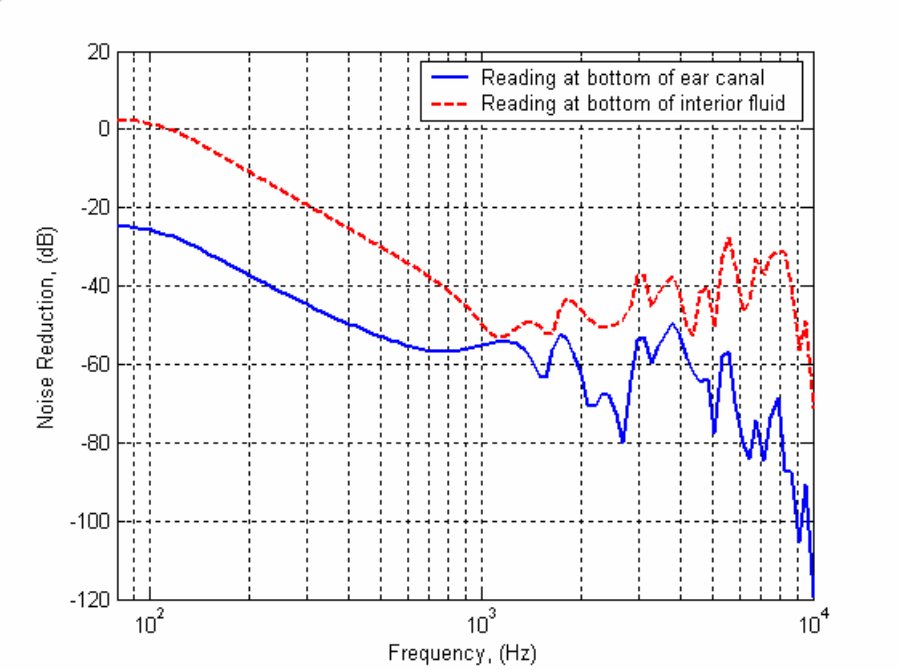

Figure 3.8 Comparing noise reduction at the bottom of the ear canal and at the bottom of the interior acoustic domain.

This plot shows a small difference in noise reduction at the claimed earplug resonance around 1,100 Hz. A more complete understanding can be gained from taking the noise reduction difference of these two noise reduction curves in Figure 3.8, and plotted in Figure 3.9. This is the difference of the noise reduction due to the pressure reading at the bottom of the interior fluid and the bottom of the ear canal and is positive valued. Higher noise reduction difference values indicate better attenuation performance; analogous to transmission loss.

$$NR_{diff} = NR_{\text{int } fluid} - NR_{ear\,canal} \tag{3.2}$$

Note how this curve closely resembles a characteristic transmission loss curve, where the left section of the curve resembles the stiffness controlled region, and the right the mass controlled region. The lowest noise reduction difference is around 1,100 Hz, at a difference of only 2 dB. Since this plot distinguishes the noise reduction of the EAR foam earplug, the lowest noise reduction point can be construed as the resonance of the earplug. This follows closely with the interpretation of a typical transmission loss curve.

The resonance of the EAR foam earplug material greatly effects the overall noise reduction of the DHP system, and depending on the material properties the resonance could be shifted in frequency. This is an important facet of the DHP system, because incorrect material properties of the earplug could drastically change the DHP model performance.

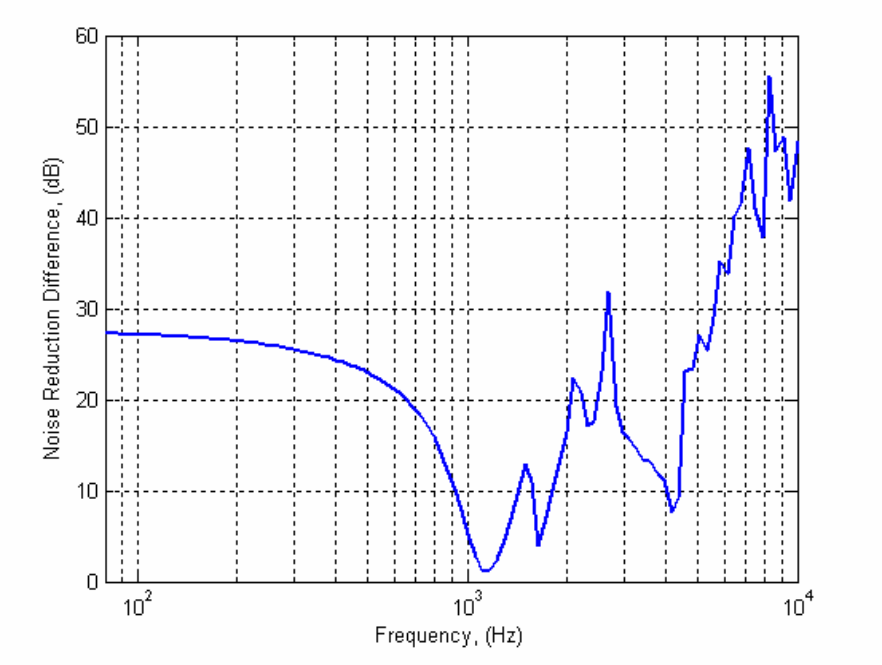

Figure 3.9 Difference in noise reduction; transmission loss of the EAR foam earplug in the ABAQUS DHP model.

This behavior of earplug resonance affecting the DHP system can be speculated to exist in real DHP HPD systems. As pointed out in Chapter 2, Berger observed a significant loss in noise attenuation in almost all human test subjects wearing EAR Classic foam earplugs in the 2 kHz octave band region, shown again here in Figure 3.10. Berger [7] suggested this loss was due to bone conduction limits, although findings in this thesis now point to the possibility of the EAR earplugs influencing the noise attenuation of the DHP system, as previously explained in this section. Acceleration must be detected in the experimental DHP test configuration to prove this observation.

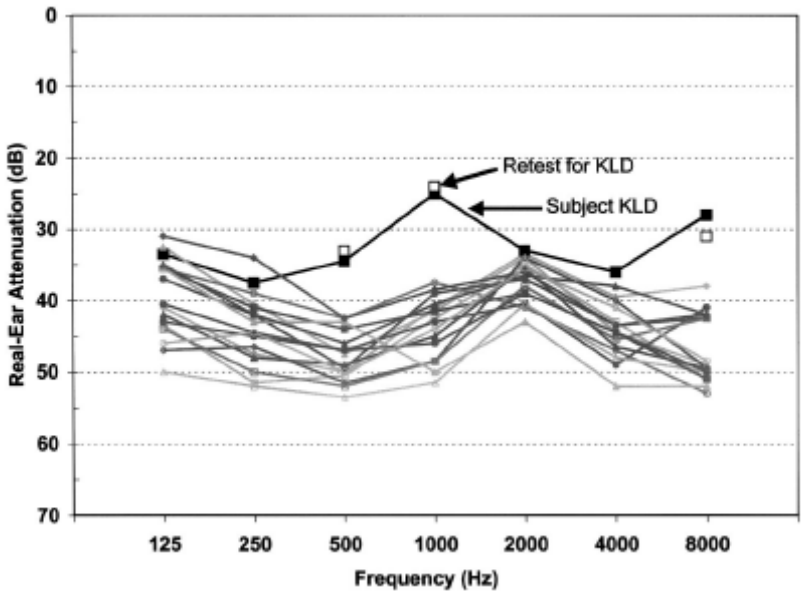

Figure 3.10 Plot of real-ear noise attenuation of human subjects equipped with Classic EAR foam earplugs [7].

3.3.2c Elastic/Acoustic Earcup regime

The third regime, the *Elastic/Acoustic Earcup* regime, is a hybrid of elastic earcup vibration and interior acoustic modes. The elastic earcup has many modes in this frequency range (1,600 to 10,000 Hz). The elastic deformation of the earcup structure transmits energy to the seal and flexlayer materials, then finally to the earplug assembly which creates relatively large deformations, and therefore acoustic pressures. This regime resembles the *Piston Mode* regime in that the earcup and seal vibration are directly responsible for the flexlayer vibration. The difference is that the earcup in the *Piston Mode* regime behaves as a rigid body, where as in the *Elastic/Acoustic Earcup* regime it is a deformable body. The interior acoustic modes of the earcup add to the pressures perceived in the ear canal, but as will be explained in the following section, these pressures do not influence the earplug response as heavily as the structural vibration does. Appendix B contains plots of the deformed earcup, and identifies each dominant deformation mode experienced in this regime. Appendix C contains a plot and explanation of the earcup structural frequency response function at a point at the top of the earcup.

3.4 Concerning earplug deformation

It is easily seen from animations of the structural deformation that the earcup assembly is acoustically excited in the frequency range under discussion. However, it is not as apparent whether the large pressures in the ear canal assembly are due only to structural vibration excitation, or to large acoustic pressure spikes, or a combination of both. Cremer, Heckl and Unger [3] stated that deformations on the order of $1x10^{-8}$ meter could induce large acoustic pressures in small contained volumes. To investigate this statement, the displacement of the bottom of the earplug in the direction of the long dimension of the ear canal is recorded and plotted in Figure 3.11. As can be seen, most displacements are within the order described to create large pressures.

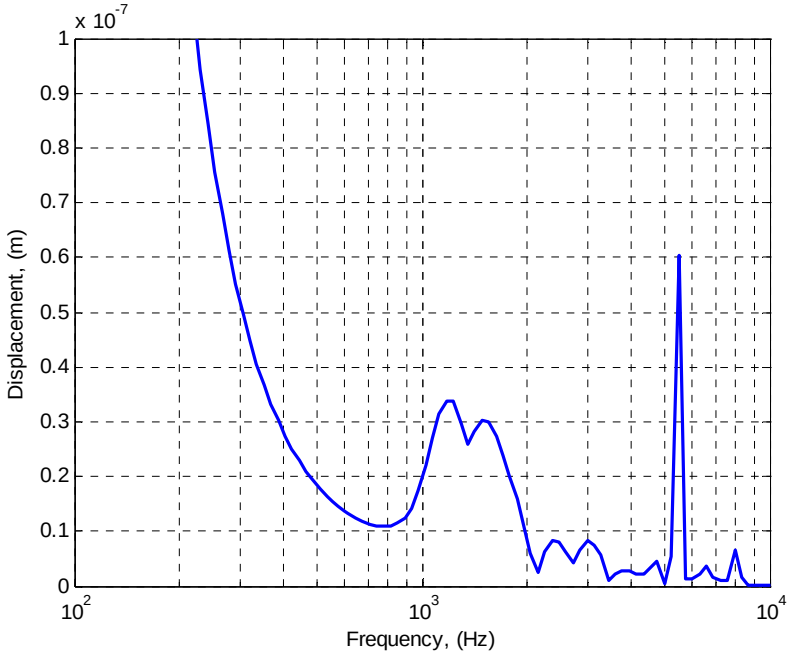

Figure 3.11 Linear displacement of the bottom of the earplug material.

This high sensitivity to the earcup deformation could mean that high pressures inside the interior acoustic cavity are being overpowered, and therefore insignificant. It is believed that the acoustic excitation energy is being transferred by the earcup and flexlayer structures through the flexlayer to the earplug, which results in a piston mode vibration of the earplug in the ear canal creating the high acoustic pressure response in the ear canal. To investigate this effect further, an ABAQUS DHP model was created that contained the same components of the previous model, except it did not tie, or connect

the nodes, of the interior acoustic domain and the entire earcup assembly (previously displayed in Figure 3.7). In other words, the fluid-structure coupling between the earcup and the interior acoustic fluid was removed. This will isolate the effect of the interior acoustic pressure on the overall pressure reading at the bottom of the ear canal. Figure 3.12 shows the different noise reduction curves for each model. Figure 3.12 shows that the ear canal pressure response in the untied model is almost exactly the same as the original model with the tied sections. This implies that the structural vibration is the significant factor in energy reaching the ear canal. The discrepancies in the tied and untied models are discussed. The lower noise reduction levels in low frequencies in the tied model can be attributed to the addition of higher pressure levels in the earcup piston mode region. This difference is minimal, at about 3 dB. At higher frequencies, the untied model seems to have slightly lower noise reduction levels. This could be because of less influence of the inner air cavity having a damping effect on the flexlayer vibration in the untied model.

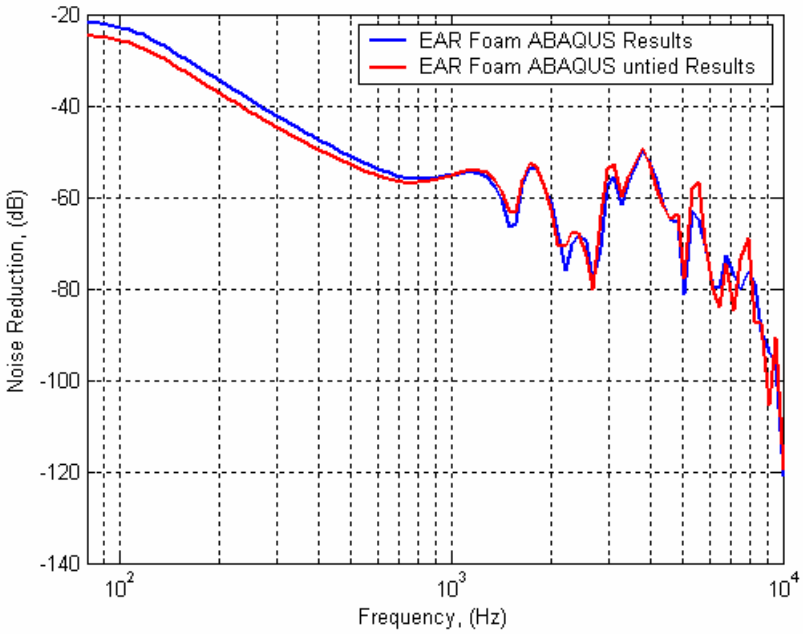

Figure 3.12 Comparing the ABAQUS models of tied and untied inner air to earplug sections.

This result implies that the primary energy path of the ABAQUS DHP model is derived from structural vibration paths. The excited earcup assembly transmits energy to the composite seal, which transmits energy to the flexlayer material, which excites the earplug assembly. Also, the exterior flexlayer material, not covered by the earcup assembly, is also acoustically excited, and its resulting vibration energy is transferred to the earplug assembly. The result is that little contribution in earplug response comes from the acoustic pressures present in the interior acoustic domain, but from the structural vibration of the entire DHP structure. This emphasizes the importance of properly characterizing the EAR foam earplug material, to determine whether this highly deformation sensitive component is being modeled correctly. Figure 3.13 outlines the discussed transmission paths. The actual contributions of each structural component will be addressed and compared in Chapter 6.

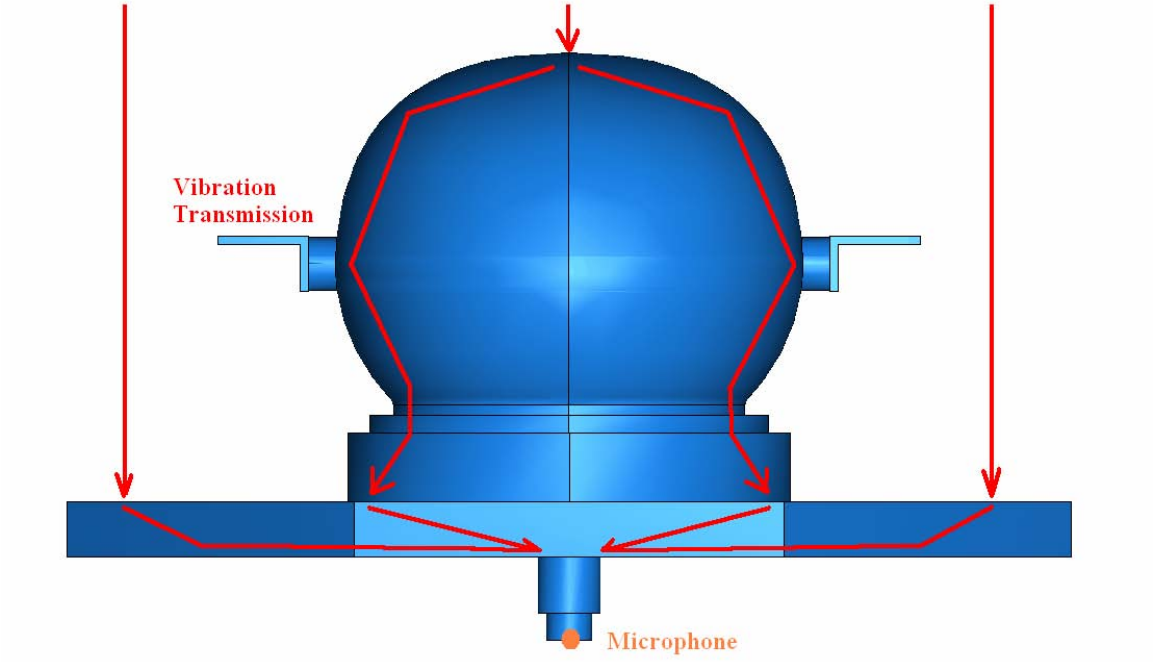

Figure 3.13 Energy transmission through structural paths, minimal energy is transferred acoustically inside the earcup.

3.5 Conclusion

The overall behavior of the ABAQUS DHP model has been explored and understood. The *Flexlayer Driven* regime exists because of the reaction of the flexlayer, Siliclone RTV and EAR foam earplug components. The *Piston Mode* regime is seen in the ABAQUS model where it was predicted to exist by Anwar [9]. The *Elastic/Acoustic Earcup* regime is attributed to structural vibration, and to a lesser degree from interior acoustic cavity modes.

It was found that the primary source of noise in the ear canal cavity is due to vibration of the DHP structural assembly. The resonance of materials in specific frequency ranges contribute to the overall structural system response, where the ear canal pressure is due to the vibration of the earplug itself.

In order to better model and understand this behavior, the material properties used for these materials must be refined and investigated. The material properties used are results from the DMA tests, which are all in an axial state of stress. Unfortunately shear is the dominant behavior mode in these three materials, and the simple axial state of stress data cannot accurately model this behavior. Therefore, shear material properties are needed to more accurately model the ABAQUS DHP system. Correct modeling of the DHP system could allow for fine tuning of the earplug material property selection, allowing for a custom DHP system to combat noise reduction performance reducing mechanisms from other components of the DHP system, for instance earcup deformation modes. More representative material properties must be obtained to more accurately model the DHP system. This process will be discussed for the EAR foam earplug material in the following chapters.

Chapter 4

Experimental process

The experimental process is the most important step in evaluating the material response. The experimental configuration must be carefully constructed and validated in order to get meaningful results. The experimental setup must accurately represent the real application configuration; the mode of deformation, material sizing and geometry and the state of stress must all be correlated for best results. Material sizing is especially important, because it is believed that viscoelastic materials at finite scale levels do not scale well. The experimental results must be explored to understand the material behavior, in this case the finite element program ABAQUS is used to visualize the response.

4.1 Experimental equipment

The general data acquisition assembly involves a FFT analyzer, small vibration exciter, a miniature accelerometer, force gage (or impedance head) and necessary conditioners and amplifiers. The Hewlett Packard 35665A Dynamic Signal Analyzer (DSA) is a real time FFT analyzer, and provided all FFT calculations and necessary transfer function computations internally. The vibration exciter used is a Ling Dynamics V203 - 4 lb. shaker powered by an AudioSource AMP 5.1A. The PCB 352C23 ICP miniature accelerometer is used for measurements on top of the EAR foam earplug because of its small mass (0.2 grams), which is the same order of magnitude as the earplug material. The miniature accelerometer also exhibits less than 5% signal error from 2 to 10,000 Hz. The PCB 288D01 impedance head (containing a force gage and an accelerometer) is used for measuring the excitation, and is chosen because of small size and availability. The PCB 480E09 variable gain signal conditioners and supplied BNC cables are used. The transfer functions are output from the HP 35665A DSA and are transformed into MATLAB .mat files using conversion software original to the HP unit. The complete setup diagram can be seen in Figure 4.1, and a picture can be seen in Figure 4.2.

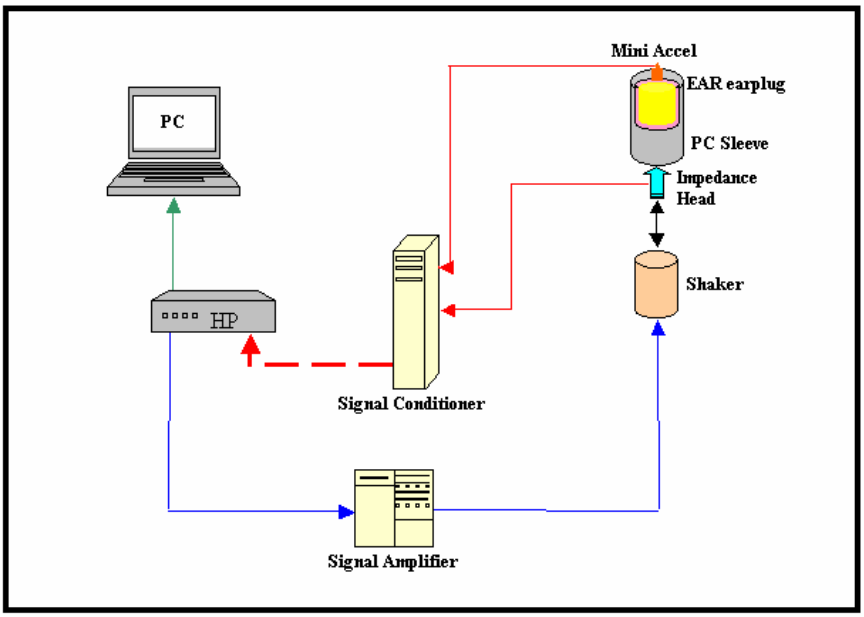

Figure 4.1 Diagram of experimental setup (shear case considered).

Figure 4.2 Picture of all experimental components.

4.2 System calibration

In order to make sure the results being obtained experimentally are correct, certain calibration techniques must be utilized. Each system component must be accurately weighed, and all cables checked for faults. The HP 35655A DSA is checked against baseline cases to understand its operational behavior. Most importantly the gains are checked for the signal conditioners and analyzer.

4.2.1 System gain calibration

Determining the correct unit output of the experimental setup is essential to obtaining usable material properties. The gains for each transducer must be applied to the raw experimental voltage output of the HP 35665A unit. The transfer function out of the analyzer multiplies out the gains set on the signal conditioners, and care must be taken when unequal gain values are used for each signal. If the linear spectrum is being used, care must be taken in determining whether the unit has output peak voltage or RMS voltage.

4.2.2 System mass calibration

The mass above the force gage on the impedance head is a crucial measurement to the performance of the analytical model. A few percent error in the mass measurement can result in significant error in the extracted material properties. To acquire this reading, the impedance head is placed upright on the shaker. It is excited and the effective mass transfer function of the force gage over the impedance head accelerometer is taken. This transfer function estimates the effective mass of the system at low frequencies. It is defined as the impedance head force over the resulting accelerometer acceleration

$$m_{eff} = \frac{F}{\ddot{x}} = \frac{F}{a} \qquad (4.1)$$

Several readings are taken, and these effective mass results are averaged over the constant slope, low frequency region. The effective mass above the force gage for the PCB 288D01 impedance head is determined to be 5.75 grams +/- 0.1 grams.

This value is checked by adding the PCB 081B05 aluminum plate and mounting stud used to mount the axial EAR foam specimen, and the above process is repeated with this added mass. The difference between the effective mass readings should be the mass of the added plate and stud. The difference in effective mass readings is 2.20 grams, where the actual measured mass of the plate and stud is about 2.23 grams.

4.3 Polycarbonate sleeve calibration

The polycarbonate sleeves are analyzed to determine if their resonant frequencies will affect the EAR foam earplug system's response. The cylindrical sleeves under

consideration are 1.25 inches in diameter by 2 inches in height. Three different preload configurations will be needed for the shear cases; therefore three different polycarbonate sleeves with different inner diameter holes will be needed. The three inner hole diameters used in this study are 1/2", 7/16" and 3/8" which are machined 1.25 inches deep into the polycarbonate sleeves. A 10-24 thread hole is tapped in the bottom to allow for attachment to the impedance head by use of a beryllium copper stud. A picture of the 7/16" sleeve can be seen in Figure 4.3.

Figure 4.3 Actual 7/16" diameter hole polycarbonate sleeve photograph.

4.3.1 Polycarbonate sleeve calibration results

Each individual sleeve is attached to the impedance head and the miniature accelerometer is connected to the top of the sleeve by accelerometer wax. The use of the wax for mounting purposes lowers the effective resonance of the accelerometer to about 50 kHz, which is well above the intended frequency range. Because of the holes in each polycarbonate sleeve, the miniature accelerometer cannot be placed directly on top center of the system as desired, however bending effects are considered negligible and slight placement offset will not significantly affect the system. The effective mass transfer functions are obtained from the analyzer, and a plot of the effective mass response of all

three sleeves can be seen in Figure 4.4. The data is plotted from 1,000 to 11,000 Hz to show the resonances around 10,500 Hz, and to not display the noisy results below 1,000 Hz. It is difficult to see in the displayed decibel format for the effective mass magnitude, but all sleeves' low frequency effective mass value was the corresponding mass of the sleeve plus the mass above the impedance head force gage.

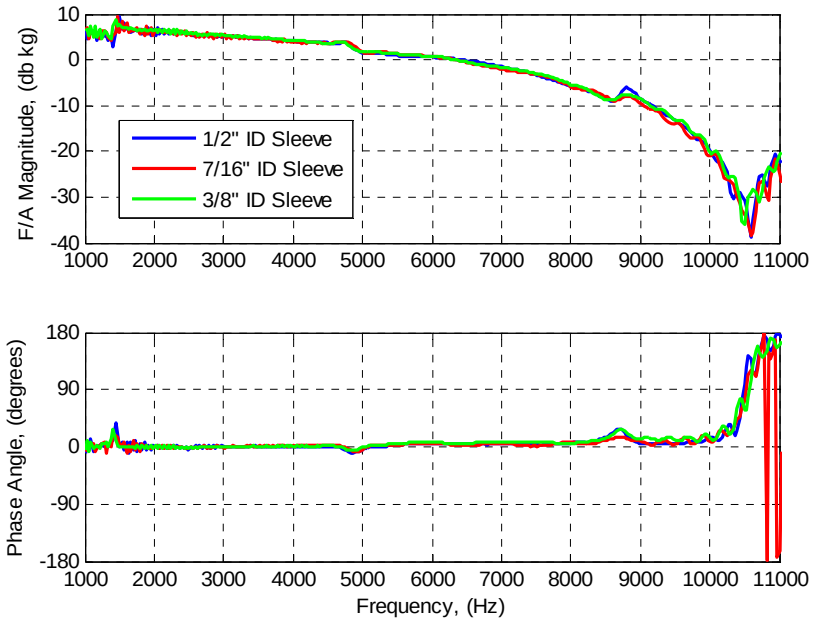

Figure 4.4 Effective mass magnitude and phase for the three polycarbonate sleeves.

4.3.2 Polycarbonate sleeve simple models

The experimental results are verified by simple hand calculations. All three sleeves exhibit about the same resonance, at 10,500 Hz. All three resonances are similar because each sleeve's reduction in mass (by increasing the inner hole) is accompanied by a proportional decrease in cross sectional stiffness, therefore leaving the system resonance unchanged. These resonances are explored with a simple one degree of freedom model, a more complicated distributed parameter system model, and finally with the finite element software ABAQUS.

Single degree of freedom model

A one degree of freedom model is used to verify the first resonance of the polycarbonate sleeves. The first resonant frequency is defined by the simple equation

$$f_n = \frac{1}{2\pi}\sqrt{\frac{k}{m}} \tag{4.2}$$

where m is the effective mass of the sleeve (1/3 of the total mass is used to account for the boundary condition and distributed system) and k is defined as the axial stiffness

$$k = \frac{AE}{L} \tag{4.3}$$

where E is the elastic modulus (taken for all models as 2.2 GPa which is an average value obtained for polycarbonate material), A is the averaged area of the sleeve cross section and L is the entire height of the sleeve. The resulting resonance for the sleeves is determined to be about 7,300 Hz. This is 30% too low therefore a more complicated distributed parameter system model is examined.

Distributed parameter system model

To further explore the polycarbonate sleeve experimental results, a distributed parameter system solution is formulated. This method accounts for distributed mass and stiffness throughout the structure. Since the simple solid rod assumption is used, it will not account for any differences in cross-sectional area, therefore all natural frequency solutions will be the same for each differing sleeve (which is also observed in the experimental data). The solution for a fixed-free bar from Inman [19] follows the form

$$f_n = \frac{1}{2\pi}\frac{(2n-1)\pi c}{2L} \tag{4.4}$$

where n is the current number of the resonance desired, L is the entire height of the sleeve and c is the wave speed of the material which is defined as

$$c = \sqrt{\frac{E}{\rho}} \tag{4.5}$$

where E is the elastic modulus and ρ is the density of the polycarbonate material. This model results in a first natural frequency of about 6,770 Hz, which is now 36% lower than the experimental value.

The polycarbonate sleeve is not completely fixed to the impedance head as was assumed in the fixed-free solution. The sleeve is attached to the impedance head by a small 10-24 stud, and therefore is allowed to move freely (except for the center impedance head area) in the plane of its bottom surface. Therefore a combination of fixed-free and free-free boundary conditions is present. The free-free distributed parameter model is of the form

$$f_n = \frac{1}{2\pi}\frac{n\pi c}{L} \tag{4.6}$$

where the variables are previously defined. The result of applying this equation yields a second natural frequency of 13,540 Hz (the first being n=0, a rigid body mode of 0 Hz). This solution is 19% too high, but since a combination of boundary conditions is expected the solution should fall between these two values. The middle value of these frequencies is about 10,150 Hz, which is only 350 Hz or 3% higher than the experimental results.

ABAQUS model verification

To finalize the simple models and understand the mode in question a three dimensional ABAQUS finite element model is constructed. The 1/2" polycarbonate sleeve is used as a verification model. Quadratic three dimensional continuum elements are used. The bottom of the polycarbonate sleeve is fixed according to the same area in contact with the impedance head in the experimental configuration. An eigensolver is employed and the modes of the model are obtained. The resonance corresponding to the first axial mode of the polycarbonate sleeve is recorded at 11,000 Hz. This is 5 percent higher than the experimentally obtained value. A graphic of the polycarbonate sleeve model can be seen in Figure 4.5, notice the inner hole on top and the fixed boundary conditions on bottom. The above solutions are placed in Table 4.1 for comparison.

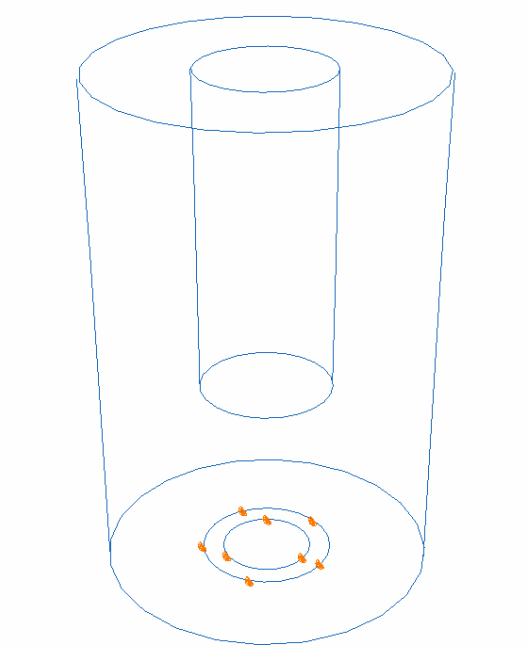

Figure 4.5 Polycarbonate sleeve finite element model geometry and loading.

Table 4.1 Resonances of each method for the polycarbonate sleeve compared.

	Experimental results	Single degree of freedom model	Average distributed parameter system	Finite element model
Axial resonant frequency	10,500 Hz	7,300 Hz	10,150 Hz	11,000 Hz
Percent error (%)	N/A	- 30% error	+ 3% error	+ 5% error

4.4 Axial case

The experimental setup of the axial foam earplug configuration is explained. This thesis will refer to the axial case as the one in which the EAR foam earplug is glued to the mounting plate and excited on its base with the miniature accelerometer glued to the top of the earplug. An annotated picture of the setup can be seen in Figure 4.6.

Figure 4.6 Picture of axial experimental case with component labels.

4.4.1 Axial case – experimental setup

The bottom aluminum mounting plate is attached to the impedance head by a beryllium copper stud with relatively high stiffness. The force gage on the impedance head is connected to the appropriate signal conditioner by the supplied microdot lead. The EAR foam earplug is glued to the bottom aluminum plate with cyanoacrylate (superglue); the PCB 352C23 miniature accelerometer is attached to the top of the EAR foam earplug with cyanoacrylate as well. The accelerometer is run to the signal conditioner with the supplied microdot lead. Due to the small mass of the foam earplug specimen, care must be taken to ensure the attached lead is not applying a load or boundary condition to the accelerometer. This effect can be minimized by firmly attaching the lead to an object the same height as the miniature accelerometer on top of the specimen.

4.4.2 Axial case – signal verification

The signal to noise ratio of the system should be checked to verify that valid data is taken. The coherence (γ) of a transfer function signal is defined as

$$\gamma^2 = \frac{H_1(\omega)}{H_2(\omega)} \tag{4.7}$$

where $H_1(\omega)$ and $H_2(\omega)$ are defined as

$$H_1(\omega) = \frac{S_{fx}(\omega)}{S_{ff}(\omega)} \tag{4.8a}$$

$$H_2(\omega) = \frac{S_{xx}(\omega)}{S_{xf}(\omega)} \tag{4.8b}$$

where $S_{xx}(\omega)$ *and* $S_{ff}(\omega)$ are the autospectra of the response excitation signals, and $S_{fx}(\omega)$ and $S_{xf}(\omega)$ are the cross-spectrum of these two signals, from Ewins [20]. A coherence level of 0.95 or better typically suggests excellent signal quality. The coherence of the axial experiment for signal conditioner gains of 10 and 100 are plotted in Figure 4.7. Figure 4.7 shows the superior signal quality of the response when both signal conditioner gains are set to 100 (maximum level). Therefore the gain is set at maximum throughout all experiments.

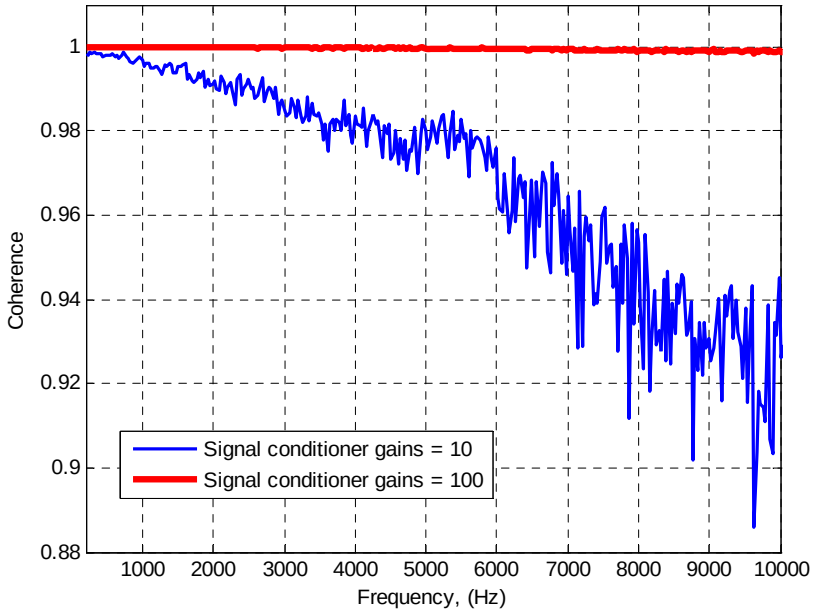

Figure 4.7 Comparing coherence for different signal conditioner gains.

4.4.3 Axial case – Results

The effective mass transfer function is taken and averaged one hundred times to ensure the smoothest characteristic possible and to minimize sampling error. The finalized experimental frequency response function can be seen in Figure 4.8. The first natural frequency occurs when the phase angle crosses +90 degrees, at 1,632 Hz. The second natural frequency occurs when the phase angle crosses -90 degrees (270 degrees unwrapped), at 5,568 Hz. Several hand calculations are proposed to validate the experimental data and understand the material behavior.

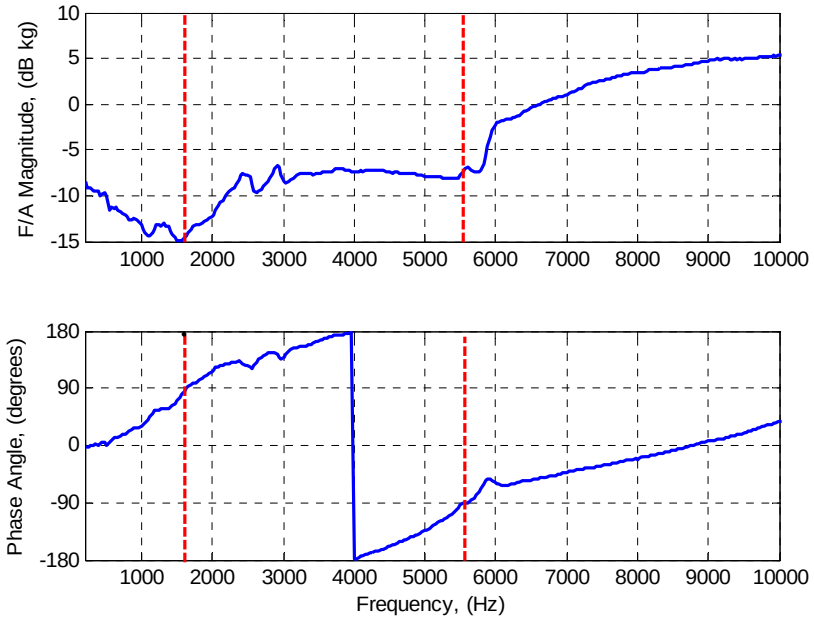

Figure 4.8 Axial experimental data FRF with marked resonances.

4.4.4 Axial case – hand calculations

To help predict and understand the behavior of the EAR foam earplug, simple hand calculations are constructed. A simple one degree of freedom model, a more complicated distributed parameter system model and the finite element program ABAQUS is used to understand the system behavior.

Single degree of freedom model

The single degree of freedom model is used to obtain a rough estimate of the resonances in the EAR foam earplug system. Equation 4.1 is used with the mass and

stiffness being of the EAR foam earplug. One half the total mass is used to simulate the effective mass due to boundary conditions. A constant elastic modulus of 1.5 MPa is used because this is an estimated value from previous data obtained from Dynamic Material Analyzer (DMA) testing. The diameter and length of the earplug material are 13.5mm and 19mm respectively. The computed first and second resonances are 1,390 and 2,780 Hz, respectively. These values are 15% and 50% lower than the experimental values, requiring a more descriptive system model. Results are placed in Table 4.2 for comparison.

Distributed parameter system model

A distributed parameter system is formulated to obtain a better estimate of the system behavior. Since the miniature accelerometer glued to the top of the EAR foam earplug is almost as massive as the foam itself, its mass must be taken into account. A continuous rod with end mass is used to model the system. The resulting equation to solve for the resonances is not as straight forward as Eq. 4.4, but involves satisfying two independent equations. The system of equations from Inman [19] is displayed below

$$\cot \lambda_n = \left(\frac{m}{\rho A L} \right) \lambda_n \tag{4.9}$$

where ρ is the density, A the cross-sectional area, L the length of the earplug, m is the end mass, and λ_n is the parameter being solved for. Once this equation is solved for each λ_n, they are placed into Eq. 4.9

$$\omega_n = \frac{\lambda_n c}{L} \tag{4.10}$$

where c is defined above in Eq. 4.5.

The same elastic modulus (E=1.5 MPa) as the single degree of freedom solution is used. The solutions of Eq. 4.6 are plotted on the same plane and their intersections yield the resonances of the system. The results yield the first and second natural frequencies of 967 and 3,478 Hz, respectively. This is an error of 30% and 60% low, respectively. Both estimates contain significant error, which might be attributed to the difference in placement of the accelerometer end mass. The miniature accelerometer used in the experiments only constrains the center of the earplug, where the distributed

parameter system models the end mass as constraining the entire top of the EAR foam material. This does not accurately model the experimental system, therefore a more accurate three-dimensional finite element model is created.

ABAQUS model verification

A three-dimensional model of the axial earplug system is constructed in ABAQUS to verify and investigate the previous hand calculations. The EAR foam earplug is the entered geometry with the entire bottom of the earplug constrained to simulate the glued boundary condition. The accelerometer mass is added to the top of the earplug as a lumped mass. The constant elastic modulus of 1.5 MPa is again used. The first and second axial natural frequencies are 1,604 and 4,585 Hz, respectively. This is an error of 2% and 18%, respectively. The second natural frequency exhibits the most error suggesting more accurate material properties as a function of frequency are needed. The ABAQUS model mesh can be seen in Figure 4.9. The hand calculation results for the axial case are tabulated in Table 4.2. The hand solutions are shown to model the first resonance well with a constant elastic modulus, but that same elastic modulus is shown inadequate at the higher frequency resonance. Since the experimental DHP EAR foam earplug configuration involves compressed preloading in a shear state of stress, a shear experimental extraction model is proposed.

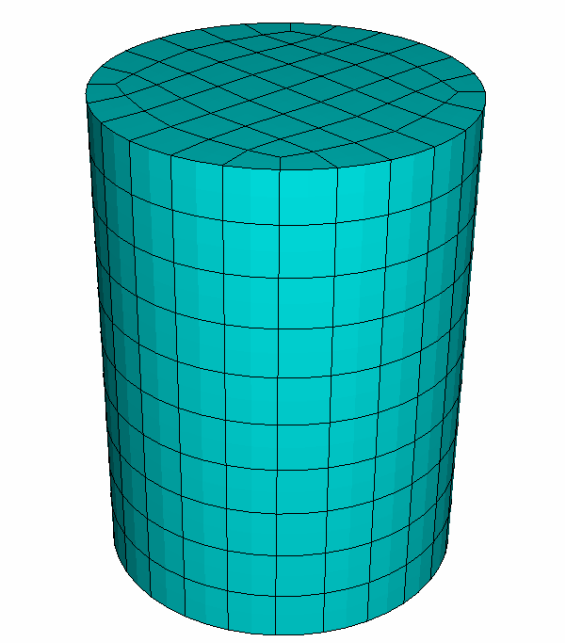

Figure 4.9 EAR foam earplug mesh in ABAQUS.

Table 4.2 Resonances of each method for the EAR foam earplug axial case.

	Experimental results	Single degree of freedom model	Distributed parameter system	Finite element model
First axial resonance	1,632 Hz	1,390 Hz (15% low)	967 Hz (30% low)	1,604 Hz (2% low)
Second axial resonance	5,568 Hz	2,780 Hz (50% low)	3,478 Hz (60% low)	4,595 Hz (18% low)

4.5 Shear case

The shear earplug case is constructed to better model the earplug in its original experimental configuration; the compressed single and double hearing protection models. The shear case will be declared as the case containing the EAR foam earplug compressed and installed into the inner hole of one of three different polycarbonate sleeves. The accelerometer is glued to the top of the earplug. An annotated picture of the configuration can be seen in Figure 4.10.

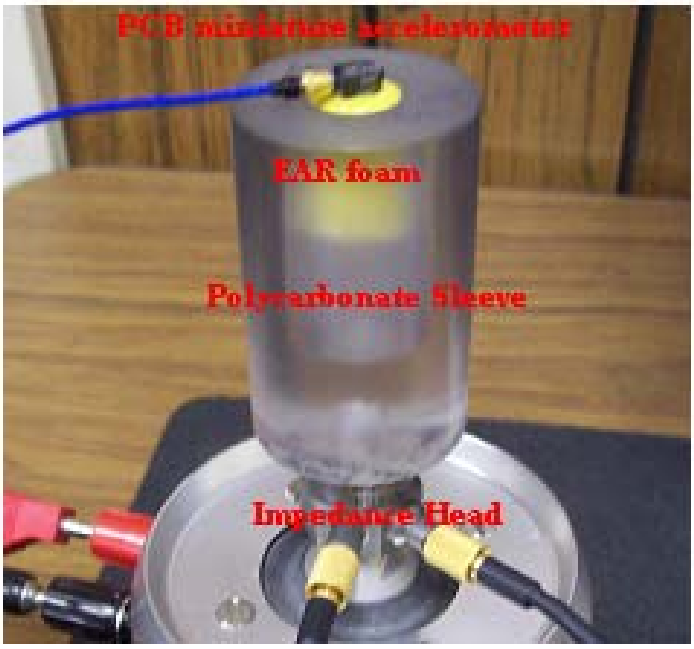

Figure 4.10 Picture of the shear experimental case with labeled components.

4.5.1 Shear case – experimental setup

The sleeves used have inner diameter holes of 1/2”, 7/16” and 3/8”. The inner diameter holes provide preload on the compressed earplug. To quantify the amount of preload on the earplug, radial compressive strain is introduced. The radial strain of the compressed earplug is defined as the reduction in its radius

$$\varepsilon_{radial} = \frac{r_p - r_0}{r_0} \tag{4.11}$$

where r_0 is the radius of the earplug in its uncompressed state, and r_p is the radius of the compressed earplug. The measure of radial strain will be referred to throughout the rest of the thesis. The 1/2”, 7/16” and 3/8” sleeves translate to 6%, 18% and 30% radial strain, respectively. Note that Eq. 4.11 will give a negative (compression) strain value, although the radial strains will be referred to as positive for ease of use.

The polycarbonate sleeve is connected to the impedance head by a 10-24 beryllium copper stud of relatively high stiffness. The EAR foam earplug is rolled until a diameter smaller than the hole in the current polycarbonate sleeve is achieved, and then it is carefully installed with attention given to the shape upon expansion. A good clean and even fit inside the hole must be ensured, and any experienced offset should warrant reinsertion of a fresh earplug. The PCB 352C23 miniature accelerometer is glued to the top of the earplug with cyanoacrylate, and then the supplied microdot lead is attached. Once again, care must be taken in constraining the lead so no unnecessary loads or boundary conditions are applied to the accelerometer or EAR foam sample.

4.5.2 Shear case - signal verification

The coherence of the affective mass transfer function is evaluated to determine the quality of the signal. A coherence level of 0.95 or better typically suggests excellent signal quality. The coherence from all three preload cases is plotted against one another in Figure 4.10. The coherence level does not drop below 0.99 in the shear preload experiment cases.

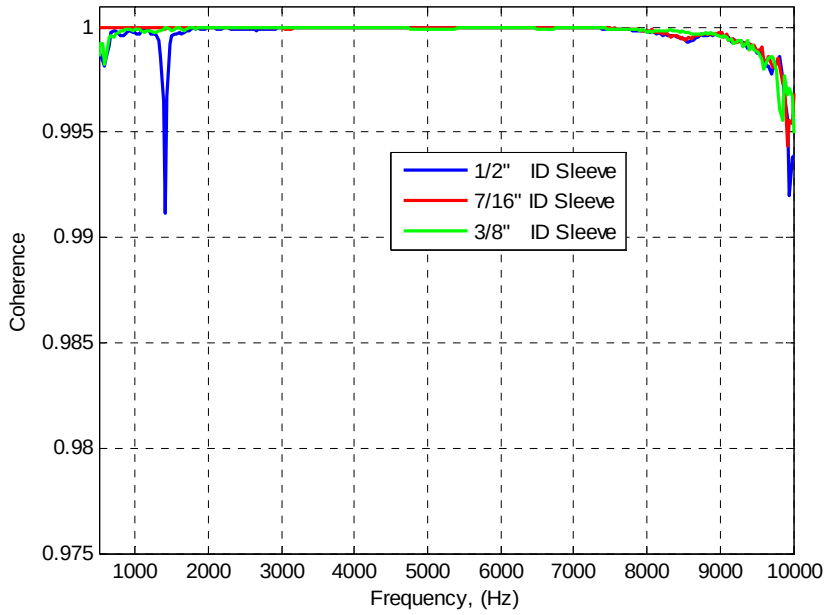

Figure 4.11 Coherence for all three shear preload cases.

4.5.3 Shear case - experimental results

The effective mass transfer functions are plotted in Figure 4.11 for all shear experimental cases. Figure 4.10 indicates that the increase in preload amount increases the frequency of the first resonance of the system response. Resonance is defined when the phase shift reaches +/- 90^{o}, and a resulting minimum will be seen in the effective mass magnitude. The first resonance of the 1/2" ID sleeve (6% radial strain) is about 3,510 Hz. Reducing the ID to 7/16 (18% radial strain) results in a first resonance of 4,300 Hz. Decreasing the ID to 3/8" (30% radial strain) results in a first resonance of 5,050 Hz. To verify and explore these results, simple hand calculations and a three dimensional finite element model are constructed.

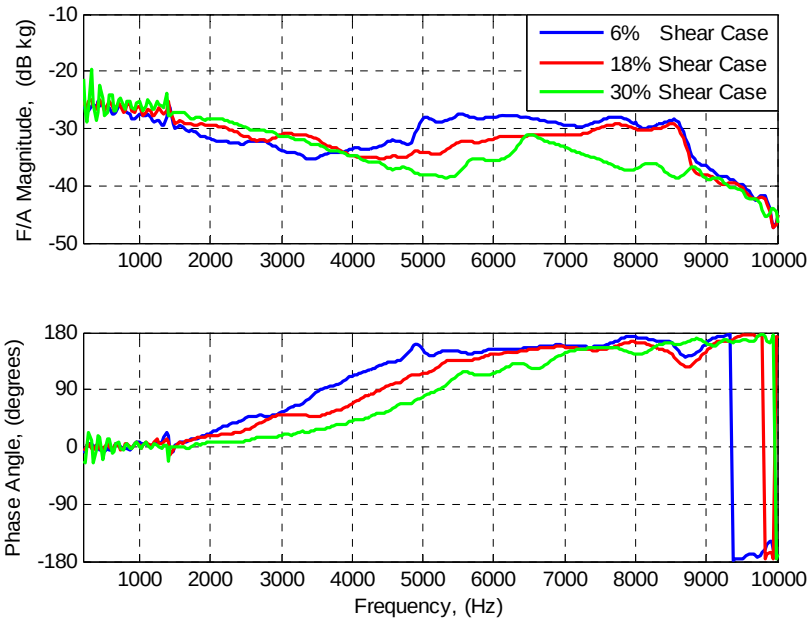

Figure 4.12 Experimental results for shear preload cases.

4.5.4 Shear case - hand calculations

Several hand calculations are constructed to verify the experimental results. A simple one-degree-of-freedom model and a three dimensional finite element model are created.

Single degree of freedom model

A rough estimate is obtained by utilizing a simple one-degree-of-freedom model, while using the same constant modulus of elasticity from the axial case. It is obtained for the 6% strain preload case only, because this is the easiest case to model with its small amount of preload. Equation 4.1 is again used, except the effective stiffness is for a shear spring rather than the axial spring previously used. The shear stiffness is defined as

$$k_s = \frac{A_s G}{L} = \frac{\pi D E}{2(1+\nu)} \tag{4.12}$$

where ν is Poisson's ratio of the material (being 0.1 for soft elastomeric foams), G and E are the shear and elastic moduli of the material, respectively, D is the diameter of the specimen and A_s is the shear area defined as

$$A_s = \pi DL \tag{4.13}$$

Half the total mass is again taken as the effective system mass. The first natural frequency of the single-degree-of-freedom model occurs at 2,220 Hz. This estimate is 37% low from the experimental result. To further investigate the system behavior an ABAQUS model is constructed.

ABAQUS model verification

A two dimensional axisymmetric model is created for each inner diameter sleeve. The bottom of the sleeve is fixed according to the same area of the impedance head contact area. The earplug is modeled as a linear elastic material which is completely constrained to the interior surface of the sleeve. Quadratic elements are used for the entire model, and the previous linear elastic modulus is the same for all cases (2.2 GPa). The ABAQUS eigensolver is used to find the resonances of the system. The first shear mode of the 6% radial strain model is found to be 4,490 Hz, 4,230 Hz for the 18% radial strain model and 4,030 Hz for the 30% radial strain model. Note how these results do not increase with preload as the experimental data does. This is because the same elastic modulus is used for all cases; the effect of preload is ignored because no information of the state of stress in the earplugs due to the compression is known. Not knowing the influence of the preload on the effective modulus of elasticity prohibits the finite element models from obtaining realistic results. These results along with the experimental data and hand calculations are displayed in Table 4.3.

Table 4.3 Resonance of each method for the EAR foam material in preloaded shear.

	Experimental results	Single degree of freedom model	Finite element model
Shear resonant frequency (6% radial strain)	3,510 Hz	2,220 Hz (37% low)	4,490 Hz (28% high)
Shear resonant frequency (18% radial strain)	4,300 Hz	N/A	4,230 Hz (2% low)
Shear resonant frequency (30% radial strain)	5,050 Hz	N/A	4,030 Hz (20% low)

4.6 Conclusion

The shear case experimental data is not modeled accurately with constant value of the linear elastic modulus of elasticity. The effective elastic modulus could be adjusted to obtain the first shear case resonance for each preload, but this would not accurately model the entire frequency range without complete material data. Also, the modulus of elasticity not only varies with frequency, but with compressed preload as well. In the following section, an analytical method is introduced to extract the material properties from the experimental data as a function of frequency in the axial case and as functions of frequency and preload in the shear cases.

Chapter 5

Material property extraction

In the previous section, a constant linear elastic modulus does not satisfactorily model the earplug material over the entire usable frequency range. The system damping is also unknown, which appears to be quite high from the experimental data. Damping is also not a constant value over the frequency range, and must be determined to obtain an accurate material model. Several extraction methods and models are considered, with the Inverse Nyquist Plane Parameter Method chosen to best obtain the unknown storage and loss moduli as a function of frequency. The question of numerical solvers is addressed, with justification for solver selection. A proven method for material property extraction is given, along with results for the axial and preloaded shear cases. Finally, an interpolation method is applied to the extracted shear data, which is accomplished by utilizing a quadratic finite element representation.

5.1 Extraction methods

5.1.1 Finite element method

The initial method considered for material property extraction is a simple one dimensional, three-degree-of-freedom finite element model. The model is shown in Figure 5.1, with masses designated for the axial case.

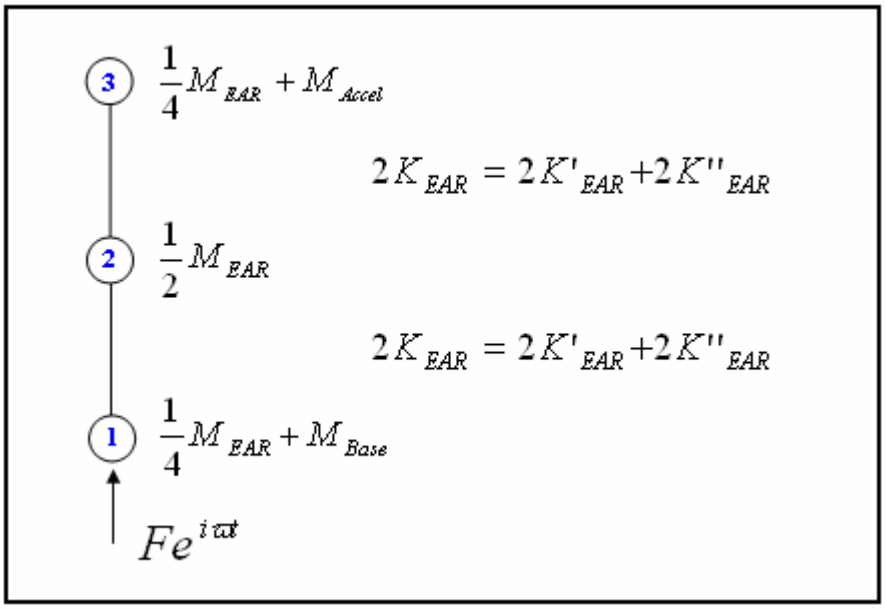

Figure 5.1 Simple finite element model.

The finite element mass, complex stiffness, known load and acceleration are specified and the unknown acceleration value at the top of the structure is solved for. The resulting effective mass transfer function is determined, which is the force at node 1 over the resulting acceleration at node 3. The matrix equation is described as

$$-\omega^2[M]\{u\} + k'[K]\{u\} + k''[K]\{u\} = \{F\} \quad \text{where} \quad [K] = \begin{bmatrix} 1 & -1 \\ -1 & 1 \end{bmatrix} \tag{5.1}$$

and ω is the circular frequency in radians per second, [M] is the lumped mass matrix, k' is the real component of the complex stiffness value, k'' is the imaginary component of the complex stiffness value, {F} is the load vector and {u} is the displacement vector. The complex stiffness can also be described as

$$k^* = k' + ik'' \tag{5.2}$$

This method is easy to formulate and process, unfortunately the optimization of this method requires cycling through various unknown complex stiffness values. This constant variation may provide ill-conditioned matrices, which do not provide viable solutions when the matrices must be inverted to obtain a solution. A working model can be obtained; unfortunately time constraints require that a proven method must be used.

5.1.2 Inverse Nyquist Plane Parameter Method

The Inverse Nyquist Plane Parameter Method is considered from previous work of Sun and Mitchell [16] and Agee and Mitchell [17]. This method involves a simple three-degree-of-freedom system, identical to the one previously used in the finite element model. A schematic of the model is shown in Figure 5.2 with graphical changes to better express the idea of the system model, where k^* is the complex stiffness defined in Eq. 5.2.

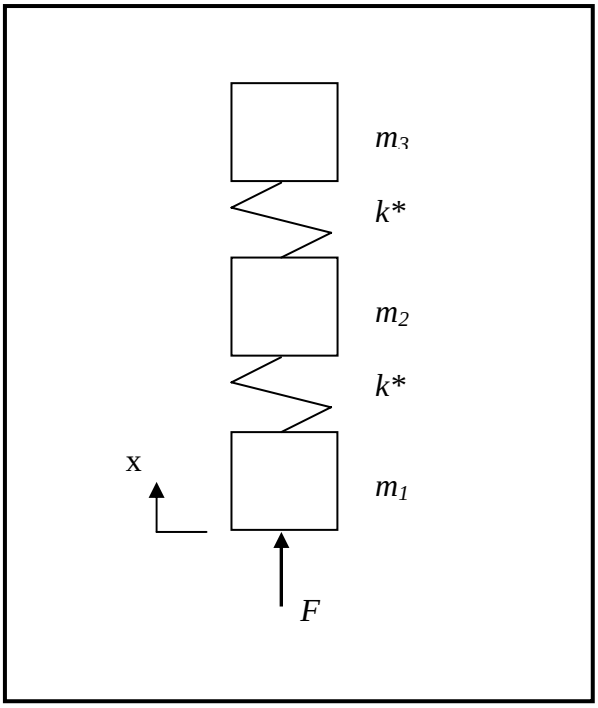

Figure 5.2 Three degree of freedom model used in the Inverse Nyquist Plane Parameter Method.

Transfer matrices are used to multiply the respective mass and stiffness matrices for each degree of freedom to obtain the total system response. The result for the required degrees of freedom (the acceleration at the top mass and the load at the bottom mass) are obtained through algebraic manipulation. Details of the formulation are given in Sun and Mitchell [16] and Agee and Mitchell [17]. The resulting expression for the effective mass transfer function of the system is

$$\frac{F}{\ddot{x}} = (m_1 + m_2 + m_3) - \frac{(m_1 m_2 + m_2 m_3 + 2m_1 m_3)}{k^*}\omega^2 + \frac{m_1 m_2 m_3}{k^{*2}}\omega^4 \qquad (5.3)$$

where the left side of the equation is taken be the known complex value of the experimental effective-mass transfer function, m_1, m_2 and m_3 are the masses of the first, second and third degrees of freedom, respectively. Note that k^* is the complex stiffness of the structure consisting of real (storage) and imaginary (loss) values. Notice that the model requires the effective stiffness be twice the specimen stiffness which is due to the two springs being in series. This method is preferred because of its ease of use and proven effectiveness. Since this approach utilizes a three-degree-of-freedom model it can model the system up to its third natural frequency. Criterion has been proposed by Agee and Mitchell [17] to determine the effective frequency range of the model. The minimum and maximum frequency values can be estimated using

$$f\ \min = 0.15\, f_{n2} \qquad f\ \max = 10^{[(\log f_{n2} + \log f_{n3})/2]} \tag{5.4}$$

where f_{n2} and f_{n3} are the second and third resonances of the system. The first resonance is considered to be the rigid body mode of the system at very low frequencies. This expression will be used for the axial and shear cases to determine the validity of the results. The three-degree-of-freedom analytical model is chosen over the two-degree-of-freedom model because it more accurately describes the higher frequency range; or it could be said that it takes into account the important contribution from the third resonance.

Equation 5.3 is an indirect summation of the contributions from all resonances to determine the appropriate response at the spectral line in consideration. More exploration of this approach will be undertaken when analyzing each experimental case. The three-degree-of-freedom model is already established, but the physical interpretation of that system must be discovered for the experimental system in question.

5.2 Axial case analytical model

The axial case and its experimental data put forth in the previous chapter are considered. The three-degree-of-freedom model that must be solved using the Inverse Nyquist Plane Parameter Method will be fit to the physical system. The model presented in Agee and Mitchell [17] will be followed with changes in physical properties. The actual masses used are described in reference to Figure 5.2. The mass m_1 is considered the sum of the mass above the force gage, the mass of the mounting plate and one quarter

the mass of the EAR foam material. The mass m_2 is taken to be one half the mass of the EAR foam material, and m_3 is the sum of the miniature accelerometer mass and one quarter the mass of the EAR foam material. The stiffness is the unknown complex stiffness of the EAR foam material. Placing these parameters into the Inverse Nyquist Plane Parameter Method expression (Eq. 5.3) along with the complex effective mass experimental data transfer function yields a system of one unknown, the complex stiffness value. This is the value sought to be extracted from the experimental data. The following section will cover the development of the three-degree-of-freedom analytical model for the shear case.

5.3 Shear case analytical model

The EAR earplug in shear is a different physical system from the axial case, and cannot be accurately explained by the analytical model of Figure 5.2. An axisymmetric drawing and a top view of the physical system represented in the shear model can be seen in Figure 5.3.

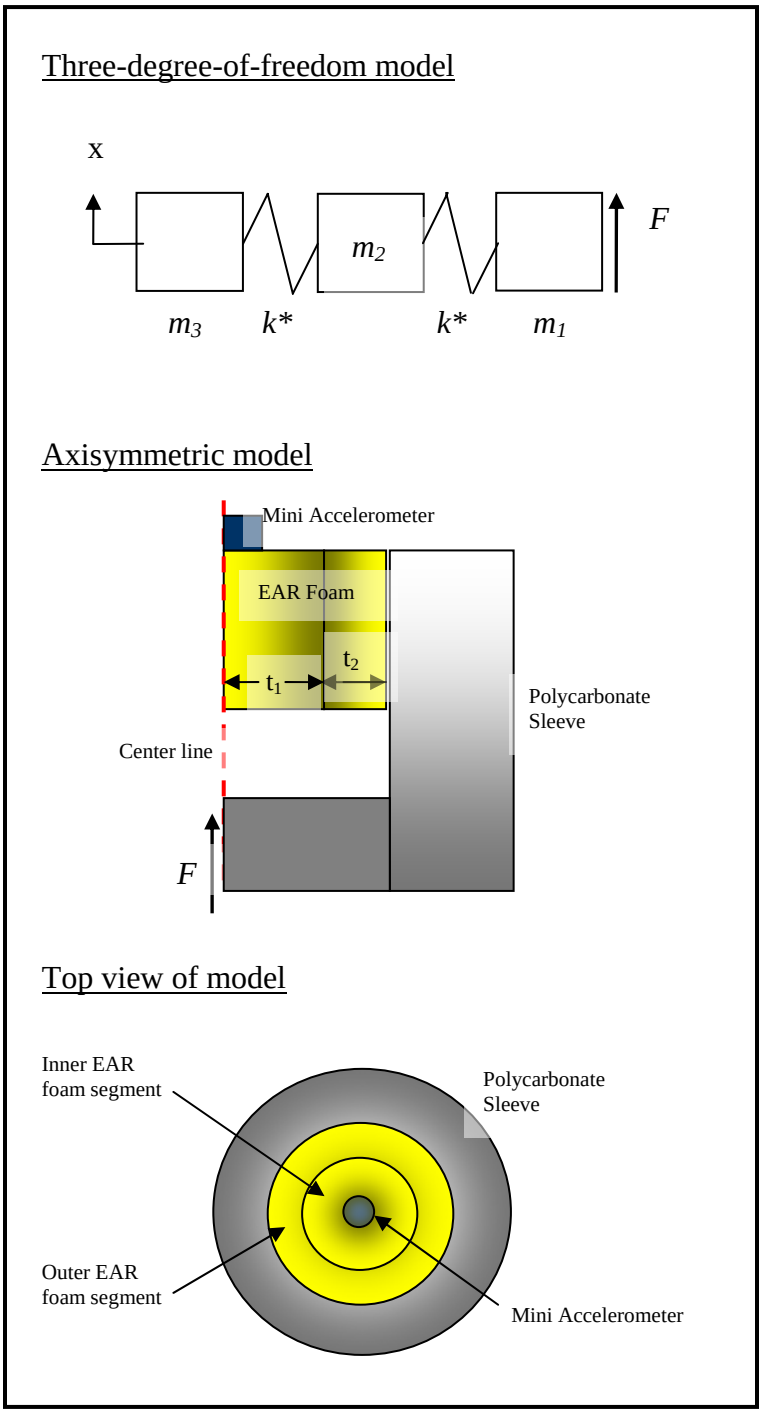

Figure 5.3 Representation of the preloaded shear case.

The mass m_1 is considered the sum of the mass above the force gage (5.75 grams) and the polycarbonate sleeve. To be able to utilize the same model and governing equation (Eq. 5.3) the two spring stiffnesses must equal each other. In order to

accomplish this, their respective top surface areas were equalized, resulting in optimal inner and outer radii for the two shear segments. This was formulated by Sun and Mitchell [16], and is comprised of the following

$$t = t_1 + t_2 \qquad \frac{t_1}{A_1 C_1} = \frac{t_2}{A_2 C_2} \tag{5.5}$$

where t is the total thickness of the EAR foam specimen (equal to the specimen radius), t_1 and t_2 are the thicknesses of the inner (closest to axis of symmetry) and outer divided specimens, respectively. The constants C_1 and C_2 are defined as

$$C_n = \frac{1}{1 + \frac{t_n^{\,2}}{36 r^2}} \tag{5.6}$$

where r is the radius of gyration, which is defined as the specimen length divided by the square root of 12 for this cylindrical geometry,

$$r = \frac{l}{\sqrt{12}} \tag{5.7}$$

Equations 5.5 are solved by a simple minimization technique, and the resulting specimen divisions are determined for each preload case.

Note that the drawing in Figure 5.3 is drawn similar to an axisymmetric model, however the model is a complete system model and is only drawn in this fashion for ease of visualization. The analytical models have been established for both experimental cases, and the numerical solver method is discussed in the following section.

5.4 Solvers

A numerical solver method is required to determine the unknown stiffness values. Several methods are considered, with note given to their results and overall usefulness. The final method chosen is Muller's complex root finding method, the applicability of the method is also presented.

5.4.1 Minimization techniques

Several minimization techniques were first considered to find the unknown stiffness values. No minimization technique tried could solve for a complex unknown

value, therefore the equation was broken up into the real and imaginary components, listed as

$$\mathrm{Re}\left(\frac{F}{\ddot{x}}\right) = \frac{C_3(1-\eta^2)\omega^4 - C_2k(1+\eta^2)\omega^2 + C_1k^2(1+\eta^2)^2}{k^2(1+\eta^2)^2} \tag{5.8}$$

$$\mathrm{Im}\left(\frac{F}{\ddot{x}}\right) = \frac{[C_2k(1+\eta^2)\omega^2 - 2C_3\omega^4]\eta}{k^2(1+\eta^2)^2} \tag{5.9}$$

where η is the loss factor, k is the real component of the complex stiffness value, C_1, C_2, and C_3 are defined as

$$C_1 = m_1 + m_2 + m_3 \tag{5.10}$$

$$C_2 = m_1m_2 + m_2m_3 + 2m_1m_3 \tag{5.11}$$

$$C_3 = m_1m_2m_3 \tag{5.12}$$

and all other variables have been previously defined. The difference between the experimental and analytical real and imaginary components are summed and squared, the values of stiffness and loss factor are attempted. This method simply finds the minimization of the least square error function, and does not explicitly solve for the zero of the equation. This technique creates solution problems, as there is no single solution. Depending on the step increment, discontinuous solutions can be found. Severe bounds must be placed on the solver for continuous results, often requiring a priori knowledge of the unknown solution. When the solution converges accurately, the runtime is significantly higher than Muller's method. This led to investigation and eventual selection of Muller's complex solver method.

5.4.2 Muller's complex root finder

Muller's method is a simple complex root finder with the following steps:

1. Takes in two points that must bracket the unknown zero, complex solution to Eq. 5.2.
2. Creates a midpoint of these two points by bisection.
3. Fits a quadratic to Eq. 5.2.
4. Solves for the roots of this quadratic equation.
5. Chooses new bounds based on the roots found. It will continue with the iteration until the appropriate root of Eq. 5.2 is found.

The reader is directed to the resource of Crenshaw [21] for more information, and the annotated code used is attached in Appendix C. This method converges quickly, usually in two iterations, assuming the system has a solution. Quickness of convergence, the simplicity of the algorithm and the uniqueness of the solution make this method the ideal choice for the material extraction problem. Since there are two possible complex roots viable for every spectral line, care must be taken in manipulating the results. The best process for extracting the resulting material properties is discussed next.

5.5 Extraction process

The process found for extracting material properties has been developed and is described. Since the raw experimental data may contain irregularities due to noise, the data should be curve fit. The real and imaginary experimental values from the data acquisition system's effective-mass transfer function should be curve fit individually. Generally a fourth or fifth order function will fit the data well. Care must be taken when tuning the curve fit. The real and imaginary components of the effective-mass transfer function should approach a constant value at zero frequency. The real component of the effective mass will approach the total mass of the system ($m_1 + m_2 + m_3$) and the imaginary component of the effective mass must approach zero. If the fitted equation does not approach these values, the offset may be added or subtracted to ensure these conditions are met. A fifth order fit to the axial experimental results is plotted in Figure 5.4, while the residuals of the magnitude and phase between the two curves can be seen in Figure 5.5.

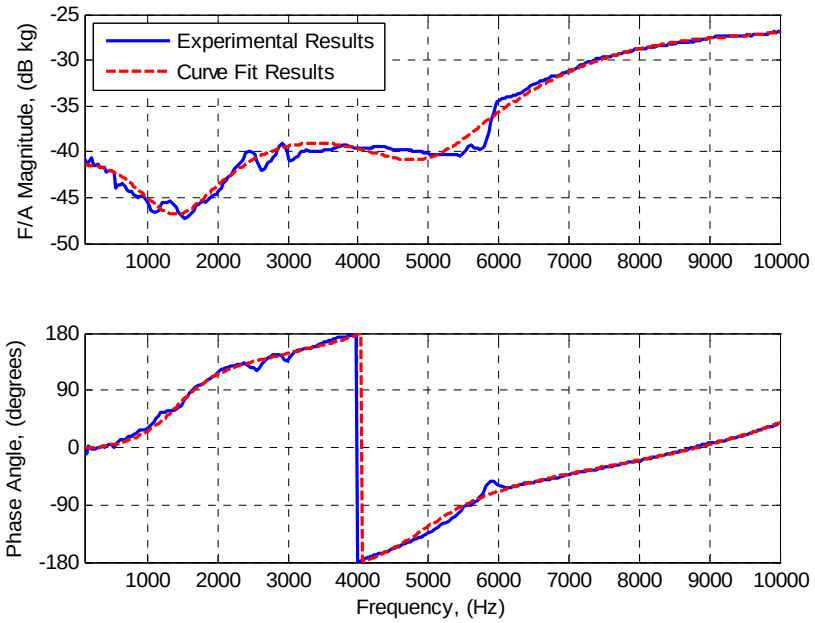

Figure 5.4 Axial experimental FRF and fifth order curve fit.

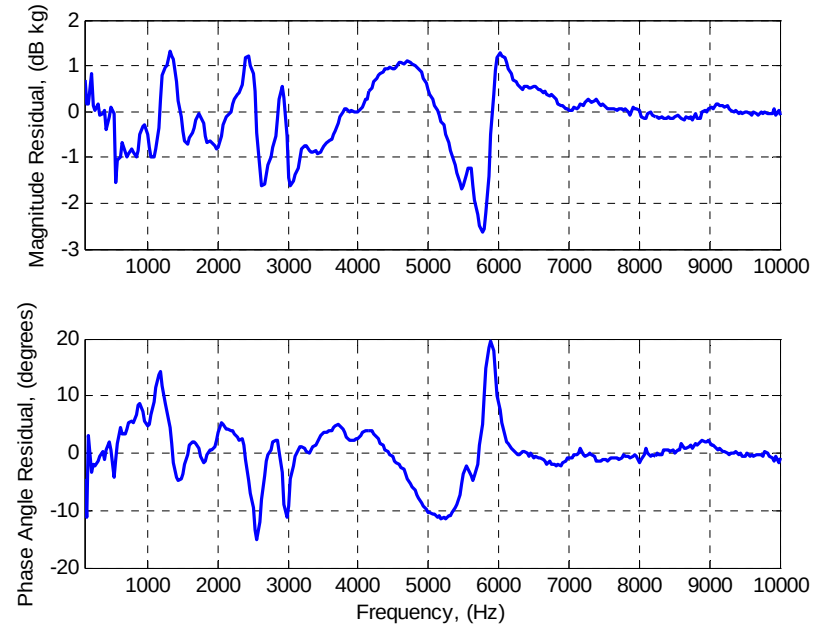

Figure 5.5 Residual of magnitude and phase between the experimental and curve fit results.

Since Muller's complex root finder chooses the root of the quadratic equation closest to the mid point, the viable solution is found almost every time. Care must be taken to ensure that the solved root is the correct one, so it is suggested that both roots are solved for and observed. This will ensure that the infeasible root is being left out of the solution. Infeasible roots are defined as roots that produce negative-valued roots. This will be seen more in certain solutions where the roots have solutions close to each other in the feasible domain.

The Inverse Nyquist Plane Parameter Method is essentially an indirect summation of contributions from the three modes, named an indirect summation because the expression in Eq. 5.3 is not a modal decomposition. This can be seen by the three terms in Eq. 5.3, where the contribution from the first mode (considered to be the rigid body mode) is described by the term ($m_1 + m_2 + m_3$). This rigid body mode can be observed in the experimental data at low frequencies when the real value approaches the total system mass and the imaginary value approaches zero. The contribution from the second and third modes is contained in the summation of the second and third terms of Eq. 5.3. If the desired material property extraction range falls largely between two natural frequencies, a discontinuity in the extracted results may occur. This greatly affects the useful range of the extracted data. This is seen in the lower frequency results of the axial and shear cases. The solution of this problem leads to the formulation of a new method to determine the usable bounds of the extracted material properties.

5.6 Extraction results

The material property results are given for the axial and shear cases. A closer look at the usable frequency range for the EAR foam material is taken.

5.6.1 Axial case extraction results

The above extraction method is applied to the EAR foam earplug axial case. The solution over the entire frequency range (32 to 10,000 Hz) for both solved roots can be seen in Figure 5.6.

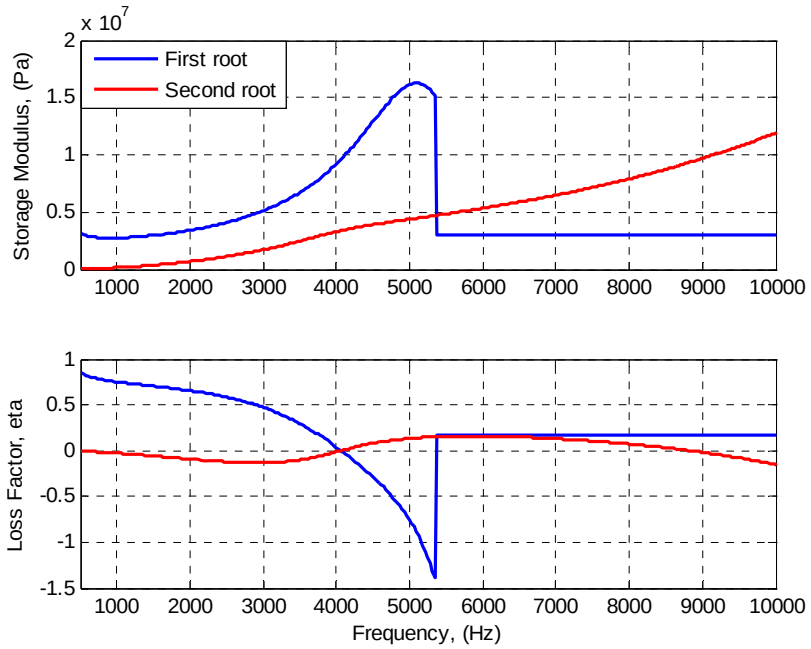

Figure 5.6 Both extracted root solutions for the axial case.

To obtain a positive loss factor through most of the frequency range, the chosen root solution must be switched. This creates a large discontinuity in both extracted properties at 4,000 Hz. This large discontinuity and unrealistic loss factor results suggests a refinement of the valid frequency range of results be considered.

The usable frequency range proposed in Eq. 5.4 is applied to the axial extraction results. This enforces a usable frequency range of 250 to 3,000 Hz. The lower frequency limit is an unbelievable value; there is an inflection point at about 800 Hz. Data before this inflection point cannot be accepted, because this trend does not mimic expected results. A more suitable lower frequency limit might be presented as

$$f\ \min = 0.5\, f_{n2} \tag{5.13}$$

which would yield a usable frequency range of 800 to 3,000 Hz. This defines the feasible range of the axial extraction results. Change in the lower frequency limit can be attributed to the relatively low mass EAR foam material whose mass is the same order as the accelerometer. The limits in Eq. 5.4 were obtained through observations, as was the change to the lower limit in Eq. 5.13. The results with the new frequency range can be seen in Figure 5.7.

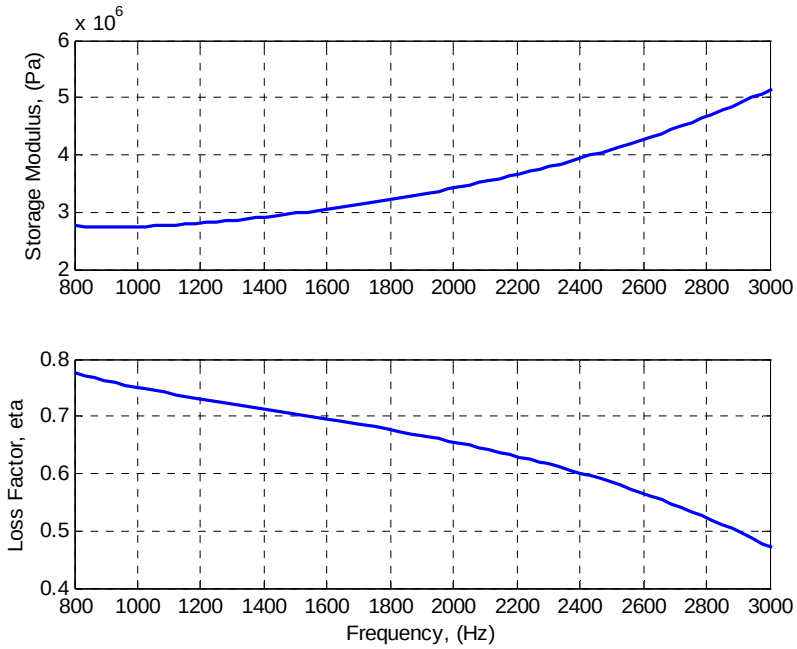

Figure 5.7 Extracted axial results with the final adjusted frequency range.

The extracted axial results are compared to the baseline DMA results and are plotted in Figure 5.8. The two results exhibit different trends, with the storage moduli of the DMA results biased high throughout the frequency range. The DMA storage moduli are at higher than the extracted axial results at the maximum difference by a factor of two, although their values approach one another as the frequency increases. The loss factors for the extracted axial results are almost four times higher than the DMA results at the low frequency range, but decrease to about twice as high at 3,000 Hz. The difference in data may be attributed to material scaling, where in the extracted axial tests the entire 19mm EAR foam specimen was utilized, where in the DMA axial tests a shortened 10mm plug was used.

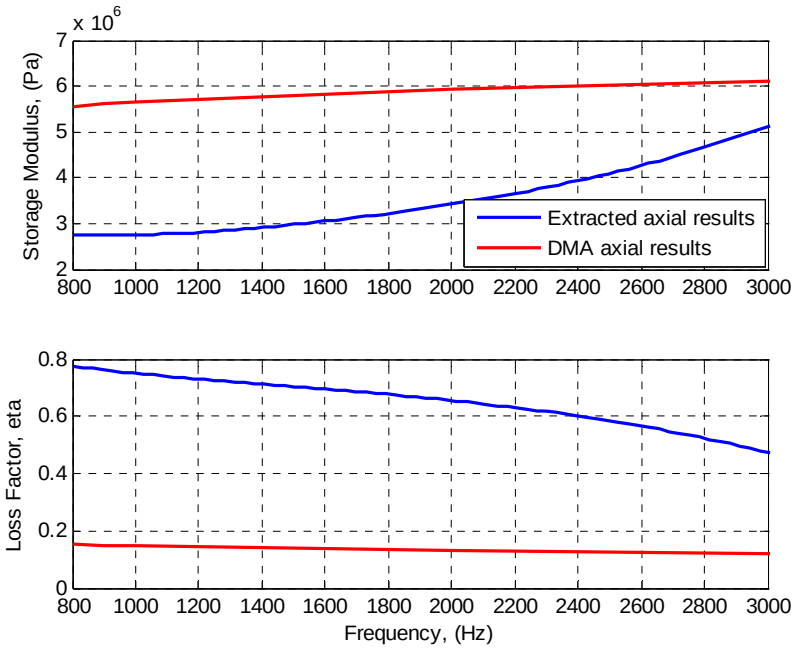

Figure 5.8 Comparing extracted axial and DMA axial results.

5.6.2 Shear case extraction results

The above extraction method is applied to the EAR foam earplug shear case. The solution over the entire frequency range (32 to 10,000 Hz) for the feasible chosen roots can be seen in Figure 5.9.

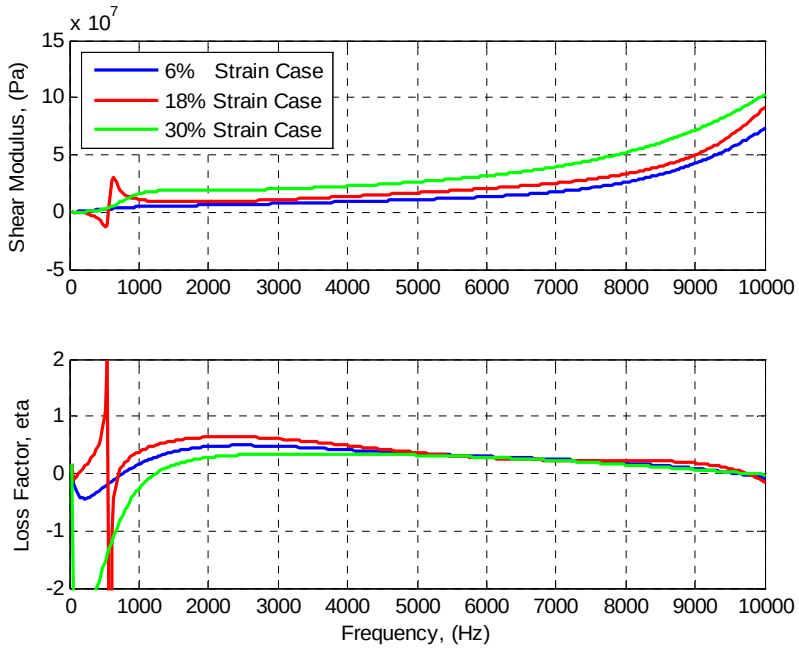

Figure 5.9 Entire frequency range solution for all three shear preload cases.

Since there are three different preload cases, the 18% strain case is considered the median, and all frequency range adjustments are based on this test. The 6% case would have a slightly lower set of frequency limits, and the 30% strain case a slightly higher range. The small variation at low and high limits caused by using the median strain case does not significantly affect the results, and makes comparison of these results much easier to view and understand. The criteria proposed in Eq. 5.4 are applied to the median 18% strain case, which results in an overall usable frequency range of 650 to 7,180 Hz. Notice the discontinuities and negative values at the lower frequency limit, until about 1,000 Hz. Also, the data is increasing from negative loss factor values at lower frequencies. This trend is suspicious, and the data below 2,000 Hz is therefore neglected. The same new lower limit as proposed in Eq. 5.13 is applied which yields a new frequency range of 2,000 Hz to 7,000 Hz, the higher limit obtained by adhering strictly to Eq. 5.4. This allows for positive-valued loss factors, despite the fact that the storage moduli are constant throughout the negative-valued loss factors. Note that all loss factors approach the same value at about 5,200 Hz. This phenomenon is currently unexplainable. The finalized plot with applied frequency limits is shown in Figure 5.10.

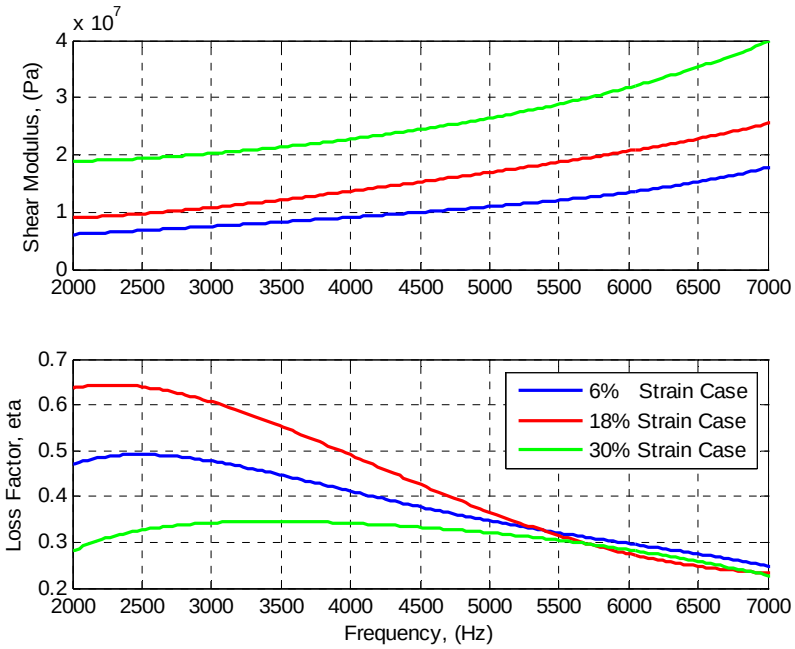

Figure 5.10 Extracted shear results with the final adjusted frequency range.

The new lower frequency limit, described in Eq. 5.13, enables feasible results for both the axial and shear cases. Since the original bounds were constructed from similar empirical methods, it can be said that for the EAR foam material in the shear and axial cases, the final form of determining the upper and lower limits is

$$f\ \min = 0.5\, f_{n2} \qquad\qquad f\ \max = 10^{[(\log f_{n2} + \log f_{n3})/2]} \tag{5.14}$$

where all variables are previously defined. It is suggested that the original limits (from Eq. 5.4) be used as guidelines upon every new material analysis, but altering them to suit the results of that system are necessary.

5.7 Interpolation method

The method chosen to interpolate material properties from any given frequency and preload (within test bounds) is a finite element method interpolation. Two nine-node quadratic elements are used, two elements are used over the frequency range to fully capture the response of the extracted data. Quadratic elements are used because the shear elastic moduli and loss factors for each preload show a quadratic trend as a function of frequency and preload. A picture of the element can be seen in Figure 5.11.

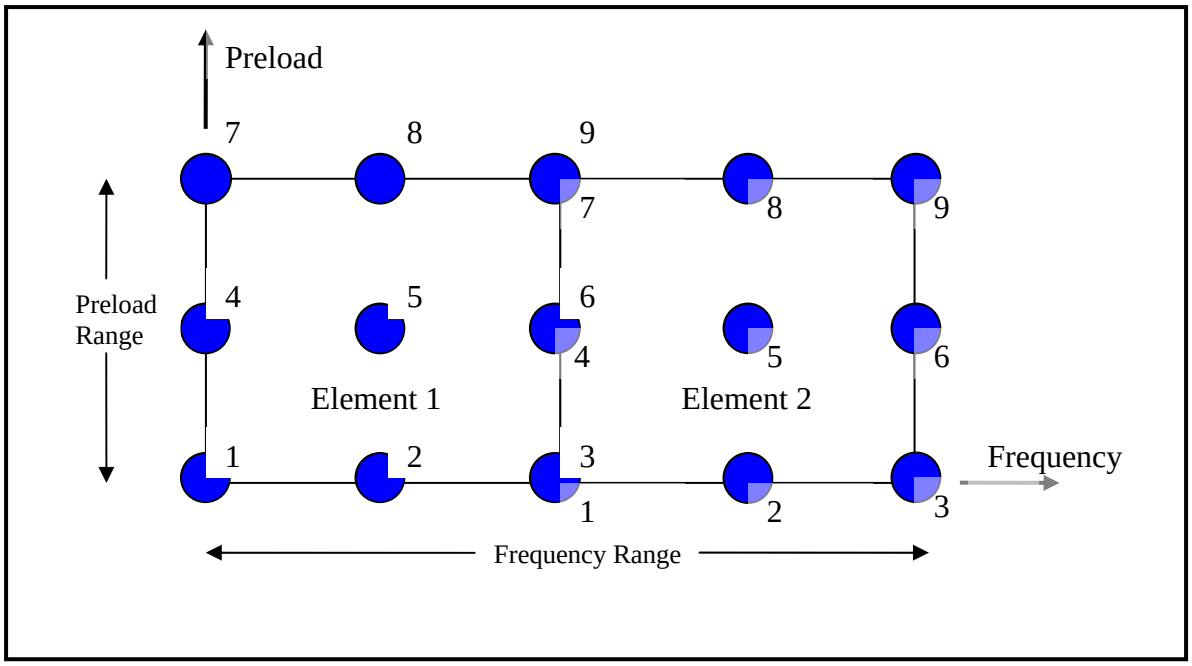

Figure 5.11 Quadratic elements with labeled nodes and axis.

To interpolate from any given preload range, the quadratic element interpolation functions are applied for each node. The interpolation functions are listed in Figure 5.12. Also, the values of storage moduli and loss factors are needed for each preload value and frequency value for each node, which are listed in Table 5.1.

$$\psi_1 = \left(1 - \frac{2f_i}{f_R}\right)\left(1 - \frac{f_i}{f_R}\right)\left(1 - \frac{2P_i}{P_R}\right)\left(1 - \frac{P_i}{P_R}\right)$$

$$\psi_2 = \frac{4f_i}{f_R}\left(1 - \frac{f_i}{f_R}\right)\left(1 - \frac{2P_i}{P_R}\right)\left(1 - \frac{P_i}{P_R}\right)$$

$$\psi_3 = \frac{f_i}{f_R}\left(\frac{2f_i}{f_R} - 1\right)\left(1 - \frac{2P_i}{P_R}\right)\left(1 - \frac{P_i}{P_R}\right)$$

$$\psi_4 = \left(1 - \frac{2f_i}{f_R}\right)\left(1 - \frac{f_i}{f_R}\right)\frac{4P_i}{P_R}\left(1 - \frac{P_i}{P_R}\right)$$

$$\psi_5 = \frac{4f_i}{f_R}\left(1 - \frac{f_i}{f_R}\right)\frac{4P_i}{P_R}\left(1 - \frac{P_i}{P_R}\right)$$

$$\psi_6 = \frac{f_i}{f_R}\left(\frac{2f_i}{f_R} - 1\right)\frac{4P_i}{P_R}\left(1 - \frac{P_i}{P_R}\right)$$

$$\psi_7 = \left(1 - \frac{2f_i}{f_R}\right)\left(1 - \frac{f_i}{f_R}\right)\frac{P_i}{P_R}\left(\frac{2P_i}{P_R} - 1\right)$$

$$\psi_8 = \frac{4f_i}{f_R}\left(1 - \frac{f_i}{f_R}\right)\frac{P_i}{P_R}\left(\frac{2P_i}{P_R} - 1\right)$$

$$\psi_9 = \frac{f_i}{f_R}\left(\frac{2f_i}{f_R} - 1\right)\frac{P_i}{P_R}\left(\frac{2P_i}{P_R} - 1\right)$$

Figure 5.12 Quadratic element nodal interpolation functions.

where f_R is the frequency range of the extracted results (2,000 to 7,000 Hz), P_r is the preload range of the extracted results (6% to 30% radial strain), f_i is the frequency value of interest and P_i is the preload value of interest.

Table 5.1 Nodal values of elastic moduli and loss factor.

Element 1 (2000-4500 Hz)			Element 2 (4500-7000Hz)		
Node Number	Elastic Modulus (Mpa)	Loss Factor	Node Number	Elastic Modulus (Mpa)	Loss Factor
1	6.15	0.47	1	10	0.38
2	10	0.38	2	12.7	0.31
3	17.6	0.25	3	17.6	0.25
4	9	0.34	4	15.3	0.42
5	15.3	0.42	5	19.7	0.29
6	25.3	0.23	6	25.3	0.23
7	18.9	0.28	7	24.5	0.33
8	24.5	0.33	8	30.3	0.29
9	39.5	0.23	9	39.5	0.23

To interpolate the results the following method is used

$$E(P_i, f_i) = E_1\psi_1 + E_2\psi_2 + E_3\psi_3 + E_4\psi_4 + E_5\psi_5 + E_6\psi_6 + E_7\psi_7 + E_8\psi_8 + E_9\psi_9 \tag{5.15}$$

$$\eta(P_i, f_i) = \eta_1\psi_1 + \eta_2\psi_2 + \eta_3\psi_3 + \eta_4\psi_4 + \eta_5\psi_5 + \eta_6\psi_6 + \eta_7\psi_7 + \eta_8\psi_8 + \eta_9\psi_9 \tag{5.16}$$

where E_n and η_n are the known elastic modulus and loss factor at the respective nodes. This method allows for any value to be interpolated by weighting the value at the unknown point with the nodal values and interpolation functions. Since the material properties as a function of preload are usually required over the entire frequency range and not just at specific spectral lines, the unknown frequency values are taken as a frequency vector (2,000 to 7,000 Hz) and the preload is taken as a constant at the preload of interest. The reader is referred to Reddy [22] for further information on finite element formulations.

To verify these results, the algorithm is run over the entire frequency range, with the preload amount taken at each experimental preload state (6%, 18% and 30% radial strain). The results are plotted on the previously extracted results to observe any discrepancies in the interpolation algorithm. This is displayed in Figure 5.13.

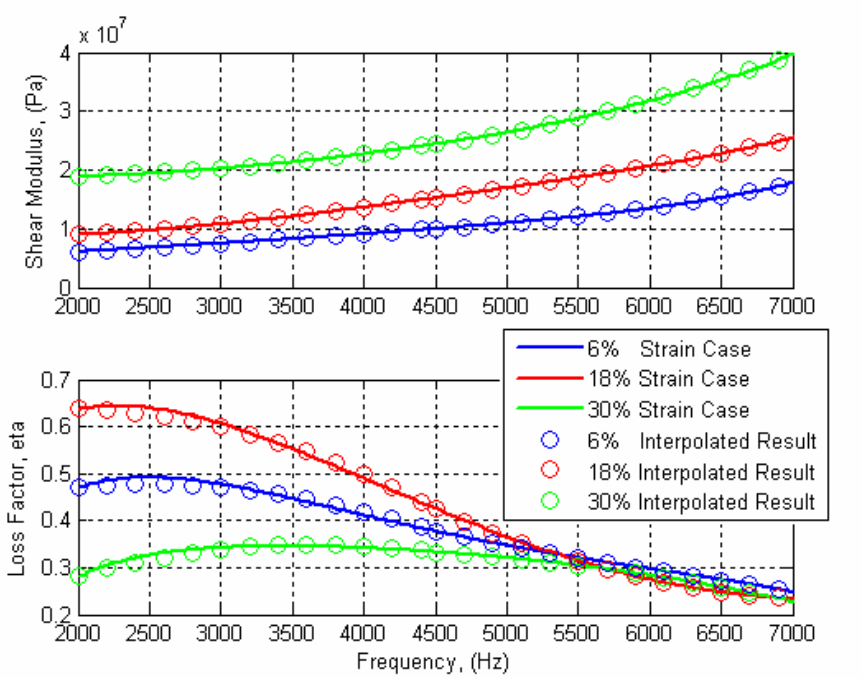

Figure 5.13 Comparing experimental extraction results with the interpolated results.

Figure 5.13 shows that the error in interpolation values for the elastic moduli is very small. The most error occurs in the loss factor at lower frequencies. This is because the quadratic function cannot handle the curvature present in this region with a single element. Two or more interpolation elements are used over the frequency range to accurately model this region which allows for greater fidelity in the interpolation model. More elements could be added to reduce the error between experimental and extracted results.

Care must be taken in processing the results. Since the interpolation function involve the terms f_R and P_R which are the ranges of the frequency and preload values, they involve offset values starting at zero. The lower limit of the frequency and preload range used to create the interpolation function must be subtracted off of the value of inquiry to obtain correct results. This is explained in the following equation

$$Value_{entered} = Value_{inqury} - Limit_{lower} \tag{5.17}$$

Where the value entered into the interpolation function is the value of interest minus the lower limit value. For example, if the lower frequency limit used to calibrate the interpolate function is 2,000 Hz, and the interpolated values at 3,000 Hz is needed, the

frequency value input into the interpolation function is 1,000 Hz. Not adjusting for this offset will result in extrapolating outside the valid frequency range and obtaining erroneous results.

5.8 Conclusion

Storage and loss moduli have been extracted for both the axial and shear experimental cases. The valid frequency ranges have been determined empirically for both cases and applied. Since material properties for any preload, within the test range, is required, an interpolation method was applied to the extracted storage moduli and loss factor results. Since the loss factor for each strain case brackets the original 6% strain value, an in depth look at this nonlinearity is necessary. The effects of increasing preload on the response of the shear case need attention, and are joined by the interpolation method discussion in the following section.

Chapter 6

Results and analysis

The effect of radial preload on the shear experimental case is analyzed, providing insight into both the extracted material properties which helps better understand the response of the updated ABAQUS DHP results. The resulting material properties are discussed with insight provided into their behavior. Finally, the results are placed into the updated ABAQUS DHP model and the result is compared to the previous model with axial material properties, and the changes in model results will be addressed.

6.1 Shear preload analysis

To understand the effects of preload on the shear system, several studies will be conducted. The experimental data will be looked into first, with a comparison of the resonant frequencies seen as a function of the radial strain. This will help understand the general response of the EAR foam earplug due to preload. The resulting material properties for each preload will be studied and compared to the base case (6% radial strain). This will determine the change in material properties with increase in preload. The entire system will be analyzed and discussed qualitatively by utilizing a three dimensional plot of the response space. Finally, the amount of confidence in these results is discussed.

Resonance analysis

The resonances are analyzed with respect to each radial strain value. The resonance of 3,510 Hz, 4,300 Hz and 5,050 Hz for the 6%, 18% and 30% radial strain cases, respectively. The plot of these values is shown in Figure 6.1.

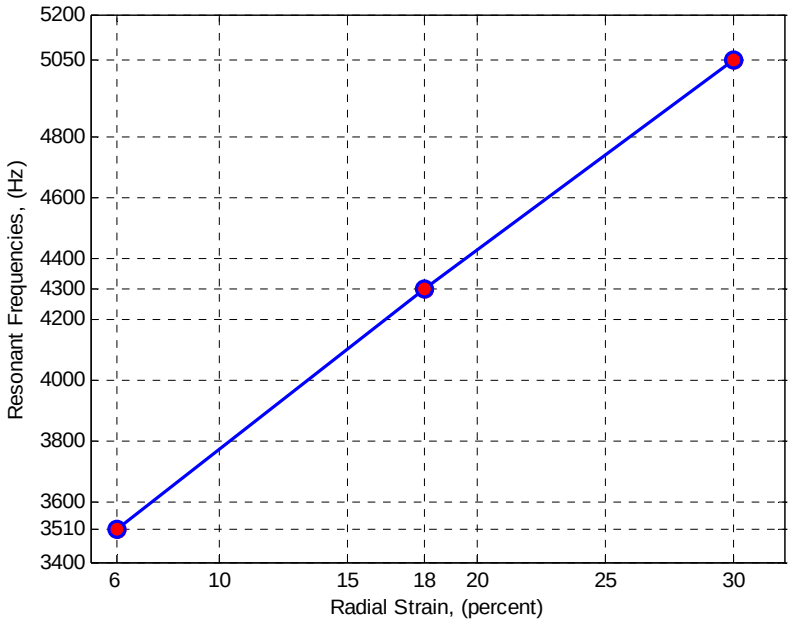

Figure 6.1 Resonance frequencies for each radial strain case.

The plot shows that the relationship of the resonances to the radial strain is nearly linear. Intuition would suggest that the material properties are also linear as a function of radial strain, but the nonlinear nature of the analytical effective mass equation (Eq. 4.2) results in a nonlinear response. An analysis of the material properties is now considered.

Analyzing shear results – design space

A closer look at the shear case extracted material properties is taken. Three dimensional plots are constructed and displayed to better represent the results and examine the shear material properties closer. The storage moduli as a function of preload and frequency are plotted in Figure 6.2, while the loss factors as a function of preload and frequency are displayed in Figure 6.3. Notice the largest value of the loss factor in Figure 6.3 is present in the 18% radial strain case. It is unknown why the loss factor for the 18% case is higher than the 6% and 30% cases. It is speculated that this high loss factor it is due to the compression characteristics of the foam material. The 18% radial strain could simply be near the point of highest damping due to compression for the shear configuration. It is possible the highest damping is experienced in this radial strain region, and further compression buckles the cell walls in the foam and presents a more

rigid, less damped material. Detailed experiments tailored to exploring the material damping are needed to verify or disprove this idea. This thesis will not investigate the damping effect any further.

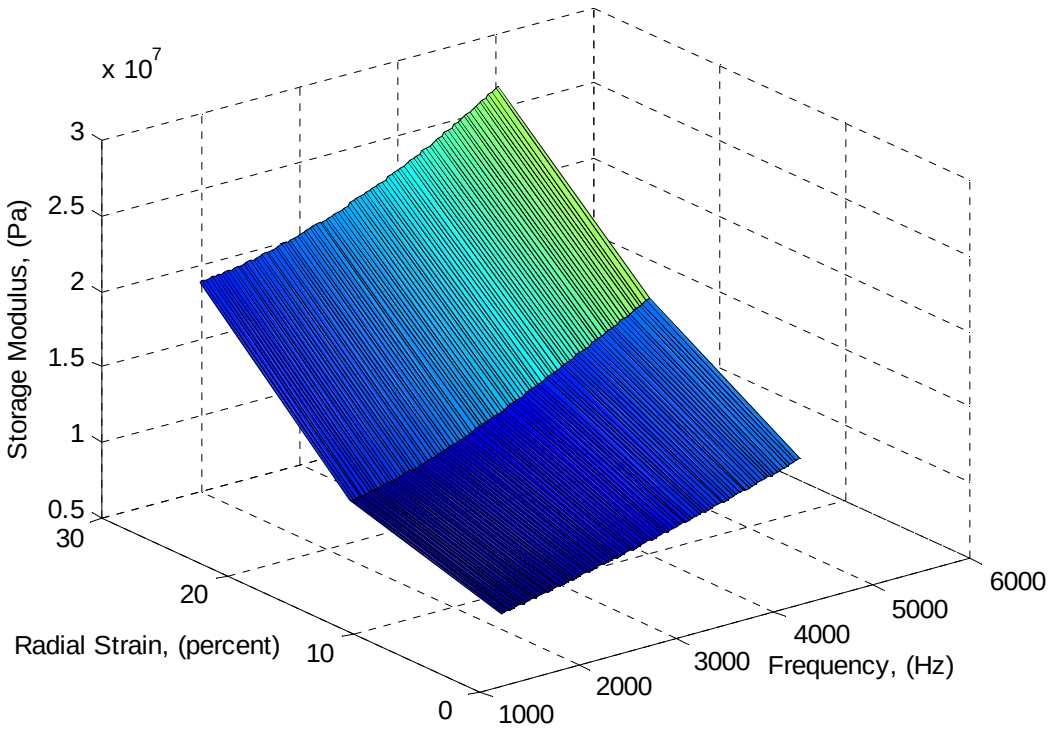

Figure 6.2 Storage moduli for each preload over the valid frequency range.

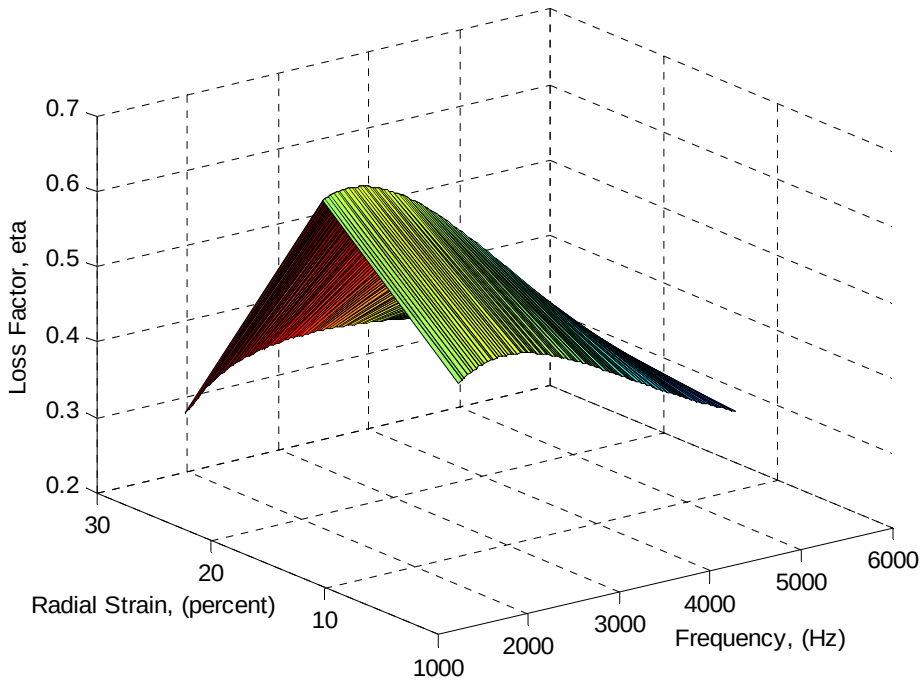

Figure 6.3 Loss factors for each preload over the valid frequency range.

Analyzing shear results - normalization

To better understand the effects of preload on the system response, the resulting extracted material properties are studied as a function of radial strain. The 6% radial strain case (1/2" ID sleeve) is taken to be the reference case for the comparison. The other two compressed cases will be normalized to the 6% radial strain case to determine their change with applied preload. A normalized plot of the elastic moduli and loss factors can be seen in Figure 6.4.

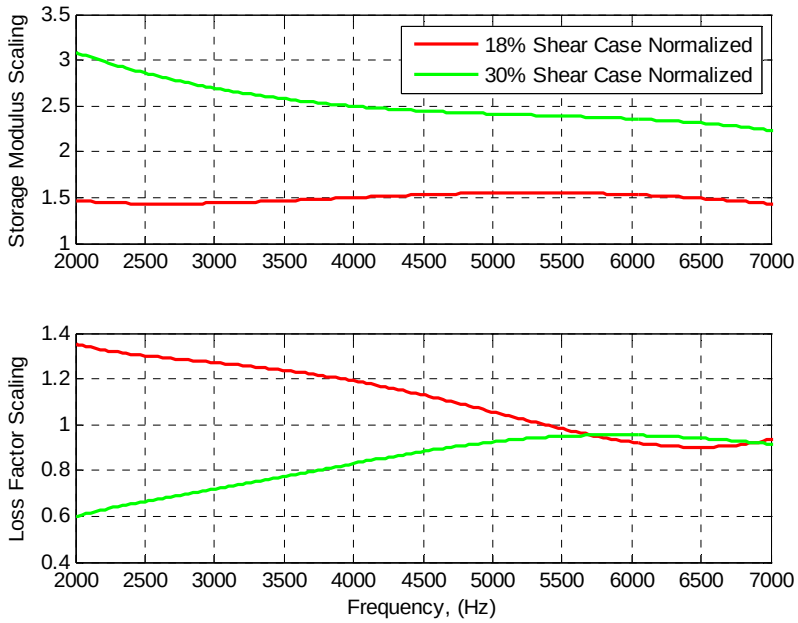

Figure 6.4 6% and 18% shear cases normalized to the 6% shear case.

The shear moduli follow an intuitive trend. The 18% strain case is on average 1.5 times higher than the base 6% strain case. The 30% strain case is about 2.5 times higher than the base 6% case on average. The loss factor does not follow expected trends. The 18% case starts at 1.3 times higher than the base 6% strain case and approaches the 6% strain case value around 5,500 Hz.. The 30% case is about 0.6 times lower than the 6% strain case, but approaches unity around 5,500 Hz as well. This suggests that damping for all cases may approach the same limit at higher frequencies.

Transformed axial results versus shear results – boundary condition check

The results from the axial case will be modified to see if they can adequately represent the shear configuration. If this is possible, it would suggest that boundary conditions do not play a large role in the material properties of the shear case, and the old axial-based material properties adequately describe the system. The axial case elastic modulus is transformed to the shear modulus by the constitutive equation

$$G = \frac{E}{2(1+\nu)} \tag{6.1}$$

This transformation is applied to the previously extracted axial case results and plotted with the 6% radial strain shear case results in Figure 6.5.

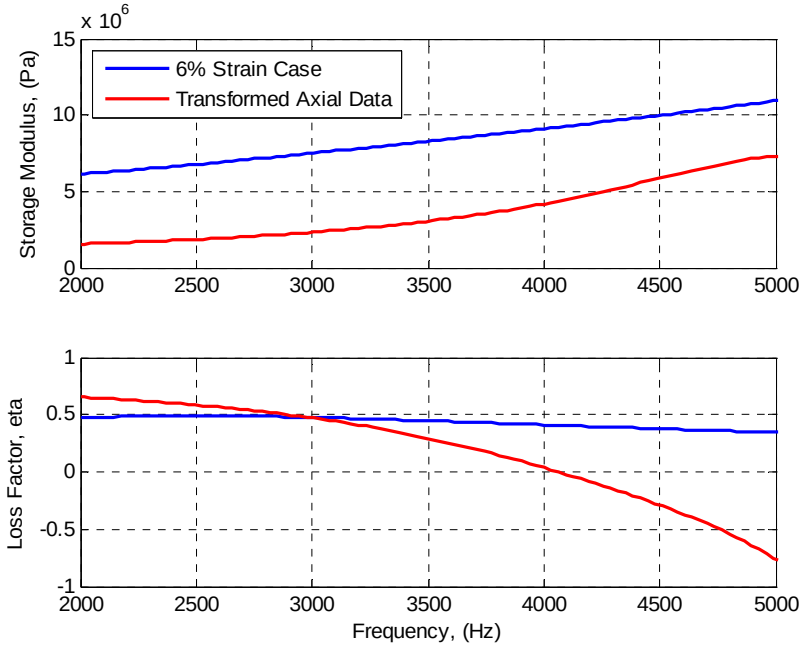

Figure 6.5 Comparing the transformed axial data to the 6% strain shear case.

The transformation of the axial elastic modulus to a shear modulus does not adequately mirror the extracted shear modulus. The shear case is on average 3 times higher than the transformed axial case. This offset is nonlinear, and decreases with the increase in frequency. The loss factor is nearly constant for the extracted shear results, but approaches zero in the transformed axial results. It should be noted that the range frequency range being compared is the valid range for the extracted shear results, but above the usable range in the transformed axial results. Therefore this comparison is for qualitative purposes only. An idea of the axial transformation results usefulness can be obtained, but no direct conclusions can be drawn.

Confidence in extracted properties

The extracted shear material properties were qualitatively compared to transformed axial results, and the axial extracted results were compared to the previous DMA axial data in Chapter 5. All data was shown to be within reasonable range of each other (up to three times apart), although not similar enough to definitively state that the

results are verified. As stated in the previous section, the axial-extracted results cannot be scaled to shear results using simple constitutive equations. The boundary conditions, loading methods and specimen scaling have profound effects on the system response, which are not reflected in the simple constitutive equations. Therefore, confidence is established in the extracted results through verification of the extraction process and through satisfactory comparisons with the other data methods. The extraction method was verified using previous data and results from Sun and Mitchell [16]. The extracted shear results are of the same order of magnitude as transformed axial data, and more confidence in results can only be established by executing other experimental methods that place the specimen in similar boundary, loading and geometrical conditions.

6.2 Updated ABAQUS DHP model analysis

The final step in this research is to utilize the newly obtained shear case extracted material properties into the ABAQUS DHP model and analyze the noise reduction changes from the model with old axial DMA material properties. It was realized that the original ABAQUS DHP model was developed using a compressed EAR foam earplug with a length of 10mm, rather than the full EAR earplug length of 19mm. The length was adjusted to 10mm in the ABAQUS DHP model because the experimental DHP setup utilized a full length EAR foam earplug, inserted into the acrylic ear canal cylinder a depth of 10mm. The 9mm of EAR foam earplug hanging out of the acrylic ear canal was considered negligible and not included in the ABAQUS model to allow for easier modeling and meshing. Another experimental and material extraction process is completed for a 10mm long EAR foam specimen, compressed into the 3/8” sleeve (30% radial strain). The largest strain case is used because it most closely resembles the compressed earplug in the experiment, which is around 35% radial strain. The process is briefly outlined with experimental response and extraction results.

The old axial DMA material properties are converted to shear material properties and compared with the newly extracted shear material properties, to determine the difference in the old and updated EAR foam material properties. The updated EAR foam material properties are then inserted into the ABAQUS DHP model, and the difference in

results from previous ABAQUS DHP and experimental DHP models are thoroughly discussed.

6.2.1 10mm EAR foam earplug

Experimental process

The same experimental process is followed for the 10mm long EAR foam earplug that was used for the standard 19mm earplug. The earplug is only analyzed in the 30% radial strain condition; this closest resembles the 35% radial strain seen in the experimental DHP setup. Because of the reduction in mass, the resonance of the 10mm EAR foam earplug is about 3,650 Hz, which is about 1.4 times less than the resonance frequency of the standard 19mm EAR foam earplug compressed to 30% radial strain. The effective-mass transfer function response is displayed in Figure 6.6.

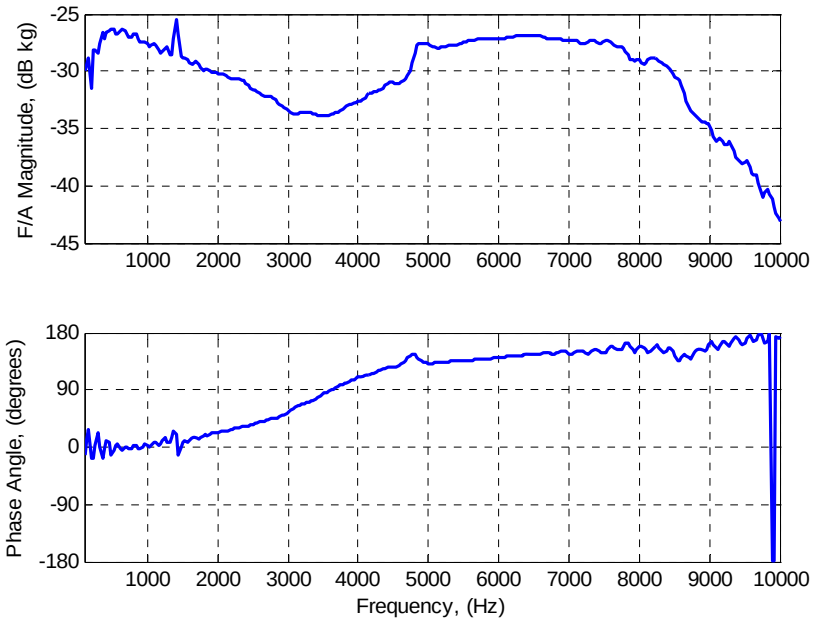

Figure 6.6 Effective-mass transfer function response of the 10mm long EAR foam earplug.

The coherence of the effective-mass transfer function signal is displayed in Figure 6.7. As can be seen, the coherence is much lower than the previous 19mm shear preloaded experiments, with an average value of 0.7. This low value indicates poor signal

strength in the experimental results, which is most likely due to the small specimen height. Caution and exploration are suggested for any future measurements on materials of this smaller mass and size.

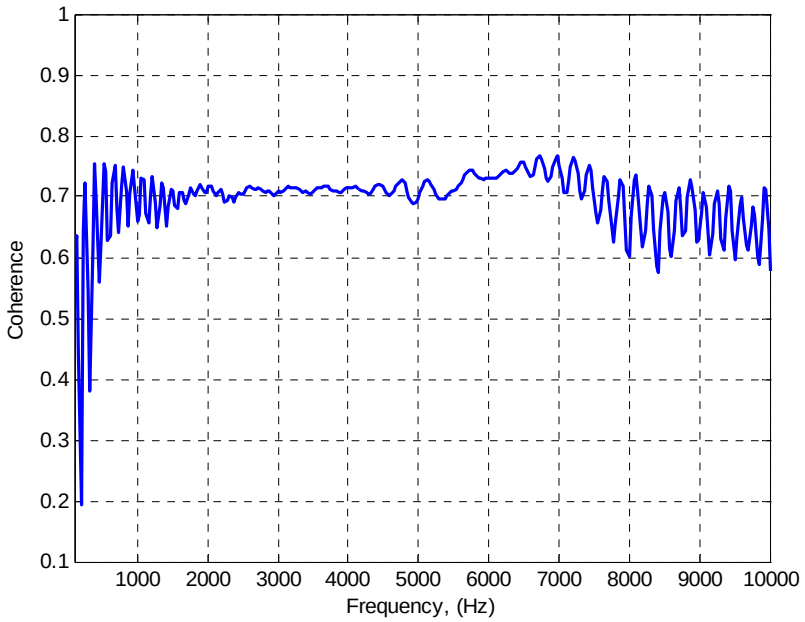

Figure 6.7 Coherence of the 10mm EAR foam material transfer function.

Material property extraction

Material property data is extracted in the same manner as the standard shear earplugs, with the 10mm length adjustment in the extraction code. The shear storage moduli and loss factors over the same usable frequency range (2,000 – 7,000 Hz) are obtained without any other modifications to the code. The extracted properties are plotted in Figure 6.8.

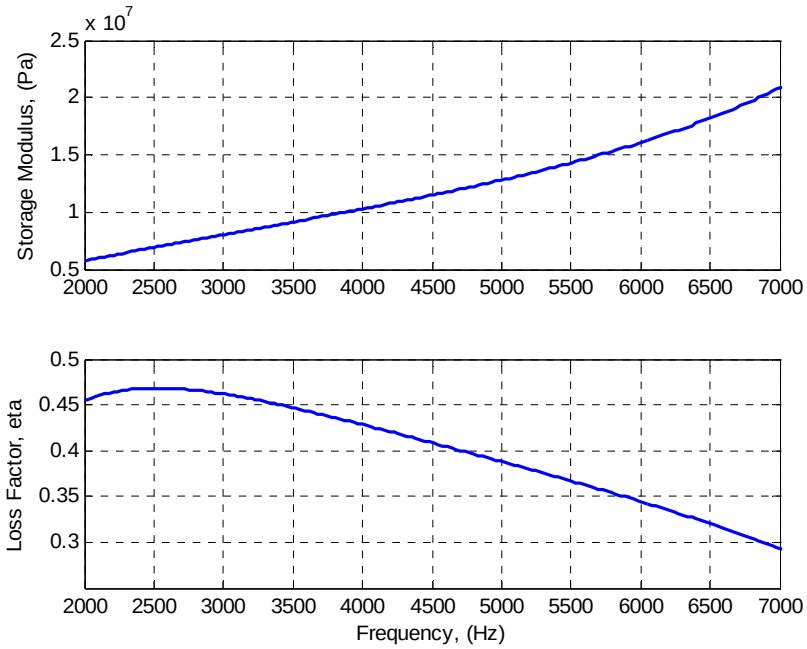

Figure 6.8 Extracted material properties for the 10mm EAR foam earplug.

Comparing old DMA shear and updated ABAQUS DHP EAR foam properties

To see the difference in the old DMA transformed shear material properties and the extracted 10mm shear material properties, a comparison is conducted. The old DMA axial elastic moduli are transformed to shear moduli by using Eq. 6.1. The results are compared in Figure 6.9. The transformed DMA shear moduli are nearly constant over the frequency range of interest, with a value of 2 MPa, while the extracted 10mm shear moduli start at 5 MPa and increase nearly linearly to about 20 MPa. This is ten times higher at the end of the frequency spectrum. The loss factor is also significantly different. The DMA transformed shear loss factors stay nearly constant at a value of about 0.12, while the extracted 10mm shear loss factors start at about 0.45 and decrease to 0.3 at 7,000 Hz. This significant difference in both shear moduli and loss factors between old transformed DMA shear and updated extracted 10mm shear should warrant a significant difference in results from the ABAQUS DHP model.

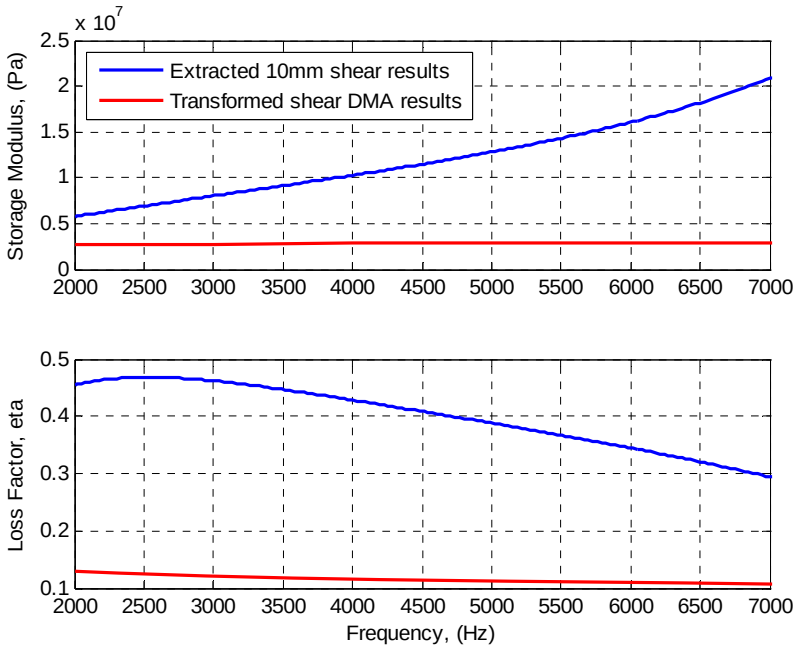

Figure 6.9 Comparing extracted and transformed DMA shear results.

Preparing material properties for ABAQUS insertion

In order to input the extracted material properties into ABAQUS, they must be transformed to fit the required formulation. ABAQUS requires the data be tabulated and entered with the following parameters per frequency:

$$\text{Omega G real}: \frac{G_{imag}}{G_{\infty}} \tag{6.2}$$

$$\text{Omega G imaginary}: 1-\frac{G_{real}}{G_{\infty}} \tag{6.3}$$

$$\text{Omega K real}: \frac{K_{imag}}{K_{\infty}} \tag{6.4}$$

$$\text{Omega K imaginary}: 1-\frac{K_{real}}{K_{\infty}} \tag{6.5}$$

where G_{imag} and G_{real} are the imaginary and real components of the shear modulus, respectively and K_{imag} and K_{real} are the imaginary and real components of the bulk modulus, respectively. G_{∞} and K_{∞} are the long-term relaxation shear and bulk moduli, respectively. The reader is referred to the ABAQUS theory manual for further

information [23]. Normally, these values are obtained by running relaxation tests in a configuration consistent with the dynamic, frequency dependent experiments. Unfortunately, no such test structure was available for use in this research, therefore the long-term moduli were taken from extrapolating the extracted shear material properties down to low frequencies. This method allows for an estimate of the long-term moduli so the above parameters can be input into ABAQUS. The bulk modulus is related to the shear modulus by the form

$$K = G\frac{2(1+\nu)}{3(1-2\nu)} \tag{6.6}$$

where G and ν are the shear modulus and Poisson's ratio, respectively.

A long-term, constant elastic modulus is entered into ABAQUS and used to scale the normalized values in Eq. 6.2 through Eq. 6.5. ABAQUS determines the appropriate long-term shear and bulk moduli from the relations in Eq. 6.1 and Eq. 6.6. Unfortunately, the entered parameters were normalized by an extrapolated value for the long-term shear and bulk moduli, therefore the correct long-term elastic modulus is unknown. To determine this unknown value, and to calibrate the finite element model for the new material properties, a three dimensional model is constructed of the EAR foam earplug. The vibration excitation is applied through boundary conditions on the outside surface of the earplug. A cylindrical object is added to the top of the earplug to simulate the accelerometer, and the resulting transfer function of the output acceleration of the top mass over the input displacement is observed. The long-term elastic modulus is adjusted until the resonance (phase shift of -90^{o}) is observed to be the same as the experimental value. The long-term modulus of the 10mm EAR foam specimen was found to be 100,000 Pa, using the same Poisson's ration of 0.1. The elastic modulus used in the previous transformed shear DMA material properties was 25,000 Pa, about 4 times softer than the updated extracted properties. This is expected, because the updated extracted results have taken into account the appropriate shear configuration, which would make the EAR foam earplug system look much stiffer than the less constrained previous axial case. The effective density was also adjusted to allow for the same mass present in the smaller model dimensions. A complete matrix of the elastic moduli and effective density for each case is included in Table 6.1, and viscoelastic properties for all tested specimens

are displayed in Appendix D. Once this information was obtained, the model was correctly validated to be input into the complete ABAQUS DHP model. The 10mm EAR foam ABAQUS model with applied load conditions is displayed in Figure 6.10.

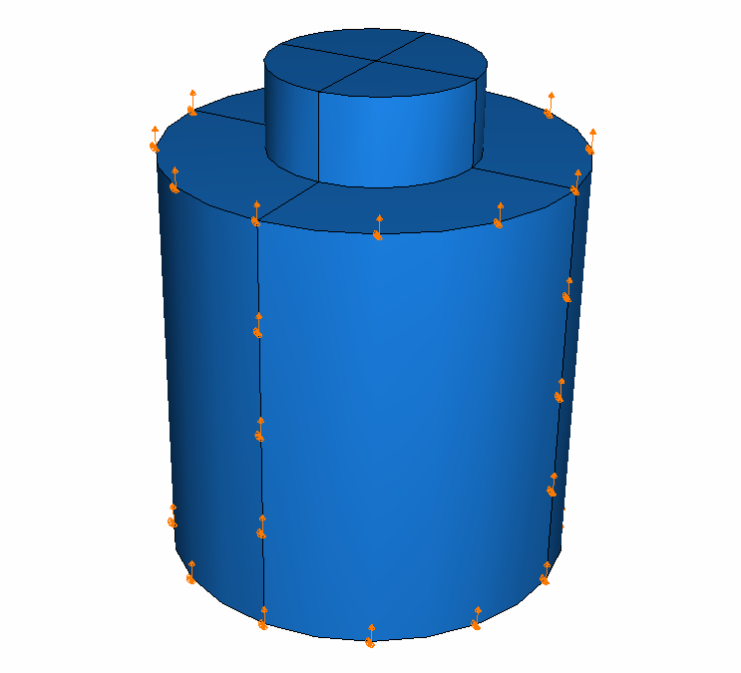

Figure 6.10 EAR foam ABAQUS model utilized to calibrate the extracted material properties with the finite element model.

Table 6.1 Final elastic moduli and effective density from the EAR foam ABAQUS calibration model.

	6% radial strain (19mm)	18% radial strain (19 mm)	30% radial strain (19 mm)	30% radial strain (10 mm)
Elastic Modulus	400 kPa	420 kPa	450 kPa	100 kPa
Effective Density (kg/m^3)	112	146	220	220

6.2.2 Updated ABAQUS DHP model results

Comparing with previous ABAQUS DHP

The extracted 10mm shear material properties are entered into the existing ABAQUS DHP model, and the result is referred to as the updated ABAQUS DHP model.

As discussed in Chapter 3, the resulting pressure frequency response function is taken at the bottom of the ear canal relative to the monopole source at the top of the hemisphere domain. The updated ABAQUS DHP model results will first be compared to the previous ABAQUS DHP model results, which utilized the DMA transformed shear material properties. The proceeding analysis is mostly qualitative, but numerical error will be expressed when appropriate. The updated and previous ABAQUS DHP model results are displayed in Figure 6.11.

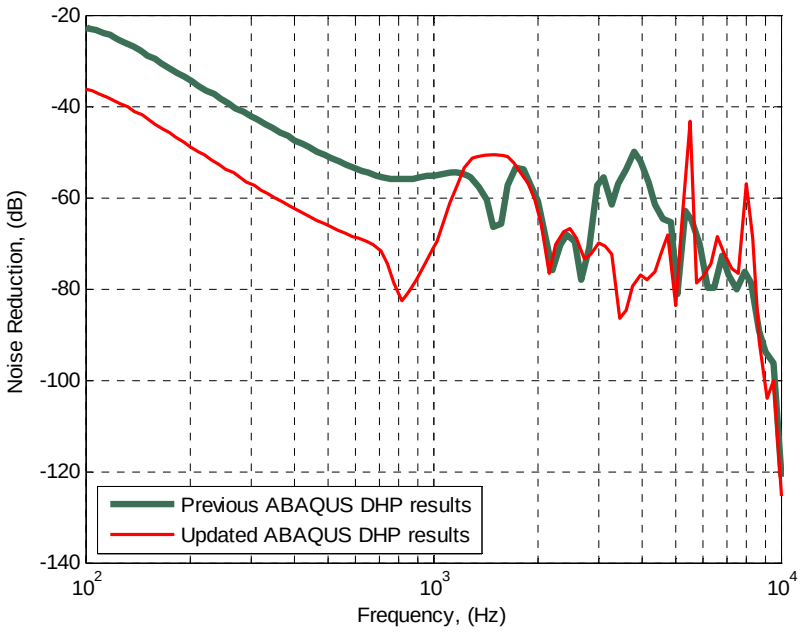

Figure 6.11 Comparing updated and previous ABAQUS DHP model results.

The updated ABAQUS DHP results are biased low by about 15 dB in the 100 to 700 Hz frequency range. This is attributed to the difference in elastic moduli entered into the respective models, as discussed in the previous chapter. The updated extracted elastic modulus is four times stiffer than the previous axial-based elastic modulus, therefore reducing the amount of energy that will be transferred through the earplug to the ear canal. This contributes to the increase in noise attenuation between the previous and updated model.

One large peak is seen at 1,485 Hz in the updated model results, overshadowing the two smaller peaks in the previous model results at 1,170 and 1,728 Hz by about 3 dB. Investigating the results of the updated ABAQUS DHP model through animations and

contour plots, it is discovered that the earcup flap mode is once again driving the system. The difference in responses is due to the respective earplug material properties and resulting vibration responses. The earplug is near a resonance and easily deformed in this frequency range, similar to the results from the previous ABAQUS DHP model. The earplug is being excited by a "pinching" motion driven by the flexlayer, visible in visualizations in the finite element postprocessor. Poisson's effect allows for deformation in the direction of the length of the ear canal, creating relatively large acoustic pressures. In summary, the resonance of the earplug contributes greatly to the pressure response experienced in the ear canal in this frequency region, much greater than seen before in the previous DHP model results. A graphic of the "pinched" earplug can be seen in Figure 6.12.

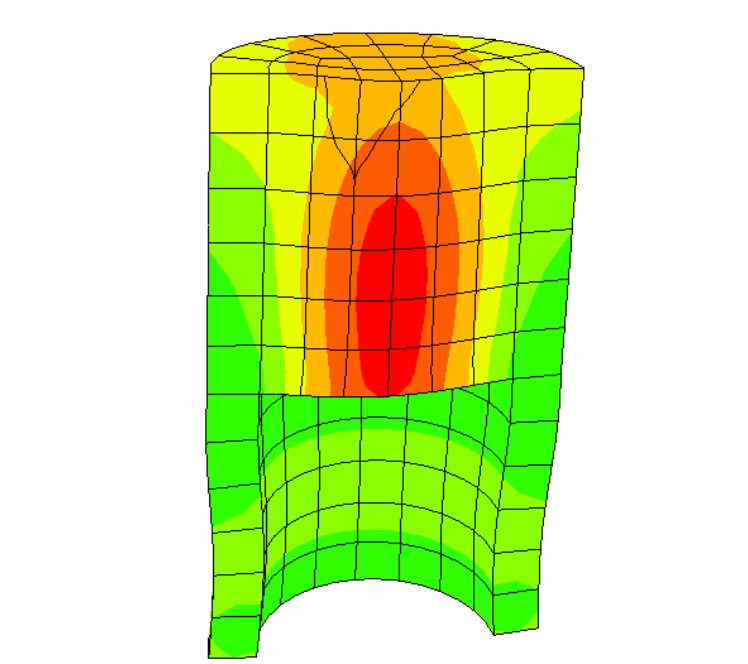

Figure 6.12 Displacement plot of the "pinched" earplug by the flexlayer.

Referring to Figure 6.11, notice the large difference in noise reduction in the 3,000-5,000 Hz frequency range where the updated DHP model exhibits a 15-25 dB increase in noise reduction performance. The major differences occur at the peaks of 3,100 and 3,700 Hz; the spectral lines corresponding to the resonance of the earcup. Because of this large difference in noise reduction performance in comparison with the rest of the *Elastic/Acoustic Earcup regime,* it is suspected the difference is in part due to

the response of the earplug assembly. If a resonance of the earplug assembly is occurring in this frequency range, it is possible that it acts as a tuned vibration absorber, reducing the amount of vibration transmitted to the bottom of the earplug material. To investigate this claim, the accelerance of the bottom and top surfaces of the earplug are taken and plotted in Figure 6.13.

The accelerance response at the bottom of the EAR foam earplug material is larger than the top of the earplug in the 1,000-2,000 Hz range, or in the *Earplug Resonance regime.* This is expected, because it has been suspected this region experiences a resonance in the earplug assembly. This topic is thoroughly explained in the upcoming sections. The accelerance response at the bottom of the earplug is less than at the top of the earplug in the 2,000-3,000 Hz range, although Figure 6.11 shows little difference in noise reduction between the previous and updated models. In the region where the major difference occurs (3,000-5,000 Hz), the accelerance at the bottom of the earplug is about 10 dB larger on average, with it being 7 dB lower at 3,000 Hz. No substantial conclusions can be drawn from this plot, or other observed data as to whether or not the earplug acts as a vibration absorber in the 3,000-5,000 Hz range. More investigation is needed to explore this theory.

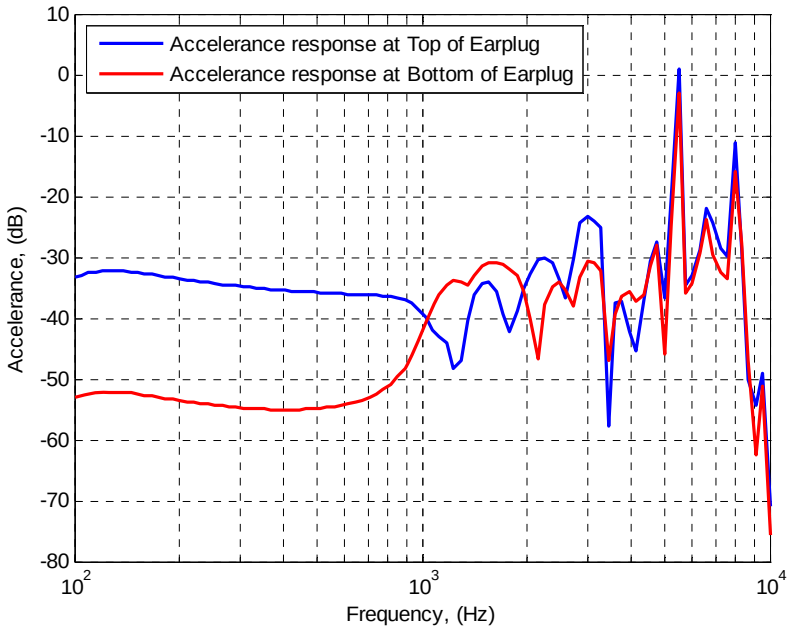

Figure 6.13 Comparing the accelerance of the top and bottom of the Ear foam earplug.

The few distinct, sharp peaks seen at 5,462 and 7,925 Hz are due to acoustic resonances in the interior air inside the earcup. These are not experienced in the previous ABAQUS DHP model due to the frequency resolution. These resonances are expected, because there is no damping of the fluid inside the acoustic interior of the earcup. These large pressure spikes exist for the previous model, it is just that the computational frequency steps did not occur close enough to one of these resonances for it to be seen. The results for the updated model occur on a frequency step near two of these resonances. A plot of the pressure distribution for each mode is displayed in Figure 6.14.

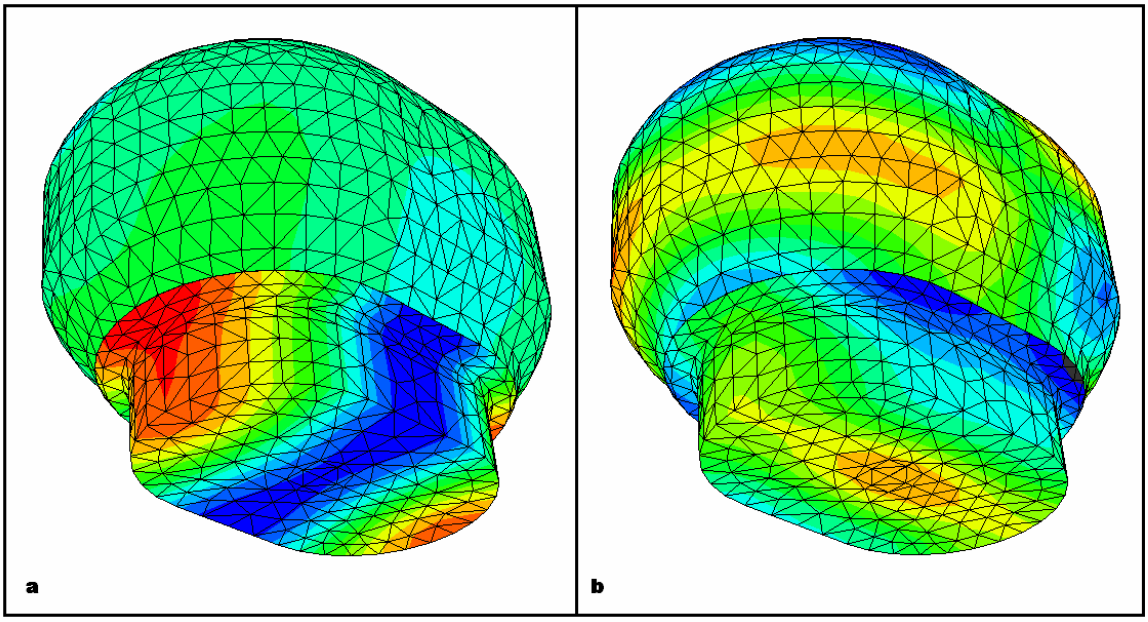

Figure 6.14 Acoustic cavity resonances at 5,462 Hz (a) and 7,925 Hz (b).

The noise reduction readings are once again taken at the bottom of the ear canal (noise reduction of earmuff and earplug assemblies) and at the bottom of the interior acoustic domain (noise reduction of earmuff assembly only) and compared. The comparison is seen in Figure 6.15 and plotted by the relation established in Eq. 3.1. The difference looks like more of an offset, with the only major discrepancy near the earplug resonances (about 1,500 Hz).

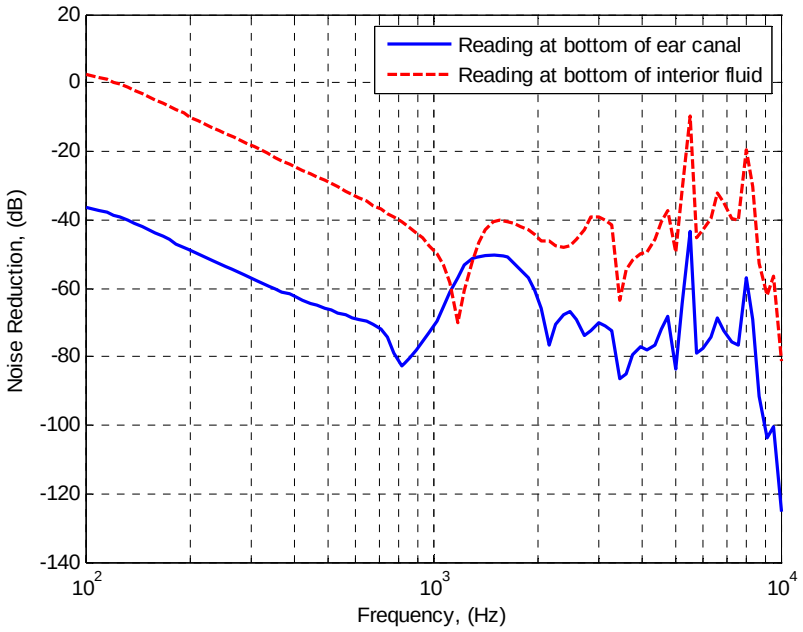

Figure 6.15 Comparing noise reductions at the bottom of the ear canal and at the bottom of the interior acoustic domain.

The difference in noise reduction levels at the bottom of the ear canal and at the top of the earplug is plotted in Figure 6.16, analogous to a transmission loss plot. The plot shows a low noise reduction difference around the earplug resonance where it is negative. It is negative valued because the earplug is actually amplifying the incident energy into the ear canal.

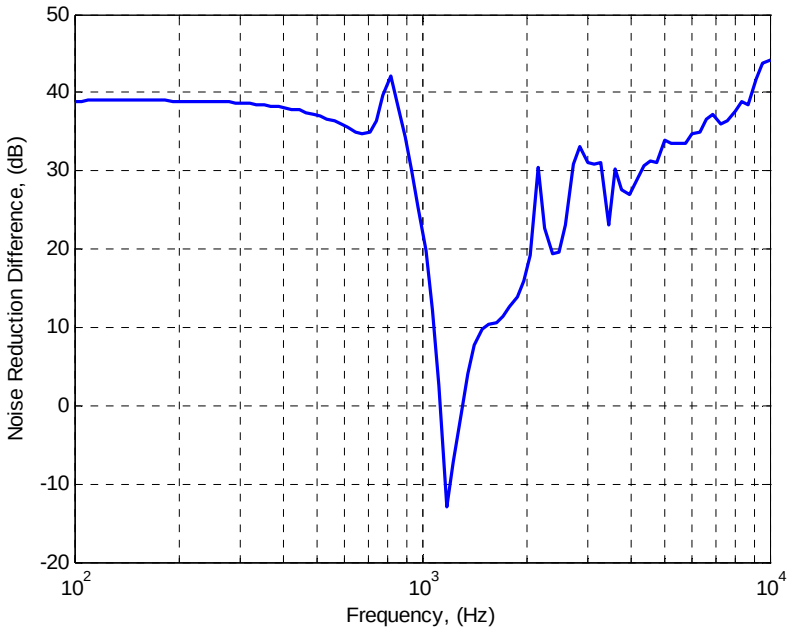

Figure 6.16 Difference in noise reduction; transmission loss of the EAR foam earplug in the updated ABAQUS DHP model.

This looks as though the performance of the updated ABAQUS DHP model is inferior to the previous ABAQUS DHP model, but a direct comparison in the transmission loss of both previous and updated results is needed to qualify the performance of each earplug. Both noise reduction difference plots are shown in Figure 6.17. The updated DHP model with updated shear EAR foam material properties outperforms the previous DHP model by about 10 dB in the low frequency range, which falls below the previous model results around 1,400 Hz (actually amplifies some acoustic energy) and then maintains better noise reduction difference through most of the upper frequency range. In comparing the updated versus previous ABAQUS DHP model results, the updated material property model outperforms the previous model, and exhibits a larger peak due to earplug resonance around 1,400 Hz.

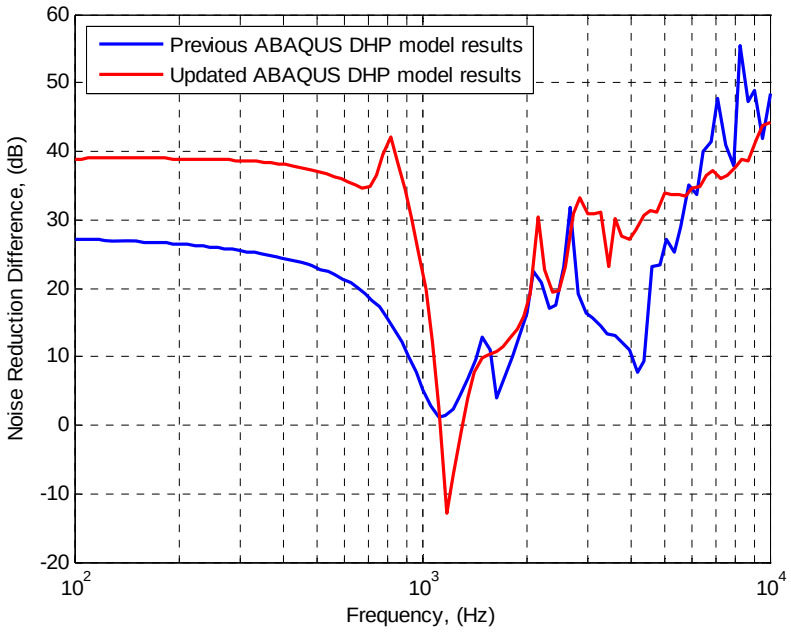

Figure 6.17 Comparing noise reduction difference for both ABAQUS DHP models, previous and updated.

Comparing with experimental DHP results

Next, the updated ABAQUS DHP model results will be compared to the experimental DHP results, to see if any new insight in behavior mechanisms can be drawn with the improved EAR foam earplug material properties. The results of the updated ABAQUS DHP model are plotted in comparison to the experimental DHP results in Figure 6.18.

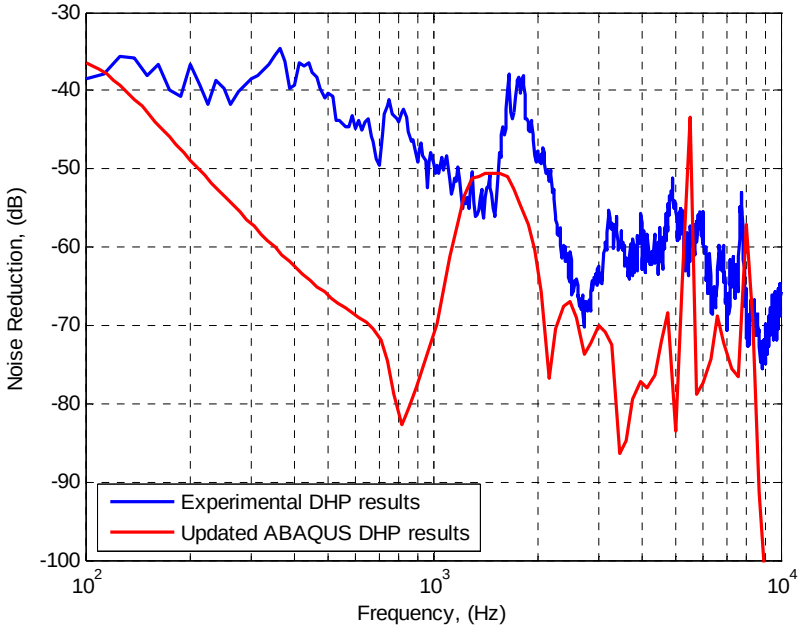

Figure 6.18 Comparing updated ABAQUS and experimental model DHP results.

The two results start off at about the same noise reduction rating, about -38 dB. There becomes significant error as the frequency increases, with the updated ABAQUS DHP model results biased low, and maximum magnitude difference of about 41 dB at 800 Hz. The difference in this frequency range is unknown, but it is suspected that the experimental data is lacking fidelity in this region. The updated model results seem to provide too much noise attenuation in this region. There are no resonance mechanisms in this frequency range in the updated ABAQUS model, although the experimental results experienced reduced noise reduction performance. The low frequency peaks in the experimental data could be due to unseen behavioral mechanisms not present in the finite element model. The piston mode is observed to be below 100 Hz, and the first known resonance afterwards is the earcup flap deformation/earplug resonance seen at 1,485 Hz. There are no identifiable mechanisms present in the finite element model between these two frequencies. Therefore, the peaks experienced in the experimental results could be due to vibration of the table structure, which is not modeled in the ABAQUS DHP models.

The most notable peaks in both the ABAQUS and experimental DHP models are located at 1,485 and 1,650 Hz, respectively. In the previous ABAQUS DHP model, this

large peak was not seen but rather two smaller peaks were in its place. As previously explained, the large peak is formed in the updated ABAQUS DHP model by the addition of resonance in the EAR foam earplug to these existing earcup modes. It is speculated that the large peaks in the updated and experimental DHP model results are the same behavior mechanisms, although it cannot be confirmed without further experimentation. Acceleration readings are needed on and around the earplug material to completely determine if the earplug resonance is affecting the noise attenuation performance. The resonant frequency of the 10mm EAR foam earplug in the shear configuration occurs at about 3,600 Hz which is significantly higher than seen in the model. However, the ABAQUS DHP models contain the Siliclone RTV material in contact with the installed earplug, changing the effective stiffness of the earplug assembly. A simple Siliclone RTV – EAR foam earplug model was created to evaluate this discrepancy.

6.2.3 Structural earplug assembly exploration

To explore the behavior of the earplug assembly, a simplified structural ABAQUS model is constructed. A circular flexlayer material is used, with a radius comparable to the footprint of the viscoelastic seal. The Siliclone RTV and EAR foam materials are recreated with the same geometry and material properties as the complete ABAQUS DHP model. Loading is applied by an outside surface of the flexlayer material, simulating input from the seal component. The bottom of the flexlayer material is completely constrained. The final result is a simulation of the earplug assembly, in geometry and boundary conditions. The resulting acceleration is read at the bottom of the earplug, determining the resonances of the complete system. The simplified structural model with applied boundary conditions and loads can be seen in Figure 6.19.

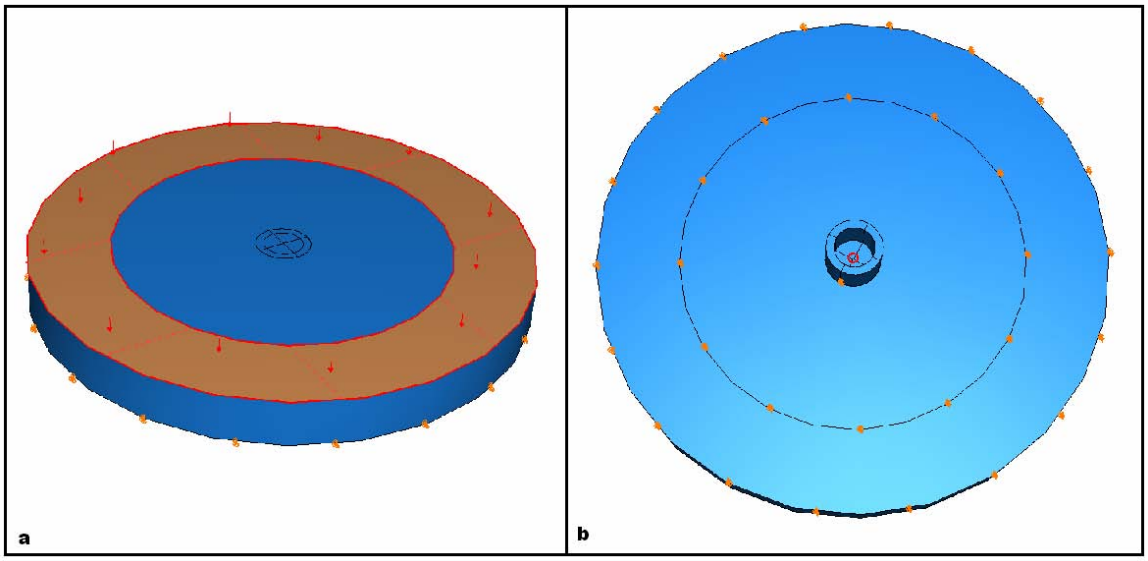

Figure 6.19 Model used to evaluate the EAR foam earplug/Siliclone RTV/Flexlayer response with top view and loading (a), and with circled acceleration response point and boundary conditions(b).

The accelerance of the system is taken from the acceleration at the bottom of the earplug and the input pressure. Since the chosen input pressure load was random, the magnitude of the accelerance response is meaningless, other than it shows the maximum of the response, which is a resonance of the earplug assembly. The result can be seen in Figure 6.20. The maximum accelerance, and therefore resonance, occurs at about 1,200 Hz. This is in the region of earplug excitation in the complete updated DHP model. This simple model shows the resonance of the earplug assembly, which is only 285 Hz lower in frequency than the large resonance peak experienced in the updated ABAQUS DHP model results. Since the resonance of the simple structural model is within 300 Hz of the suspected earplug regime resonance, it can be assumed that the major peak in the complete DHP model is in fact partially due to the earplug assembly resonance. The difference in resonant frequencies can be attributed to the simplified boundary and loading conditions present in the simplified structural model.

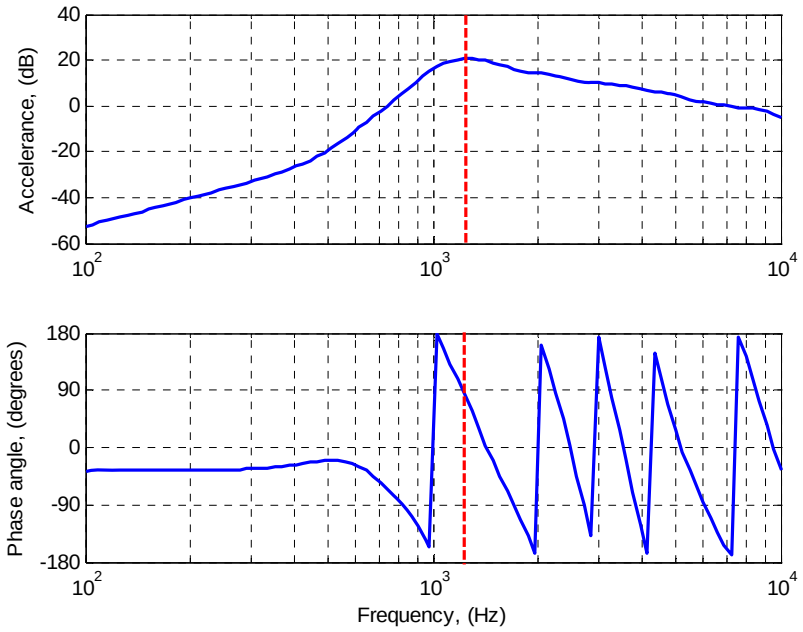

Figure 6.20 Accelerance response of the simple earcup assembly system, notice the largest resonance (marked in red) of the system.

6.3 Structural vibration of components

It has been shown, in Chapter 3, that the pressure in the bottom of the ear canal is mostly due to structural system vibration along with the energy path of the acoustic source energy to the earplug material. The updated model will now be used to explore the vibration response of the bottom of the EAR foam earplug to the response at several different points in the ABAQUS DHP model. This will allow us to determine the dominant energy paths in the updated ABAQUS DHP model. The acceleration in the vertical direction at the bottom of the earplug material is taken as the reference for all measurements, and is normalized to the vertical accelerations at the top of the earcup assembly (E_a), in the longitudinal seal direction of the flexlayer material ($F1_a$) and in the horizontal seal direction of the flexlayer ($F2_a$). Figure 6.21 shows the general locations of the readings. The decibel readings of each location can be seen in Figure 6.22.

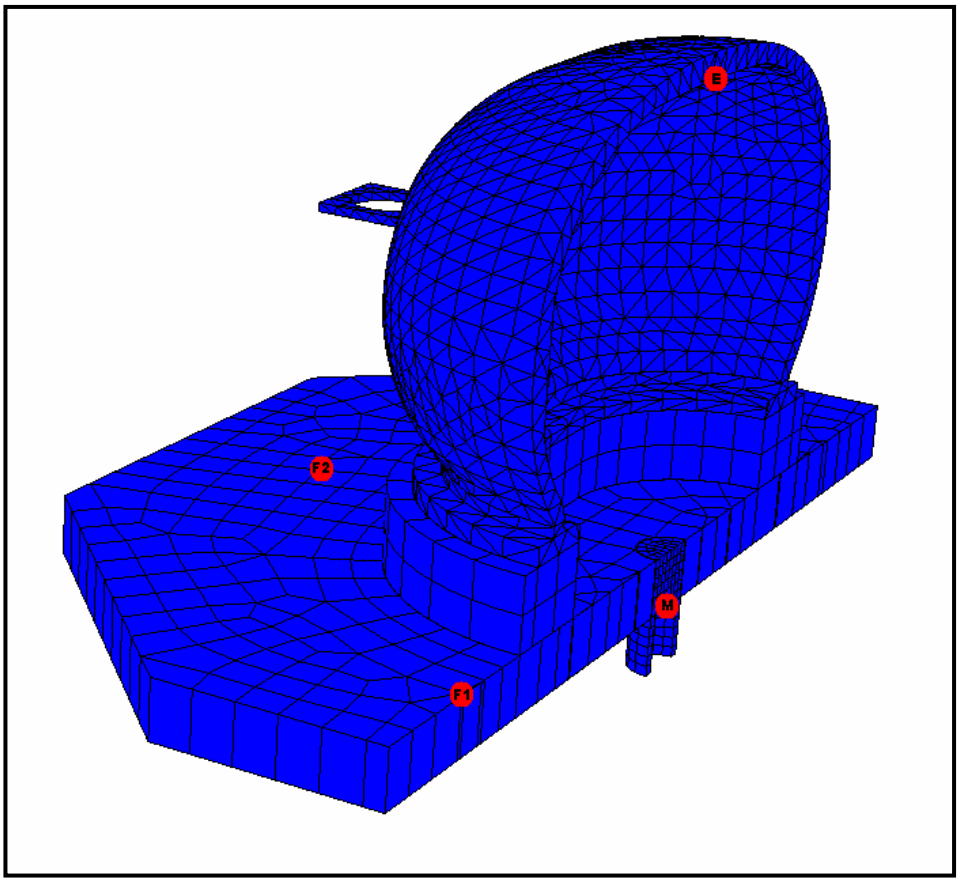

Figure 6.21 Location of the acceleration readings taken on several components.

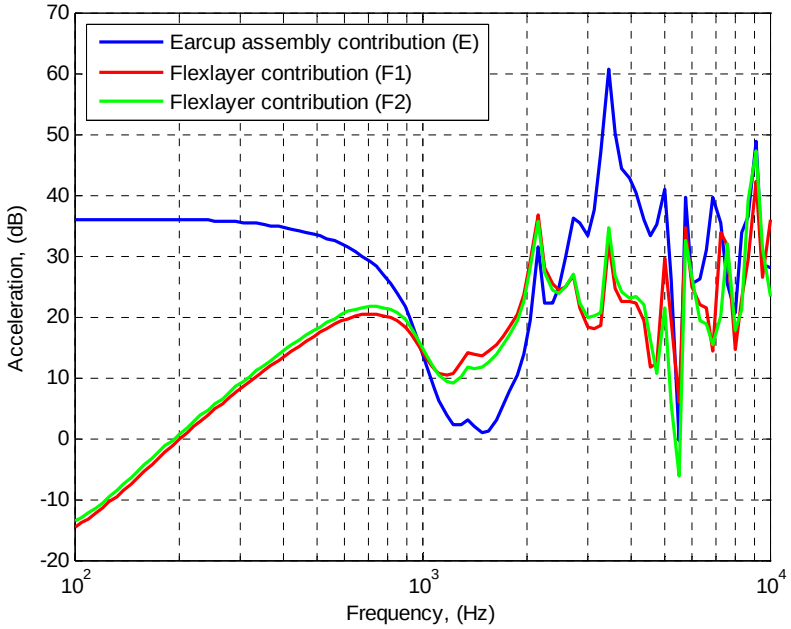

Figure 6.22 Comparing the contributions from the three locations.

In the low frequencies, or the *Piston Mode regime*, the earcup assembly is primarily responsible for transferred energy. This is explained by the piston mode resonance previously discussed. There is a higher contribution of energy by the flexlayer in the *Earplug Resonance regime*, which can be attributed to the resonance of the interior earplug assembly, as well as the flexlayer material in general. There is a significant difference in energy contribution in the 2,500-5,000 Hz region, which can be attributed to the large deformations experienced in the elastic earcup in resonance. This analysis is a first glance at the energy transfer contributions of each assembly component, but more investigation is needed to quantitatively determine the major energy transfer paths. Also note that vertical accelerations are taken for each component, therefore this analysis neglects any contributions made by non-vertical displacements.

6.4 Conclusion

The effect of radial preload on the shear experimental case was analyzed, and it was shown that a simple transformation of axial to shear material properties does not accurately model the material response. The shear material property results were compared, and the overall behavior of each preload case noted. Finally, the results were placed into the updated ABAQUS DHP model and the results were compared to the previous ABAQUS DHP model results and also the experimental DHP results. It was shown that the major mechanisms put forth in Chapter 3 were correct, the updated material properties emphasized the resonance of the EAR foam earplug material. Again, vibration of the complete ABAQUS DHP assembly is responsible for the majority of the acoustic pressure read at the bottom of the ear canal cavity. The updated ABAQUS DHP model provides more sound attenuation than the previous model, mainly because of the increased relative stiffness of the earplug. Finally, the updated ABAQUS DHP model results were compared to the original experimental DHP results. It was shown that more experimental vibration testing is needed to positively identify the mechanisms in the experimental behavior, but it is likely that the labeled regimes will be consistent with new experimental results. Also, the large peak experienced at 1,485 and 1,650 Hz in the updated and experimental model results is likely due to the earplug resonance. The difference in frequencies could be due to lack of appropriate and complete material

properties for all the viscoelastic materials and any small variations in boundary conditions from the finite element and experimental models. If this discovery of earplug vibration can in fact be verified through experimental DHP vibration testing, it will open the door for interpretation and design changes to improve the complete DHP HPD system, and single hearing protection earplug systems.

Chapter 7

Conclusion

7.1 Summary

Double hearing protection (DHP) noise reduction inhibiting mechanisms are identified and evaluated through the use of finite element models reconciled with data from comparable experimental tests. Specifically, the utilization of advanced material models and coupled structural-acoustic finite element models are used to accurately explore and accurately characterize the experimental DHP system. In order to identify these behavioral characteristics, the finite element model must contain representative material properties and boundary conditions. This thesis develops and explores the finite element models which provide insight into the actual experimental response, as well as integrates a modern analytical material property extraction method to better characterize the 19mm E-A-R Classic foam earplug (EAR foam earplug) and examines the changes these new properties have on the DHP system response.

It is believed more appropriate material properties for the EAR foam material will contribute to better correlation between the finite element and experimental results, as well as help qualitatively determine the contribution of the earplug response to the DHP system. Previous research in the hearing protection industry speculates that the EAR foam earplug vibration may contribute to DHP system response in the form of reduced noise attenuation levels at the material's resonance frequency. This phenomenon is observed in finite element DHP models, which emphasizes the importance of correctly modeling the EAR foam earplug material.

In order to identify the dominant behavioral mechanisms of the ABAQUS DHP model, certain key goals were met.

1. The finite element model must simulate the experimental system as closely as is practical. The DHP test configuration system parameters must be modeled, including boundary conditions, loading and material properties.
2. The finite element model results must be reconciled with experimental results. This allows for appropriate changes in system parameters, and helps understand the overall behavior of the finite element model response.

3. The reconciled finite element model must be thoroughly explored, and the targeted mechanisms must be identified.
4. Any system parameters shown to not accurately model the physics of the system must be changed, and the process iterated.

The overall behavior of the ABAQUS DHP model has been explored and understood. The *Flexlayer Driven* regime exists because of the reaction of the flexlayer, Siliclone RTV and EAR foam earplug components. The *Piston Mode* regime is seen in the ABAQUS model where it was predicted to exist by Anwar [9]. The *Elastic/Acoustic Earcup* regime is attributed to structural vibration, and to a lesser degree from interior acoustic cavity modes.

It was found that the primary source of noise in the ear canal cavity is due to vibration of the DHP structural assembly. The resonance of materials in specific frequency ranges contribute to the overall structural system response, where the ear canal acoustic pressure is primarily due to the vibration of the earplug itself.

In order to better model and understand this behavior the material properties used for these materials must be refined and investigated, specifically material properties in the shear configuration. Correct modeling of the DHP system could allow for fine tuning the earplug material property selection, allowing for a custom DHP system to combat mechanisms which reduce noise reduction performance from other components of the DHP system.

The shear case experimental data is not modeled accurately with a constant linear elastic modulus of elasticity. The effective elastic modulus could be adjusted to obtain the first shear case resonance for each preload, but this would not accurately model the entire frequency range without complete material data. Also, the modulus of elasticity not only varies with frequency, but with compressed preload as well. The experimental system utilized to explore the EAR foam earplug was validated with numerous hand calculations and simple finite element models. An axial case is explored to calibrate the experimental equipment and extraction method. The EAR foam material was experimentally tested in the shear configuration analogous to the experimental DHP configuration, and the

material properties extracted. Radial compressive strains of 6%, 18%, and 30% are explored for the EAR foam earplug.

Storage moduli and loss factors were extracted for both the axial and shear experimental cases. The valid frequency ranges were determined empirically for both cases and applied. Since material properties for any preload, within the test range, are required, an interpolation method was applied to the extracted storage moduli and loss factor results. Since the loss factor for each strain case brackets the original 6% strain value, an in-depth look at this nonlinearity is necessary. A novel finite element based interpolation method was discussed, allowing storage moduli and loss factors to be extracted for any amount of preload between the tested limits (6% to 30% radial strain) for the entire frequency range.

The effect of radial preload on the shear experimental case was analyzed, and it was shown that a simple transformation of axial to shear material properties does not accurately model the material response. Difference in boundary and loading conditions have a large impact on the response of this viscoelastic foam material, therefore the experimental extraction method of placing the material in the actual shear case was deemed necessary. The shear material property results were compared, and the overall behavior of each preload case noted.

Finally, the results were placed into the updated finite element DHP model (with the new EAR foam shear material properties) and the results were compared to the previous finite element DHP model results (pre-existing EAR foam axial-based material properties) and also the experimental DHP results. It was shown that the major mechanisms put forth in Chapter 3 were correct, the updated material properties emphasized the resonance of the EAR foam earplug material in the simulated ear canal. The updated finite element DHP model provided more sound attenuation than the previous finite element DHP model, mainly because of the increased relative stiffness of the earplug. Finally, the updated finite element DHP model results were compared to the original experimental DHP results. It was shown that more experimental vibration testing is needed to positively identify the mechanisms in the experimental behavior, but it is likely that the labeled regimes will be consistent with new experimental results. Also, the large peaks experienced at 1,485 and 1,650 Hz in the updated and experimental model

results is likely due to the earplug resonance. The difference in frequencies could be due to lack of appropriate and complete material properties for all the viscoelastic materials, and any small variations in boundary conditions from the finite element and experimental models. If this discovery of earplug vibration can in fact be verified through experimental DHP vibration testing, it will open the door for interpretation and design changes to improve the complete DHP HPD system, and also single hearing protection earplug systems.

7.2 Conclusions

This research identified the dominant behavior mechanisms in a finite element DHP model that simulates the DHP experimental configuration. More appropriate material properties for the EAR foam earplug were obtained through an analytical extraction process. The results, with certain unresolved issues of this research are as follows:

1. ABAQUS DHP models were constructed, correlated with experimental data and explored.
    - There is still some discrepancy in the low frequency range (100-700 Hz) between ABAQUS and experimental DHP results, although it is now believed to be due to vibration of the heavy base in the experimental DHP model.
    - Obtaining representative material properties for the ABAQUS DHP model are the most time consuming and complicated procedure of the entire analysis.

2. Pressure in the ear canal of the ABAQUS DHP model is primarily a result of structural vibration.
    - Earplug deformations in the ear canal were shown to be on the order of $1x10^{-8}$, which was shown by Cremer et. al. [3] to produce large noise levels.
    - This theory cannot be confirmed at this time for the experimental DHP configuration due to the lack of vibration data present in the experimental

system.

- There is still uncertainty as to how much the bottom of the EAR foam earplug deforms relative to the top. Only the acceleration at the top of the earplug is measured in experiment.
- The resulting behavior of the ABAQUS DHP system is dependent on the relative stiffness between system components. Since acoustic influences on the system response are minimal, all model changes for increasing noise reduction performance should be aimed at limiting the entire system vibration.

3. The resonance of the earplug assembly is known to be responsible for the large peak in the 1-2 kHz region of the ABAQUS DHP model, and this behavior is also expected to be responsible for the experimental DHP system's peak in this frequency range.
    - This speculation remains unproven until the acceleration of the earplug and its surrounding materials can be measured in the experimental DHP configuration.
    - Vibration of the earplug assembly in the experimental DHP configuration would suggest the possibility of earplug system vibration playing a role in real human DHP systems.

7.3 Contribution of this work

The dominant mechanisms described pertain to the DHP finite element model, and are speculated to exist in the experimental DHP configuration. These mechanisms cannot be directly connected to behavior in human DHP systems although some speculations can be made.

- If structural vibration is a dominant mode in the human DHP system, then relative stiffness and damping parameters could be modified to greatly improve noise reduction performance.

- If earplug material vibration is a dominant behavior in human DHP response in the 2 kHz octave band region (as described from Berger [7]), then earplug characterization and modification would be important factors in modern HPDs.

7.4 Recommendations for future work

Significant gains have been made in analyzing the experimental and finite element DHP models. Major behavioral mechanisms have been identified, but unfortunately more experimental and finite element modeling is needed to improve and verify some speculations.

1. Further refinement and reconciling of the finite element DHP model could improve current results.
    - The finite element DHP model could be further refined by adding complex contact conditions and hyperelastic material models. While some gains from model refinement will be achieved, the amount of effort required would be large.
2. The stiffness and mass of the earplug assembly greatly effects the structural response of the EAR foam earplug.
    - The Siliclone and Flexlayer RTV materials should have their material properties extracted in their characteristic (shear) configuration.
3. It is speculated that noise reduction peaks in the experimental DHP results could be primarily due to structural vibration.
    - To validate the speculations of the earplug assembly vibration in the experimental DHP configuration, more experimentation is needed. The acceleration of the EAR foam earplug and the surrounding viscoelastic materials must be experimentally measured in order to positively identify their behavior. Also, the motion of the “rigid” base in the experimental DHP model should be measured to explore the peaks seen in the low frequency region.

- Since it has been shown that the majority of sound pressure inside the ear canal results from structural vibration, future DHP systems should be designed around eliminating as much vibration as possible. This could involve utilizing more highly damped materials for system components.

4. The pressure experienced inside the ear canal assembly is directly due to the vibration of the earplug material.
    - Larger and more realistic values of radial preload of the EAR foam earplug could be investigated by employing non-contact acceleration testing methods in the experimental extraction process.
    - The amount of sound created by EAR foam earplug vibration could be determined by placing a small, vibration insensitive microphone inside the seal polycarbonate sleeve.

References

[1] Centers for Disease Control and Prevention, "Work-Related Hearing Loss," *www.cdc.gov/niosh/hpworkrel.html* (Atlanta, GA: Department of Health and Human Services).

[2] Technology Horizons, "New Twists to an Old Design," *www.afrlhorizons.com/Briefs/Apr04/HE0303.html* (Dayton, OH: Air Force Research Laboratory).

[3] Cremer L., Heckl M., and Ungar E., *Structure-Borne Sound*, 2nd edition (New York: Springer-Verlag, 1987).

[4] David Clark, "Model 19A," *www.davidclark.com/HeadsetPgs/model19a.htm* (Worchester, MA: David Clark Company, Inc)

[5] AirSourceOne, "Aviation Pilot Supplies," *www.airsource1.com/catalog.cgi/DAVID%20CLARK/HELMET* (Fort Worth, TX: AirSourceOne.com).

[6] ANSI (1957). *Method for the measurement of real-ear attenuation of ear protectors at threshold*, ANSI Z24.22-1957. New York: American National Standards Institute, Inc.

[7] Berger, R.W. Kieper, Dan Gauger, "Hearing Protection: Surpassing the Limits to Attenuation Imposed by the Bone-Conduction Pathways," *The Journal of the Acoustical Society of America*, vol.114, n4, pp1955-1967, 2003.

[8] Berger, E.H., Hearing protection devices. In E.H. Berger, W.D. Ward, J.C. Morrill, and L.H. Royster (Eds.), *Noise and hearing conservation manual* (4th ed.) (pp. 319-378) Akron, OH: American Industrial Hygiene Association, 1986.

[9] Aamir Anwar, "Low Frequency Finite Element Modeling of Passive Noise Attenuation in Ear Defenders." Master's Thesis, Virginia Poytechnic Institute and State University, Blacksburg, VA 2005.

[10] Zwislocki J, "Acoustic attenuation between ears," *The Journal of the Acoustical Society of America*, vol.25, pp.752-759, 1953.

[11] Gudmundsen G, Killion M, Wilber L, "Zwislocki was right…A potential solution to the 'hollow voice' problem with deeply sealed earmolds," *Hearing Instruments*, Jan. 1988.

[12] Khanna S.M, Tonndorf J, Queller J, "Mechanical parameters of hearing by bone conduction," *The Journal of the Acoustical Society of America*, vol.60, pp.139-154, 1976.

[13] Berger, E.H., "Laboratory Attenuation of Earmuffs and Earplugs Both Singly and in Combination," *American Industrial Hygiene Association Journal*, 44(5) 321-329, 1983.

[14] Bierman R.L, Smith G.M, Zitek S.J, "Determination of Dynamic Properties of Elastomers over Broad Frequency Range," *Experimental Mechanics*, vol.23, pp.158-164, 1983.

[15] Gade S, Nielson L.F, Wismer N.J, "An Improved Method for Estimating the Dynamic Properties of Materials," *Sound and Vibration*, Instrumentation Reference Issue, pp.20-24, 2000.

[16] Mitchell L.D, Sun F.P, "Wide-band Measurement of Frequency Dependent Viscoelastic Properties Using an Inverse Nyquist Plane Parameter Extraction Methodology," *Experimental Mechanics*, vol.XX, pp.350-356, 1989.

[17] Agee, B. L., and L. D. Mitchell, "Frequency-Dependent Viscoelastic Property Measurement Via Modal Analysis Techniques," *Proceedings of the 9th International Conference on Experimental Mechanics*, Denmark, 20-24 August, 1990.

[18] Aklonis J., MacKnight W., *Introduction to Polymer Viscoelasticity*, 2nd edition (New York: John Wiley and Sons, 1983)

[19] Inman D.J, *Engineering Vibration - Second Edition* Chapter 6, p.451, Prentice Hall, 2001.

[20] Ewins D.J., *Modal Testing: Theory and Practice* Chapter3, p.131, Brüel & Kjær, 1986.

[21] Embedded.com, "World's Best Root Finder," *www.embedded.com/shared/printableArticle.jhtml?articleID=9900570* (Manhasset, NY: CMP Medial LLC).

[22] Reddy J., *An Introduction to the Finite Element Method*, 2nd edition (New York: McGraw-Hill, 2003)

[23] "ABAQUS Theory Manual" ver.6.5, ©ABAQUS, Inc. 2005.

[24] Westone.com, "Popular Westone Earmolds," *www.westone.com/earmold_styles.html#protect* (Colorado Springs, CO: Westone Laboratories, Inc).

[25] E-A-R Hearing Protection Products, "Combat Arms," *www.e-a-r.com/e%2Da%2Dr.com/premold_detail.cfm?prod_family=Combat%20Arms&ind_prod_num=370-1000001* (Indianapolis, IN: Aearo Corporation).

[26] E-A-R Hearing Protection Products, "Classic Five Pair", *www.e-a-r.com/e%2Da%2Dr.com/roll_detail.cfm?prod_family=Classic%20Five%20Pair&ind_prod_num=316-1111001* (Indianapolis, IN: Aearo Corporation).

Appendix A
Material properties for the previous ABAQUS DHP model

Polycarbonate material

- E = 2.2 GPa
- $\nu = 0.39$
- $\rho = 972\ kg/m^3$

Siliclone RTV material

- E = 1.86 MPa
- $\nu = 0.38$
- $\rho = 1{,}275\ kg/m^3$
- Viscoelastic material properties

G_{imag}/G_∞	$1-G_{real}/G_\infty$	K_{imag}/K_∞	$1-K_{real}/K_\infty$	Frequency, (Hz)
0.047602	0.70702	0.047602	0.70702	1
0.053949	0.68142	0.053949	0.68142	2
0.057985	0.66541	0.057985	0.66541	3
0.061001	0.65357	0.061001	0.65357	4
0.063431	0.6441	0.063431	0.6441	5
0.065475	0.63617	0.065475	0.63617	6
0.067247	0.62933	0.067247	0.62933	7
0.068814	0.62329	0.068814	0.62329	8
0.070222	0.61789	0.070222	0.61789	9
0.071501	0.61299	0.071501	0.61299	10
0.080412	0.57917	0.080412	0.57917	20
0.086037	0.55803	0.086037	0.55803	30
0.090222	0.54239	0.090222	0.54239	40
0.093582	0.52987	0.093582	0.52987	50
0.096403	0.5194	0.096403	0.5194	60
0.098842	0.51036	0.098842	0.51036	70
0.10099	0.50239	0.10099	0.50239	80
0.10293	0.49525	0.10293	0.49525	90
0.10468	0.48878	0.10468	0.48878	100
0.11682	0.4441	0.11682	0.4441	200
0.12442	0.41617	0.12442	0.41617	300
0.13006	0.39551	0.13006	0.39551	400
0.13457	0.37899	0.13457	0.37899	500
0.13834	0.36515	0.13834	0.36515	600
0.1416	0.35321	0.1416	0.35321	700
0.14447	0.34268	0.14447	0.34268	800
0.14703	0.33325	0.14703	0.33325	900
0.14936	0.32471	0.14936	0.32471	1000
0.1654	0.26568	0.1654	0.26568	2000
0.17538	0.2288	0.17538	0.2288	3000
0.18273	0.2015	0.18273	0.2015	4000
0.18859	0.17967	0.18859	0.17967	5000
0.19349	0.16139	0.19349	0.16139	6000
0.1977	0.14562	0.1977	0.14562	7000
0.20141	0.13171	0.20141	0.13171	8000
0.20472	0.11926	0.20472	0.11926	9000
0.20772	0.10797	0.20772	0.10797	10000

Flexlayer RTV material

- 68,190 Pa
- $\nu = 0.45$
- $\rho = 1{,}036\ kg/m^3$
- Viscoelastic material properties

G_{imag}/G_∞	$1-G_{real}/G_\infty$	K_{imag}/K_∞	$1-K_{real}/K_\infty$	Frequency, (Hz)
23.697	-22.3949	23.697	-22.3949	737.5
23.4712	-22.5386	23.4712	-22.5386	750
23.3084	-22.6941	23.3084	-22.6941	762.5
23.0914	-22.7703	23.0914	-22.7703	775
22.9638	-22.8657	22.9638	-22.8657	787.5
22.8069	-22.9449	22.8069	-22.9449	800
22.6587	-23.0328	22.6587	-23.0328	812.5
22.5136	-23.0446	22.5136	-23.0446	825
22.3948	-23.1839	22.3948	-23.1839	837.5
22.2775	-23.2191	22.2775	-23.2191	850
22.1953	-23.3012	22.1953	-23.3012	862.5
22.1557	-23.354	22.1557	-23.354	875
22.0722	-23.4083	22.0722	-23.4083	887.5
21.9959	-23.486	21.9959	-23.486	900
21.9548	-23.5696	21.9548	-23.5696	912.5
21.8962	-23.6473	21.8962	-23.6473	925
21.8492	-23.75	21.8492	-23.75	937.5
21.7569	-23.7602	21.7569	-23.7602	950
21.7217	-23.8731	21.7217	-23.8731	962.5
21.7041	-23.9406	21.7041	-23.9406	975
21.6586	-24.0491	21.6586	-24.0491	987.5
21.5926	-24.1269	21.5926	-24.1269	1000
21.5017	-24.1562	21.5017	-24.1562	1012.5
21.4797	-24.275	21.4797	-24.275	1025
21.4122	-24.3454	21.4122	-24.3454	1037.5
21.3682	-24.3864	21.3682	-24.3864	1050
21.3213	-24.4861	21.3213	-24.4861	1062.5
21.2553	-24.5565	21.2553	-24.5565	1075
21.1893	-24.5741	21.1893	-24.5741	1087.5
21.1439	-24.6768	21.1439	-24.6768	1100
21.1263	-24.6812	21.1263	-24.6812	1112.5
21.1204	-24.7501	21.1204	-24.7501	1125
21.0339	-24.7882	21.0339	-24.7882	1137.5
21.0456	-24.8029	21.0456	-24.8029	1150
21.0295	-24.8616	21.0295	-24.8616	1162.5
21.0471	-24.9217	21.0471	-24.9217	1175
21.0119	-24.995	21.0119	-24.995	1187.5
21.0559	-25.1226	21.0559	-25.1226	1200
21.0368	-25.2619	21.0368	-25.2619	1212.5
20.9371	-25.432	20.9371	-25.432	1225
20.742	-25.5977	20.742	-25.5977	1237.5
20.4781	-25.5127	20.4781	-25.5127	1250
20.4399	-25.4335	20.4399	-25.4335	1262.5
20.4048	-25.3866	20.4048	-25.3866	1275
20.4092	-25.4042	20.4092	-25.4042	1287.5
20.3769	-25.4599	20.3769	-25.4599	1300
20.2317	-25.5831	20.2317	-25.5831	1312.5
19.9281	-25.3587	19.9281	-25.3587	1325
20.0865	-25.0111	20.0865	-25.0111	1337.5
20.415	-25.061	20.415	-25.061	1350
20.4678	-25.3147	20.4678	-25.3147	1362.5
20.3402	-25.4276	20.3402	-25.4276	1375

Flexlayer viscoelastic material properties continued…

20.2376	-25.4115	20.2376	-25.4115	1387.5
20.1584	-25.3411	20.1584	-25.3411	1400
20.1569	-25.3455	20.1569	-25.3455	1412.5
20.1892	-25.2942	20.1892	-25.2942	1425
20.198	-25.3044	20.198	-25.3044	1437.5
20.1906	-25.2736	20.1906	-25.2736	1450
20.2244	-25.2707	20.2244	-25.2707	1462.5
20.264	-25.2868	20.264	-25.2868	1475
20.2948	-25.3074	20.2948	-25.3074	1487.5
20.3314	-25.3426	20.3314	-25.3426	1500
20.3652	-25.3807	20.3652	-25.3807	1512.5
20.3681	-25.4306	20.3681	-25.4306	1525
20.3666	-25.4995	20.3666	-25.4995	1537.5
20.308	-25.5772	20.308	-25.5772	1550
20.286	-25.6637	20.286	-25.6637	1562.5
20.2053	-25.6813	20.2053	-25.6813	1575
20.1071	-25.6828	20.1071	-25.6828	1587.5
20.0645	-25.6916	20.0645	-25.6916	1600
20.0264	-25.6725	20.0264	-25.6725	1612.5
19.9663	-25.6388	19.9663	-25.6388	1625
19.9237	-25.5757	19.9237	-25.5757	1637.5
19.9208	-25.5493	19.9208	-25.5493	1650
19.9164	-25.52	19.9164	-25.52	1662.5
19.9311	-25.5303	19.9311	-25.5303	1675
19.9223	-25.4672	19.9223	-25.4672	1687.5
19.9501	-25.479	19.9501	-25.479	1700
19.9575	-25.4922	19.9575	-25.4922	1712.5
19.9472	-25.457	19.9472	-25.457	1725
19.9868	-25.4966	19.9868	-25.4966	1737.5
19.9736	-25.4907	19.9736	-25.4907	1750
19.9765	-25.5259	19.9765	-25.5259	1762.5
19.9707	-25.5552	19.9707	-25.5552	1775
19.9633	-25.5904	19.9633	-25.5904	1787.5
19.9516	-25.6109	19.9516	-25.6109	1800
19.9179	-25.6285	19.9179	-25.6285	1812.5
19.849	-25.6271	19.849	-25.6271	1825
19.8167	-25.6711	19.8167	-25.6711	1837.5
19.7815	-25.6901	19.7815	-25.6901	1850
19.7272	-25.6843	19.7272	-25.6843	1862.5
19.7038	-25.6872	19.7038	-25.6872	1875
19.67	-25.7063	19.67	-25.7063	1887.5
19.604	-25.6872	19.604	-25.6872	1900
19.5777	-25.6931	19.5777	-25.6931	1912.5
19.4999	-25.6667	19.4999	-25.6667	1925
19.4721	-25.6784	19.4721	-25.6784	1937.5
19.4295	-25.6857	19.4295	-25.6857	1950
19.3841	-25.6652	19.3841	-25.6652	1962.5
19.3166	-25.6432	19.3166	-25.6432	1975
19.2682	-25.6212	19.2682	-25.6212	1987.5
19.2213	-25.6256	19.2213	-25.6256	2000
19.1788	-25.608	19.1788	-25.608	2012.5
19.1142	-25.5684	19.1142	-25.5684	2025
19.06	-25.542	19.06	-25.542	2037.5
19.0043	-25.5347	19.0043	-25.5347	2050
18.9427	-25.5098	18.9427	-25.5098	2062.5
18.884	-25.4482	18.884	-25.4482	2075
18.8459	-25.4452	18.8459	-25.4452	2087.5
18.7784	-25.4144	18.7784	-25.4144	2100

Previous EAR foam material

- E = 22,155 Pa
- $\nu = 0.1$
- $\rho = 228\ kg/m^3$
- Viscoelastic material properties

G_{imag}/G_∞	$1-G_{real}/G_\infty$	K_{imag}/K_∞	$1-K_{real}/K_\infty$	Frequency, (Hz)
333.38	-159.05	333.38	-159.05	1
388.06	-204.33	388.06	-204.33	2
417.04	-233.33	417.04	-233.33	3
435.79	-254.85	435.79	-254.85	4
449.16	-272.02	449.16	-272.02	5
459.27	-286.31	459.27	-286.31	6
467.2	-298.56	467.2	-298.56	7
473.61	-309.27	473.61	-309.27	8
478.9	-318.79	478.9	-318.79	9
483.34	-327.36	483.34	-327.36	10
505.41	-384.39	505.41	-384.39	20
512.56	-417.83	512.56	-417.83	30
515.13	-441.35	515.13	-441.35	40
515.75	-459.38	515.75	-459.38	50
515.4	-473.94	515.4	-473.94	60
514.53	-486.11	514.53	-486.11	70
513.37	-496.53	513.37	-496.53	80
512.04	-505.63	512.04	-505.63	90
510.62	-513.68	510.62	-513.68	100
496.33	-564.38	496.33	-564.38	200
484.62	-591.97	484.62	-591.97	300
475.13	-610.54	475.13	-610.54	400
467.21	-624.34	467.21	-624.34	500
460.44	-635.22	460.44	-635.22	600
454.54	-644.14	454.54	-644.14	700
449.32	-651.67	449.32	-651.67	800
444.64	-658.15	444.64	-658.15	900
440.4	-663.82	440.4	-663.82	1000
411.78	-698.28	411.78	-698.28	2000
394.92	-716.31	394.92	-716.31	3000
383.11	-728.24	383.11	-728.24	4000
374.1	-737.05	374.1	-737.05	5000
366.88	-744	366.88	-744	6000
360.88	-749.7	360.88	-749.7	7000
355.76	-754.53	355.76	-754.53	8000
351.33	-758.71	351.33	-758.71	9000
347.42	-762.39	347.42	-762.39	10000

Air fluid material

- Bulk modulus = 153,000
- $\rho = 1.201\ kg/m^3$

Appendix B.1
Modal identification

The modes of the previous ABAQUS DHP model results are identified visually. The overall displacement vector is plotted, with red and blue contours indicating highest and lowest deformations, respectively. Frequencies of consideration are marked and labeled in red.

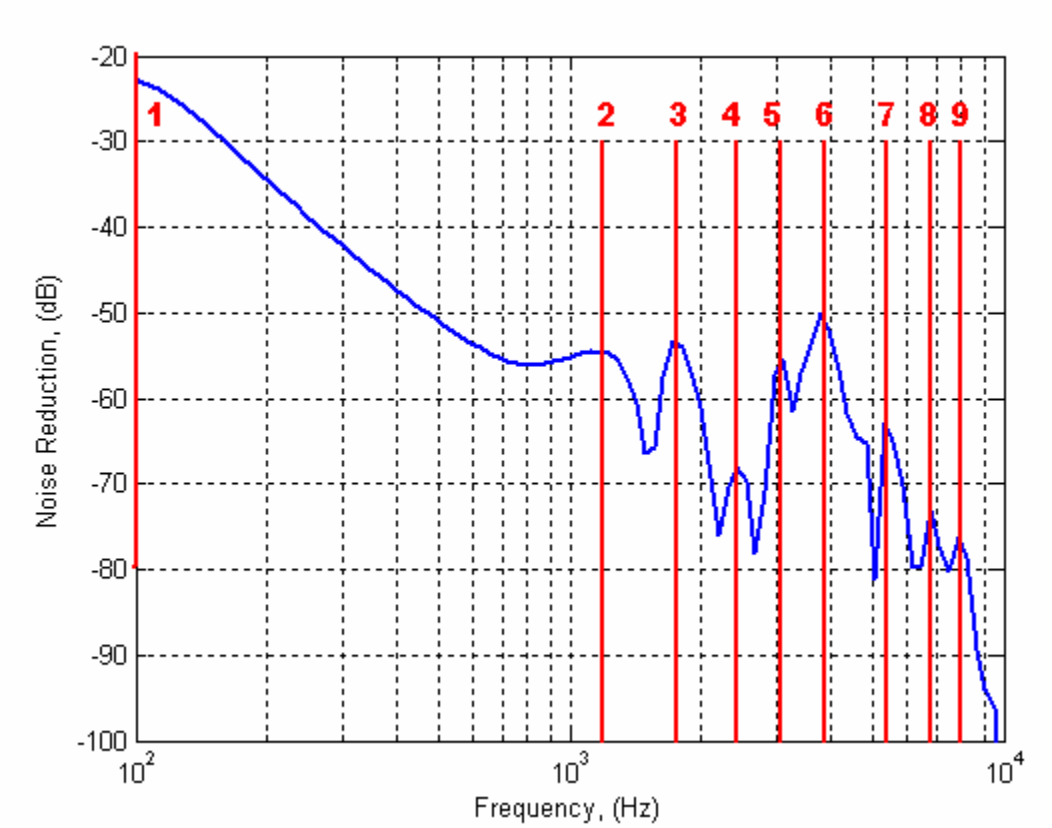

Figure B0 Resonances chosen to be visually displayed of the previous ABAQUS DHP system response.

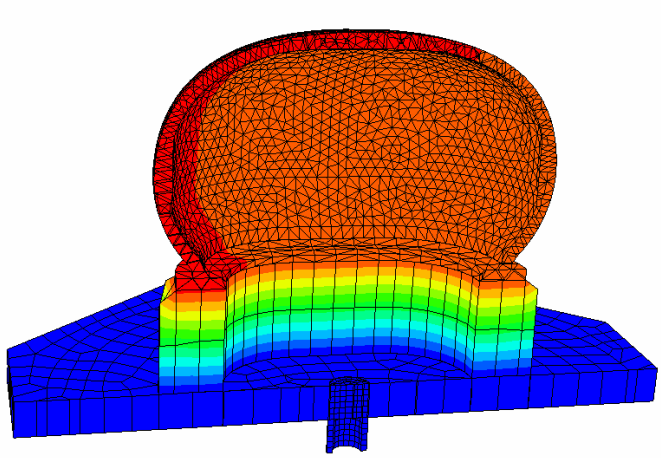

Figure B1 (1) Piston mode (1170 Hz) - *Piston Mode regime.*

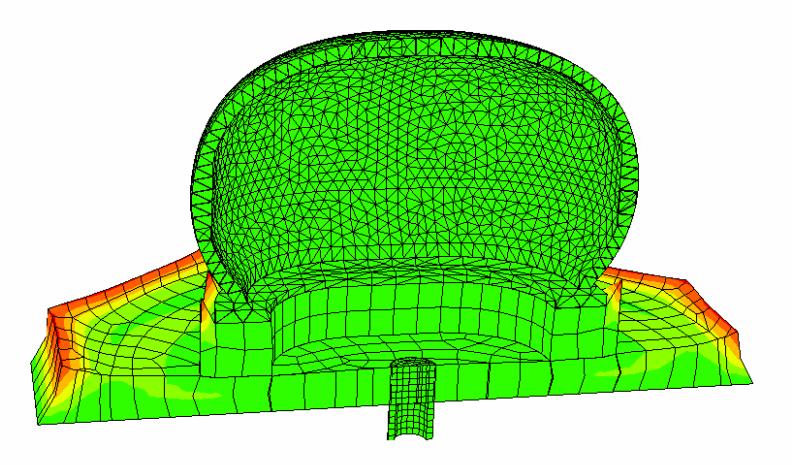

Figure B2 (2) Earplug/Earcup flap resonance (1170 Hz) - *Earplug Resonance regime.*

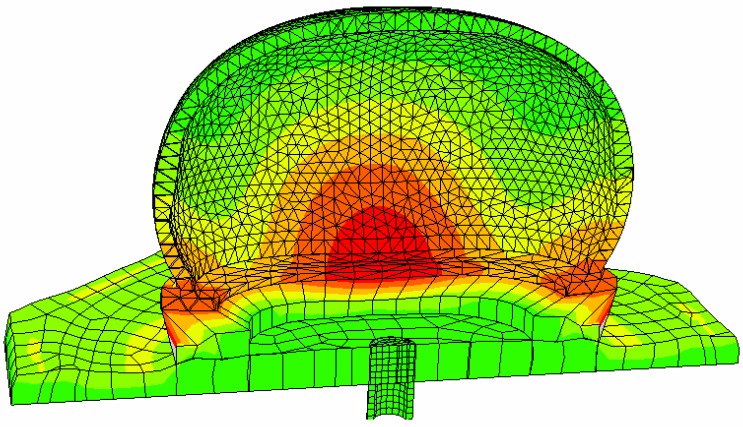

Figure B3 (3) Earcup flap resonance (1728 Hz) - *Elastic/Acoustic Earcup regime.*

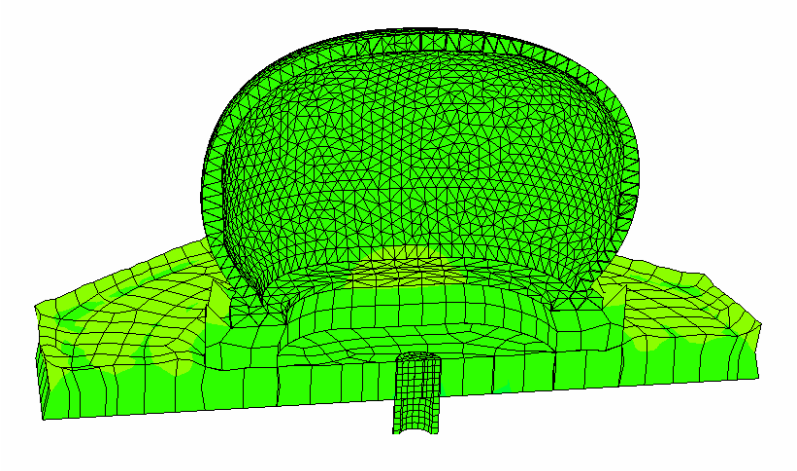

Figure B4 (4) Earcup flap resonance (2315 Hz) - *Elastic/Acoustic Earcup regime.*

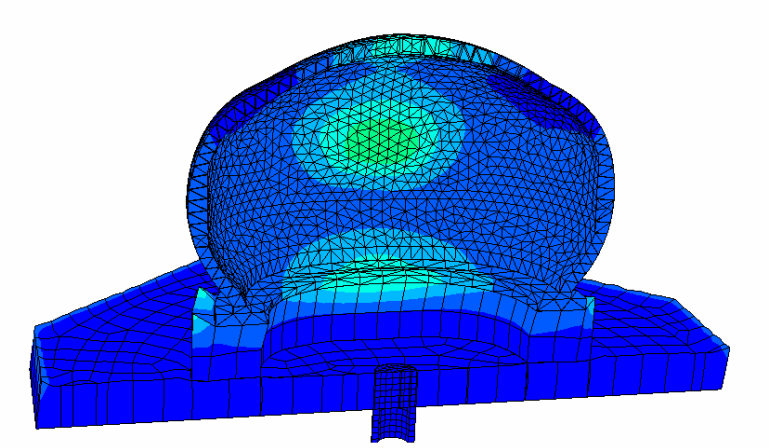

Figure B5 (5) Earcup resonance (2314 Hz) - *Elastic/Acoustic Earcup regime.*

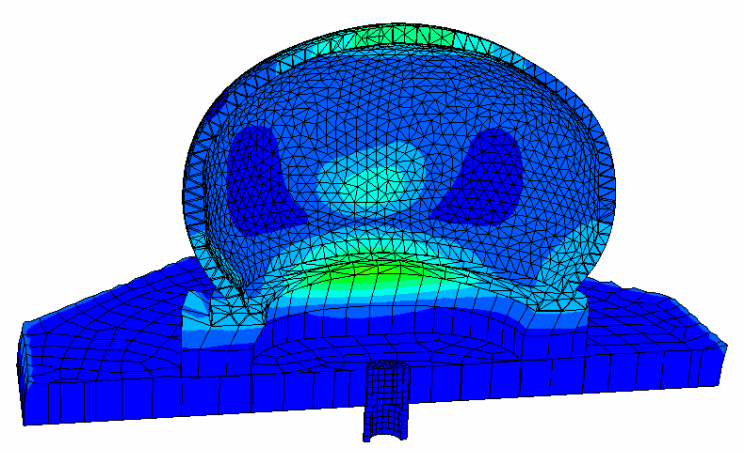

Figure B6 (6) Earcup resonance (3770 Hz) - *Elastic/Acoustic Earcup regime.*

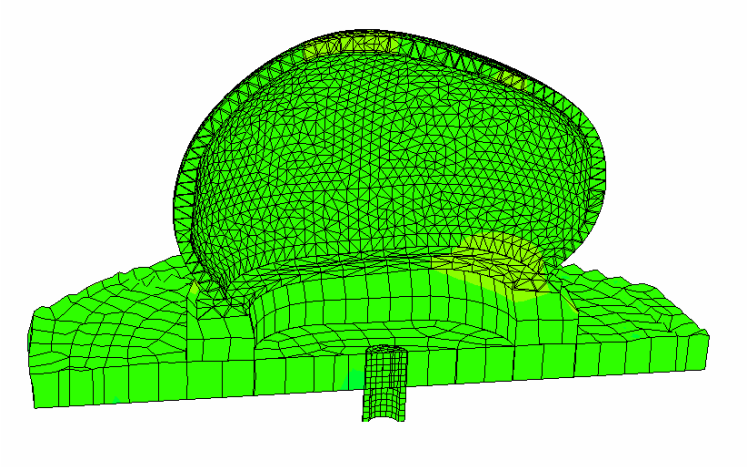

Figure B7 (7) Earcup resonance (5570 Hz) - *Elastic/Acoustic Earcup regime.*

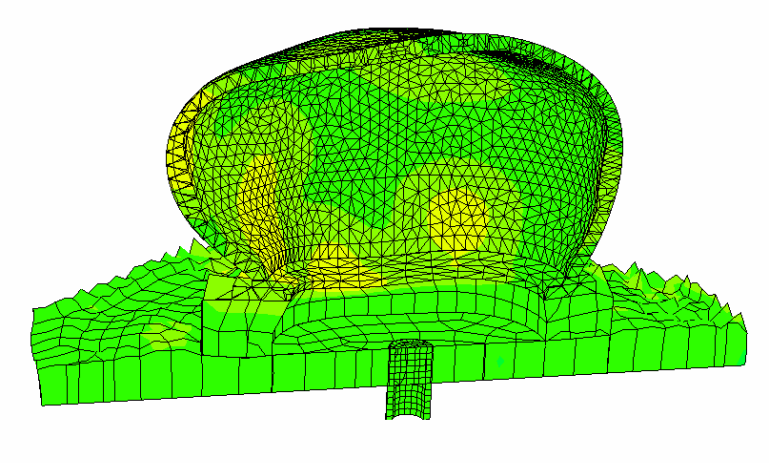

Figure B8 (8) Earcup resonance (6770 Hz) – *Elastic/Acoustic Earcup regime.*

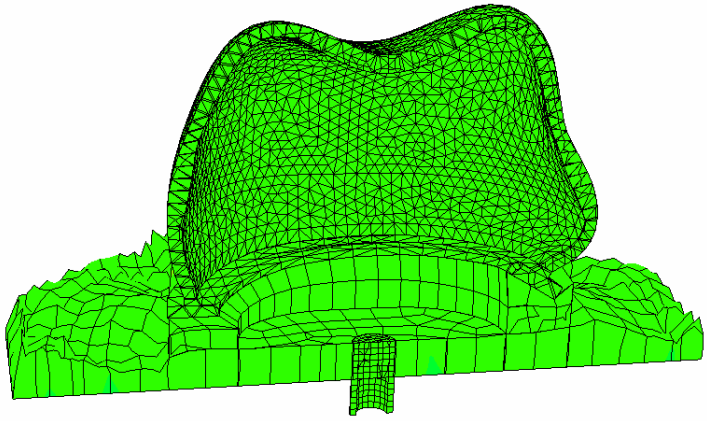

Figure B9 (9) Earcup resonance (7836 Hz) - *Elastic/Acoustic Earcup regime.*

Appendix B.2
Earcup structural FRF

To help understand the contribution of structural vibration on the overall ABAQUS DHP system behavior, the structural accelerance frequency response function of a point at the top of the earcup is taken. This is a point mobility reading, as the 1 Newton input load is placed at the same point as the acceleration output is taken. The source load and output points are read in the vertical direction, therefore neglecting any horizontal motion.

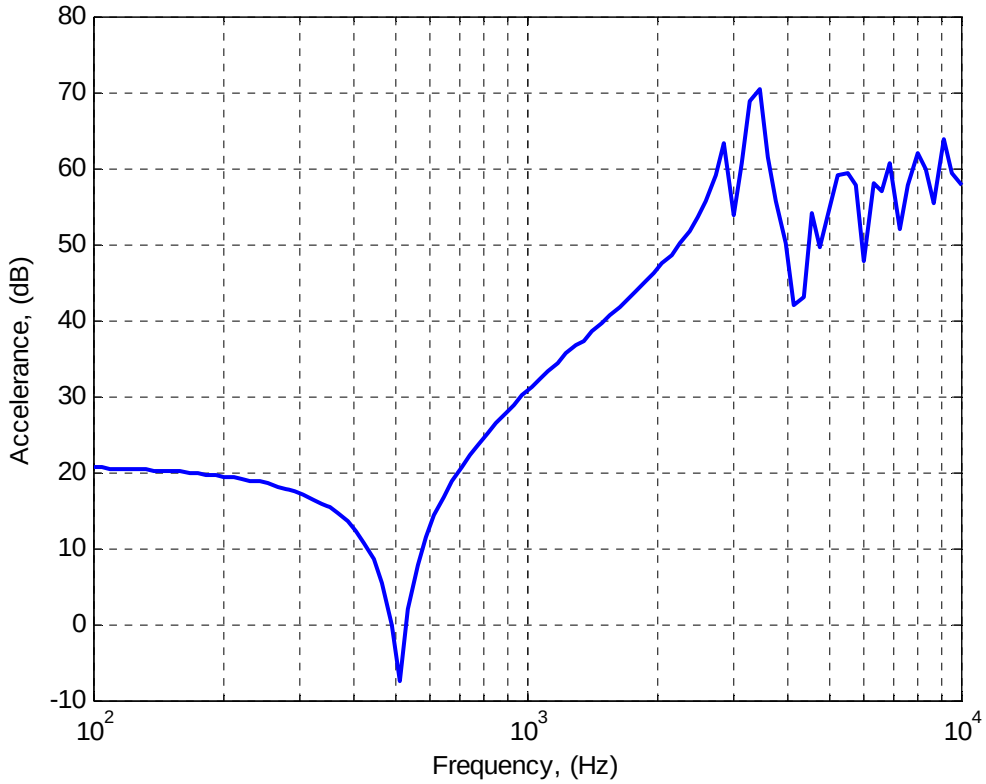

Figure B10 The structural FRF at the top of the polycarbonate earcup.

Appendix C
Muller's method code

The MATLAB code for Muller's method is displayed. This code was originally written and modified by J. Burkhardt and M. Sussman.

```
%  This is Muller's method for seeking a real root of a nonlinear
function.
%  Muller's method requires three points to start.  This function
%  uses a point a little closer to x0 than to x2 as its middle point.
%  This is a "stripped down" version with little error checking.
%
%=========================================================================
% Originally written by J. Burkardt
% Modified by M. M. Sussman
% Modified by Christian James
% Virginia Tech 2-3-06

%maximum change in iteration step results
  EPSILON = 0.000001;
%maximum number of iterations allowed
  ITMAX = 1000;

% choose x1 close to the midpoint between x0 and x2
% don't use the exact midpoint to avoid symmetries
% it would be much better to include x1 in the calling sequence.
  x1 = (.51*x0 + .49*x2);

%receiving values of chosen point through the objective function
  y0 = ObjectiveS(x0,j);
  y1 = ObjectiveS(x1,j);
  y2 = ObjectiveS(x2,j);

  for itCount=1:ITMAX

%  Determine the coefficients
%    A, B, C
%  of the polynomial
%    Y(X) = A * (X-X2)**2 + B * (X-X2) + C
%  which goes through the data:
%    (X1,Y1), (X2,Y2), (X3,Y3).
%
  A = ( ( y0 - y2 ) * ( x1 - x2 ) - ( y1 - y2 ) * ( x0 - x2 ) ) / ...
        ( ( x0 - x2 ) * ( x1 - x2 ) * ( x0 - x1 ) );

  B = ( ( y1 - y2 ) * ( x0 - x2 )^2 - ( y0 - y2 ) * ( x1 - x2 )^2 ) /
...
    ( ( x0 - x2 ) * ( x1 - x2 ) * ( x0 - x1 ) );

  C = y2;
```

```
%  Get the real roots of the polynomial, and choose the one that makes
%  the LEAST change to X2.

  if ( A ~= 0 )

    disc = B * B - 4.0 * A * C;

    q1 = ( B - sqrt ( disc ) );
    q2 = ( B + sqrt ( disc ) );

     if ( abs ( q1 ) < abs ( q2 ) )
        dx = - 2.0 * C / q2;
     else
       dx = - 2.0 * C / q1;
     end

  elseif ( B ~= 0 )
    dx = - C / B;
  else
      result = 6e6 + 1e6*i;
      disp(['muller: algorithm broke down, itCount=' num2str(itCount)])
      return
  end

  x3 = x2 + dx;
  y3 = ObjectiveS(x3,j);

  x0 = x1;
  x1 = x2;
  x2 = x3;

  y0 = y1;
  y1 = y2;
  y2 = y3;

  % print out the new point to show progress of the iteration
  disp([ 'itCount=',num2str(itCount),' x2=',num2str(x2), ...
     ' y2=', num2str(y2) ])

%  Declare victory if the most recent change in X is small, and
%  the size of the function is small.

  if ( abs ( y2 ) < EPSILON )
    result = x2;
    disp(['muller: converged after ' num2str(itCount) ' iterations.'])
    return
  end

end

error(['muller: more than ' num2str(ITMAX) ' iterations required.'])

%END FUNCTION
```

Appendix D
EAR foam earplug material properties

19mm EAR foam earplug, 6% radial strain

- E = 400 kPa
- $\nu = 0.1$
- $\rho = 112\ kg/m^3$
- Viscoelastic material properties

G_{imag}/G_∞	$1-G_{real}/G_\infty$	K_{imag}/K_∞	$1-K_{real}/K_\infty$	Frequency, (Hz)
0.497855	-0.0645455	0.497855	-0.0645455	1984
0.504273	-0.0714545	0.504273	-0.0714545	2016
0.510473	-0.0783636	0.510473	-0.0783636	2048
0.516455	-0.0852727	0.516455	-0.0852727	2080
0.522236	-0.0923636	0.522236	-0.0923636	2112
0.5278	-0.0994545	0.5278	-0.0994545	2144
0.533182	-0.106545	0.533182	-0.106545	2176
0.538364	-0.113818	0.538364	-0.113818	2208
0.543382	-0.121091	0.543382	-0.121091	2240
0.548218	-0.128545	0.548218	-0.128545	2272
0.552873	-0.136	0.552873	-0.136	2304
0.557364	-0.143455	0.557364	-0.143455	2336
0.561709	-0.150909	0.561709	-0.150909	2368
0.565873	-0.158545	0.565873	-0.158545	2400
0.569909	-0.166182	0.569909	-0.166182	2432
0.573782	-0.174	0.573782	-0.174	2464
0.577527	-0.181636	0.577527	-0.181636	2496
0.581127	-0.189455	0.581127	-0.189455	2528
0.584582	-0.197455	0.584582	-0.197455	2560
0.587927	-0.205455	0.587927	-0.205455	2592
0.591127	-0.213455	0.591127	-0.213455	2624
0.5942	-0.221455	0.5942	-0.221455	2656
0.597164	-0.229636	0.597164	-0.229636	2688
0.600018	-0.237818	0.600018	-0.237818	2720
0.602745	-0.246	0.602745	-0.246	2752
0.605364	-0.254182	0.605364	-0.254182	2784
0.607873	-0.262545	0.607873	-0.262545	2816
0.610273	-0.270909	0.610273	-0.270909	2848
0.612564	-0.279273	0.612564	-0.279273	2880
0.614764	-0.287818	0.614764	-0.287818	2912
0.616873	-0.296364	0.616873	-0.296364	2944
0.618873	-0.304909	0.618873	-0.304909	2976
0.6208	-0.313455	0.6208	-0.313455	3008
0.622618	-0.322182	0.622618	-0.322182	3040
0.624364	-0.330909	0.624364	-0.330909	3072
0.626018	-0.339636	0.626018	-0.339636	3104
0.627582	-0.348364	0.627582	-0.348364	3136
0.629091	-0.357091	0.629091	-0.357091	3168
0.630509	-0.366	0.630509	-0.366	3200
0.631836	-0.374909	0.631836	-0.374909	3232
0.633109	-0.383818	0.633109	-0.383818	3264
0.634309	-0.392727	0.634309	-0.392727	3296
0.635436	-0.401818	0.635436	-0.401818	3328
0.636509	-0.410727	0.636509	-0.410727	3360

19mm EAR foam earplug, 6% radial strain continued…

0.637509	-0.419818	0.637509	-0.419818	3392
0.638455	-0.428909	0.638455	-0.428909	3424
0.639327	-0.438182	0.639327	-0.438182	3456
0.640145	-0.447273	0.640145	-0.447273	3488
0.640927	-0.456545	0.640927	-0.456545	3520
0.641636	-0.465636	0.641636	-0.465636	3552
0.642291	-0.475091	0.642291	-0.475091	3584
0.642909	-0.484364	0.642909	-0.484364	3616
0.643491	-0.493636	0.643491	-0.493636	3648
0.644018	-0.503091	0.644018	-0.503091	3680
0.644491	-0.512545	0.644491	-0.512545	3712
0.644945	-0.522	0.644945	-0.522	3744
0.645345	-0.531455	0.645345	-0.531455	3776
0.645709	-0.540909	0.645709	-0.540909	3808
0.646055	-0.550545	0.646055	-0.550545	3840
0.646364	-0.560182	0.646364	-0.560182	3872
0.646636	-0.569818	0.646636	-0.569818	3904
0.646873	-0.579455	0.646873	-0.579455	3936
0.647091	-0.589091	0.647091	-0.589091	3968
0.647291	-0.598909	0.647291	-0.598909	4000
0.647473	-0.608727	0.647473	-0.608727	4032
0.647618	-0.618545	0.647618	-0.618545	4064
0.647764	-0.628545	0.647764	-0.628545	4096
0.647873	-0.638364	0.647873	-0.638364	4128
0.647982	-0.648364	0.647982	-0.648364	4160
0.648073	-0.658364	0.648073	-0.658364	4192
0.648145	-0.668545	0.648145	-0.668545	4224
0.648218	-0.678545	0.648218	-0.678545	4256
0.648291	-0.688727	0.648291	-0.688727	4288
0.648345	-0.699091	0.648345	-0.699091	4320
0.6484	-0.709273	0.6484	-0.709273	4352
0.648455	-0.719636	0.648455	-0.719636	4384
0.648509	-0.73	0.648509	-0.73	4416
0.648564	-0.740545	0.648564	-0.740545	4448
0.648618	-0.751091	0.648618	-0.751091	4480
0.648673	-0.761636	0.648673	-0.761636	4512
0.648745	-0.772364	0.648745	-0.772364	4544
0.648818	-0.783091	0.648818	-0.783091	4576
0.648909	-0.794	0.648909	-0.794	4608
0.649	-0.804909	0.649	-0.804909	4640
0.649109	-0.815818	0.649109	-0.815818	4672
0.649236	-0.826909	0.649236	-0.826909	4704
0.649382	-0.838	0.649382	-0.838	4736
0.649527	-0.849273	0.649527	-0.849273	4768
0.649709	-0.860545	0.649709	-0.860545	4800
0.649909	-0.872	0.649909	-0.872	4832
0.650109	-0.883455	0.650109	-0.883455	4864
0.650364	-0.895091	0.650364	-0.895091	4896
0.650618	-0.906909	0.650618	-0.906909	4928
0.650909	-0.918727	0.650909	-0.918727	4960
0.651218	-0.930545	0.651218	-0.930545	4992
0.651564	-0.942727	0.651564	-0.942727	5024
0.651927	-0.954909	0.651927	-0.954909	5056
0.652327	-0.967091	0.652327	-0.967091	5088
0.652764	-0.979636	0.652764	-0.979636	5120
0.653218	-0.992182	0.653218	-0.992182	5152
0.653709	-1.00491	0.653709	-1.00491	5184
0.654255	-1.01764	0.654255	-1.01764	5216

19mm EAR foam earplug, 6% radial strain continued…

0.654818	-1.03073	0.654818	-1.03073	5248
0.655418	-1.04382	0.655418	-1.04382	5280
0.656055	-1.05709	0.656055	-1.05709	5312
0.656727	-1.07055	0.656727	-1.07055	5344
0.657436	-1.08418	0.657436	-1.08418	5376
0.658182	-1.098	0.658182	-1.098	5408
0.658982	-1.112	0.658982	-1.112	5440
0.659818	-1.12618	0.659818	-1.12618	5472
0.660691	-1.14036	0.660691	-1.14036	5504
0.6616	-1.15491	0.6616	-1.15491	5536
0.662564	-1.16964	0.662564	-1.16964	5568
0.663564	-1.18473	0.663564	-1.18473	5600
0.6646	-1.19982	0.6646	-1.19982	5632
0.665691	-1.21527	0.665691	-1.21527	5664
0.666818	-1.23073	0.666818	-1.23073	5696
0.668	-1.24673	0.668	-1.24673	5728
0.669218	-1.26273	0.669218	-1.26273	5760
0.670473	-1.27909	0.670473	-1.27909	5792
0.671782	-1.29564	0.671782	-1.29564	5824
0.673145	-1.31236	0.673145	-1.31236	5856
0.674545	-1.32964	0.674545	-1.32964	5888
0.675982	-1.34691	0.675982	-1.34691	5920
0.677473	-1.36455	0.677473	-1.36455	5952
0.679018	-1.38255	0.679018	-1.38255	5984
0.6806	-1.40091	0.6806	-1.40091	6016
0.682218	-1.41945	0.682218	-1.41945	6048
0.683891	-1.43836	0.683891	-1.43836	6080
0.6856	-1.45745	0.6856	-1.45745	6112
0.687364	-1.47709	0.687364	-1.47709	6144
0.689164	-1.49691	0.689164	-1.49691	6176
0.691018	-1.51727	0.691018	-1.51727	6208
0.692891	-1.53782	0.692891	-1.53782	6240
0.694836	-1.55891	0.694836	-1.55891	6272
0.6968	-1.58018	0.6968	-1.58018	6304
0.698818	-1.602	0.698818	-1.602	6336
0.700855	-1.62418	0.700855	-1.62418	6368
0.702964	-1.64673	0.702964	-1.64673	6400
0.705091	-1.66982	0.705091	-1.66982	6432
0.707255	-1.69327	0.707255	-1.69327	6464
0.709455	-1.71727	0.709455	-1.71727	6496
0.711691	-1.74164	0.711691	-1.74164	6528
0.713982	-1.76636	0.713982	-1.76636	6560
0.716291	-1.79182	0.716291	-1.79182	6592
0.718618	-1.81764	0.718618	-1.81764	6624
0.721	-1.84382	0.721	-1.84382	6656
0.7234	-1.87073	0.7234	-1.87073	6688
0.725836	-1.89818	0.725836	-1.89818	6720
0.728291	-1.92618	0.728291	-1.92618	6752
0.730782	-1.95455	0.730782	-1.95455	6784
0.733291	-1.98364	0.733291	-1.98364	6816
0.735818	-2.01345	0.735818	-2.01345	6848
0.738364	-2.04364	0.738364	-2.04364	6880
0.740927	-2.07455	0.740927	-2.07455	6912
0.743527	-2.10618	0.743527	-2.10618	6944
0.746127	-2.13836	0.746127	-2.13836	6976
0.748727	-2.17127	0.748727	-2.17127	7008
0.751364	-2.20473	0.751364	-2.20473	7040

19mm EAR foam earplug, 18% radial strain

- E = 420 kPa
- $\nu = 0.1$
- $\rho = 146\ kg/m^3$
- Viscoelastic material properties

G_{imag}/G_∞	$1-G_{real}/G_\infty$	K_{imag}/K_∞	$1-K_{real}/K_\infty$	Frequency, (Hz)
0.6704	-0.0558667	0.6704	-0.0558667	2016
0.674267	-0.0598667	0.674267	-0.0598667	2048
0.678	-0.0641333	0.678	-0.0641333	2080
0.681733	-0.0685333	0.681733	-0.0685333	2112
0.685333	-0.0733333	0.685333	-0.0733333	2144
0.688933	-0.0784	0.688933	-0.0784	2176
0.692533	-0.0836	0.692533	-0.0836	2208
0.696	-0.0890667	0.696	-0.0890667	2240
0.699333	-0.0946667	0.699333	-0.0946667	2272
0.702667	-0.100667	0.702667	-0.100667	2304
0.706	-0.1068	0.706	-0.1068	2336
0.709333	-0.113067	0.709333	-0.113067	2368
0.7124	-0.119733	0.7124	-0.119733	2400
0.7156	-0.1264	0.7156	-0.1264	2432
0.718667	-0.133333	0.718667	-0.133333	2464
0.7216	-0.1404	0.7216	-0.1404	2496
0.724533	-0.147733	0.724533	-0.147733	2528
0.727333	-0.1552	0.727333	-0.1552	2560
0.730133	-0.162933	0.730133	-0.162933	2592
0.732933	-0.170667	0.732933	-0.170667	2624
0.7356	-0.178667	0.7356	-0.178667	2656
0.738133	-0.1868	0.738133	-0.1868	2688
0.740667	-0.1952	0.740667	-0.1952	2720
0.743067	-0.2036	0.743067	-0.2036	2752
0.745333	-0.212267	0.745333	-0.212267	2784
0.7476	-0.220933	0.7476	-0.220933	2816
0.749867	-0.229867	0.749867	-0.229867	2848
0.752	-0.238933	0.752	-0.238933	2880
0.754	-0.248133	0.754	-0.248133	2912
0.756	-0.257467	0.756	-0.257467	2944
0.757867	-0.266933	0.757867	-0.266933	2976
0.7596	-0.276533	0.7596	-0.276533	3008
0.761333	-0.286267	0.761333	-0.286267	3040
0.762933	-0.296	0.762933	-0.296	3072
0.764533	-0.306	0.764533	-0.306	3104
0.766	-0.316133	0.766	-0.316133	3136
0.767333	-0.326267	0.767333	-0.326267	3168
0.768667	-0.336667	0.768667	-0.336667	3200
0.769867	-0.347067	0.769867	-0.347067	3232
0.770933	-0.3576	0.770933	-0.3576	3264
0.772	-0.368267	0.772	-0.368267	3296
0.772933	-0.379067	0.772933	-0.379067	3328
0.773733	-0.389867	0.773733	-0.389867	3360
0.7744	-0.4008	0.7744	-0.4008	3392
0.775067	-0.411867	0.775067	-0.411867	3424
0.775733	-0.423067	0.775733	-0.423067	3456
0.776133	-0.434267	0.776133	-0.434267	3488
0.776533	-0.445733	0.776533	-0.445733	3520
0.7768	-0.457067	0.7768	-0.457067	3552

19mm EAR foam earplug, 18% radial strain continued…

0.777067	-0.468667	0.777067	-0.468667	3584
0.7772	-0.480267	0.7772	-0.480267	3616
0.7772	-0.491867	0.7772	-0.491867	3648
0.777067	-0.503733	0.777067	-0.503733	3680
0.776933	-0.5156	0.776933	-0.5156	3712
0.776667	-0.527467	0.776667	-0.527467	3744
0.7764	-0.539467	0.7764	-0.539467	3776
0.776	-0.5516	0.776	-0.5516	3808
0.775467	-0.563733	0.775467	-0.563733	3840
0.7748	-0.575867	0.7748	-0.575867	3872
0.774133	-0.588133	0.774133	-0.588133	3904
0.773333	-0.600533	0.773333	-0.600533	3936
0.772533	-0.612933	0.772533	-0.612933	3968
0.7716	-0.625467	0.7716	-0.625467	4000
0.770533	-0.638	0.770533	-0.638	4032
0.769467	-0.650533	0.769467	-0.650533	4064
0.768267	-0.6632	0.768267	-0.6632	4096
0.767067	-0.675867	0.767067	-0.675867	4128
0.765733	-0.688667	0.765733	-0.688667	4160
0.764267	-0.701467	0.764267	-0.701467	4192
0.7628	-0.7144	0.7628	-0.7144	4224
0.7612	-0.727333	0.7612	-0.727333	4256
0.7596	-0.740267	0.7596	-0.740267	4288
0.757867	-0.753333	0.757867	-0.753333	4320
0.756133	-0.7664	0.756133	-0.7664	4352
0.754267	-0.779467	0.754267	-0.779467	4384
0.7524	-0.792667	0.7524	-0.792667	4416
0.750533	-0.805867	0.750533	-0.805867	4448
0.748533	-0.819067	0.748533	-0.819067	4480
0.7464	-0.8324	0.7464	-0.8324	4512
0.744267	-0.845733	0.744267	-0.845733	4544
0.742133	-0.859067	0.742133	-0.859067	4576
0.739867	-0.872533	0.739867	-0.872533	4608
0.7376	-0.886	0.7376	-0.886	4640
0.735333	-0.899467	0.735333	-0.899467	4672
0.732933	-0.913067	0.732933	-0.913067	4704
0.730533	-0.926533	0.730533	-0.926533	4736
0.728133	-0.940267	0.728133	-0.940267	4768
0.725733	-0.953867	0.725733	-0.953867	4800
0.7232	-0.9676	0.7232	-0.9676	4832
0.720667	-0.981333	0.720667	-0.981333	4864
0.718133	-0.9952	0.718133	-0.9952	4896
0.7156	-1.00907	0.7156	-1.00907	4928
0.712933	-1.02293	0.712933	-1.02293	4960
0.7104	-1.03693	0.7104	-1.03693	4992
0.707733	-1.05093	0.707733	-1.05093	5024
0.7052	-1.06493	0.7052	-1.06493	5056
0.702533	-1.07893	0.702533	-1.07893	5088
0.699867	-1.0932	0.699867	-1.0932	5120
0.697333	-1.10733	0.697333	-1.10733	5152
0.694667	-1.1216	0.694667	-1.1216	5184
0.692	-1.13587	0.692	-1.13587	5216
0.689467	-1.15027	0.689467	-1.15027	5248
0.6868	-1.16467	0.6868	-1.16467	5280
0.684267	-1.1792	0.684267	-1.1792	5312

19mm EAR foam earplug, 18% radial strain continued…

0.681733	-1.19373	0.681733	-1.19373	5344
0.6792	-1.20827	0.6792	-1.20827	5376
0.676667	-1.22293	0.676667	-1.22293	5408
0.674133	-1.23773	0.674133	-1.23773	5440
0.671733	-1.25253	0.671733	-1.25253	5472
0.669333	-1.26747	0.669333	-1.26747	5504
0.666933	-1.2824	0.666933	-1.2824	5536
0.664667	-1.29747	0.664667	-1.29747	5568
0.6624	-1.31253	0.6624	-1.31253	5600
0.660133	-1.32787	0.660133	-1.32787	5632
0.658	-1.3432	0.658	-1.3432	5664
0.655867	-1.35853	0.655867	-1.35853	5696
0.653867	-1.374	0.653867	-1.374	5728
0.651867	-1.3896	0.651867	-1.3896	5760
0.65	-1.40533	0.65	-1.40533	5792
0.648133	-1.4212	0.648133	-1.4212	5824
0.6464	-1.43707	0.6464	-1.43707	5856
0.644667	-1.4532	0.644667	-1.4532	5888
0.643067	-1.46933	0.643067	-1.46933	5920
0.6416	-1.4856	0.6416	-1.4856	5952
0.640133	-1.502	0.640133	-1.502	5984
0.6388	-1.51853	0.6388	-1.51853	6016
0.6376	-1.53533	0.6376	-1.53533	6048
0.636533	-1.55213	0.636533	-1.55213	6080
0.635467	-1.56907	0.635467	-1.56907	6112
0.634533	-1.58627	0.634533	-1.58627	6144
0.633733	-1.60347	0.633733	-1.60347	6176
0.633067	-1.62093	0.633067	-1.62093	6208
0.6324	-1.63853	0.6324	-1.63853	6240
0.632	-1.6564	0.632	-1.6564	6272
0.6316	-1.67427	0.6316	-1.67427	6304
0.631467	-1.69253	0.631467	-1.69253	6336
0.631333	-1.7108	0.631333	-1.7108	6368
0.631467	-1.72933	0.631467	-1.72933	6400
0.6316	-1.74813	0.6316	-1.74813	6432
0.631867	-1.76707	0.631867	-1.76707	6464
0.6324	-1.78627	0.6324	-1.78627	6496
0.633067	-1.8056	0.633067	-1.8056	6528
0.633733	-1.8252	0.633733	-1.8252	6560
0.634667	-1.84507	0.634667	-1.84507	6592
0.635733	-1.8652	0.635733	-1.8652	6624
0.636933	-1.8856	0.636933	-1.8856	6656
0.6384	-1.90613	0.6384	-1.90613	6688
0.639867	-1.92707	0.639867	-1.92707	6720
0.6416	-1.94813	0.6416	-1.94813	6752
0.643467	-1.9696	0.643467	-1.9696	6784
0.6456	-1.99133	0.6456	-1.99133	6816
0.647733	-2.01333	0.647733	-2.01333	6848
0.650133	-2.03573	0.650133	-2.03573	6880
0.6528	-2.05827	0.6528	-2.05827	6912
0.655467	-2.08133	0.655467	-2.08133	6944
0.6584	-2.10453	0.6584	-2.10453	6976
0.6616	-2.12827	0.6616	-2.12827	7008
0.6648	-2.15227	0.6648	-2.15227	7040
0.668267	-2.17653	0.668267	-2.17653	7072
0.672	-2.20133	0.672	-2.20133	7104

19mm EAR foam earplug, 30% radial strain

- E = 450 kPa
- $\nu = 0.1$
- $\rho = 220\ kg/m^3$
- Viscoelastic material properties

G_{imag}/G_∞	$1-G_{real}/G_\infty$	K_{imag}/K_∞	$1-K_{real}/K_\infty$	Frequency, (Hz)
0.28836	-0.0178	0.28836	-0.0178	2016
0.292893	-0.0187333	0.292893	-0.0187333	2048
0.297187	-0.0197333	0.297187	-0.0197333	2080
0.301267	-0.0208667	0.301267	-0.0208667	2112
0.30514	-0.0221333	0.30514	-0.0221333	2144
0.30882	-0.0235333	0.30882	-0.0235333	2176
0.312333	-0.025	0.312333	-0.025	2208
0.315687	-0.0266667	0.315687	-0.0266667	2240
0.318893	-0.0284	0.318893	-0.0284	2272
0.32196	-0.0302	0.32196	-0.0302	2304
0.324907	-0.0322	0.324907	-0.0322	2336
0.327727	-0.0342667	0.327727	-0.0342667	2368
0.33044	-0.0364	0.33044	-0.0364	2400
0.333053	-0.0386667	0.333053	-0.0386667	2432
0.335573	-0.041	0.335573	-0.041	2464
0.338007	-0.0434667	0.338007	-0.0434667	2496
0.340353	-0.046	0.340353	-0.046	2528
0.342627	-0.0486667	0.342627	-0.0486667	2560
0.344827	-0.0514	0.344827	-0.0514	2592
0.34696	-0.0542	0.34696	-0.0542	2624
0.349033	-0.0571333	0.349033	-0.0571333	2656
0.351067	-0.0600667	0.351067	-0.0600667	2688
0.35302	-0.0631333	0.35302	-0.0631333	2720
0.354927	-0.0663333	0.354927	-0.0663333	2752
0.356787	-0.0695333	0.356787	-0.0695333	2784
0.358607	-0.0728667	0.358607	-0.0728667	2816
0.36038	-0.0762667	0.36038	-0.0762667	2848
0.362113	-0.0797333	0.362113	-0.0797333	2880
0.363813	-0.0832667	0.363813	-0.0832667	2912
0.365473	-0.0868667	0.365473	-0.0868667	2944
0.367107	-0.0906	0.367107	-0.0906	2976
0.368707	-0.0943333	0.368707	-0.0943333	3008
0.37028	-0.0982	0.37028	-0.0982	3040
0.371827	-0.102067	0.371827	-0.102067	3072
0.373347	-0.106067	0.373347	-0.106067	3104
0.374847	-0.110067	0.374847	-0.110067	3136
0.37632	-0.1142	0.37632	-0.1142	3168
0.377773	-0.1184	0.377773	-0.1184	3200
0.379207	-0.122667	0.379207	-0.122667	3232
0.38062	-0.126933	0.38062	-0.126933	3264
0.382013	-0.131333	0.382013	-0.131333	3296
0.383393	-0.1358	0.383393	-0.1358	3328
0.38476	-0.140333	0.38476	-0.140333	3360
0.386107	-0.144867	0.386107	-0.144867	3392
0.38744	-0.149533	0.38744	-0.149533	3424
0.388767	-0.154267	0.388767	-0.154267	3456
0.390073	-0.159067	0.390073	-0.159067	3488
0.391367	-0.163933	0.391367	-0.163933	3520
0.392653	-0.1688	0.392653	-0.1688	3552

19mm EAR foam earplug, 30% radial strain continued…

0.393927	-0.1738	0.393927	-0.1738	3584
0.395187	-0.178867	0.395187	-0.178867	3616
0.39644	-0.184	0.39644	-0.184	3648
0.39768	-0.189133	0.39768	-0.189133	3680
0.398913	-0.1944	0.398913	-0.1944	3712
0.40014	-0.199733	0.40014	-0.199733	3744
0.401353	-0.205133	0.401353	-0.205133	3776
0.40256	-0.210533	0.40256	-0.210533	3808
0.40376	-0.216067	0.40376	-0.216067	3840
0.404953	-0.221667	0.404953	-0.221667	3872
0.40614	-0.227333	0.40614	-0.227333	3904
0.40732	-0.233067	0.40732	-0.233067	3936
0.408487	-0.238867	0.408487	-0.238867	3968
0.409667	-0.244667	0.409667	-0.244667	4000
0.41082	-0.2506	0.41082	-0.2506	4032
0.411973	-0.2566	0.411973	-0.2566	4064
0.41312	-0.262667	0.41312	-0.262667	4096
0.414253	-0.268867	0.414253	-0.268867	4128
0.415387	-0.275067	0.415387	-0.275067	4160
0.416513	-0.281333	0.416513	-0.281333	4192
0.417633	-0.287733	0.417633	-0.287733	4224
0.418747	-0.294133	0.418747	-0.294133	4256
0.419853	-0.300667	0.419853	-0.300667	4288
0.420953	-0.307267	0.420953	-0.307267	4320
0.422047	-0.313933	0.422047	-0.313933	4352
0.423133	-0.320667	0.423133	-0.320667	4384
0.42422	-0.327533	0.42422	-0.327533	4416
0.425293	-0.3344	0.425293	-0.3344	4448
0.426367	-0.3414	0.426367	-0.3414	4480
0.427427	-0.348467	0.427427	-0.348467	4512
0.428487	-0.3556	0.428487	-0.3556	4544
0.429533	-0.3628	0.429533	-0.3628	4576
0.43058	-0.370133	0.43058	-0.370133	4608
0.431613	-0.377533	0.431613	-0.377533	4640
0.432647	-0.385	0.432647	-0.385	4672
0.433667	-0.392533	0.433667	-0.392533	4704
0.43468	-0.4002	0.43468	-0.4002	4736
0.435693	-0.407933	0.435693	-0.407933	4768
0.436693	-0.4158	0.436693	-0.4158	4800
0.43768	-0.423667	0.43768	-0.423667	4832
0.438667	-0.431667	0.438667	-0.431667	4864
0.439647	-0.4398	0.439647	-0.4398	4896
0.440613	-0.448	0.440613	-0.448	4928
0.441573	-0.456267	0.441573	-0.456267	4960
0.44252	-0.464667	0.44252	-0.464667	4992
0.44346	-0.473133	0.44346	-0.473133	5024
0.444393	-0.481733	0.444393	-0.481733	5056
0.445313	-0.4904	0.445313	-0.4904	5088
0.44622	-0.499133	0.44622	-0.499133	5120
0.447127	-0.508067	0.447127	-0.508067	5152
0.448013	-0.517	0.448013	-0.517	5184
0.448893	-0.526133	0.448893	-0.526133	5216
0.44976	-0.535333	0.44976	-0.535333	5248
0.450613	-0.5446	0.450613	-0.5446	5280
0.45146	-0.554	0.45146	-0.554	5312

19mm EAR foam earplug, 30% radial strain continued…

0.452287	-0.563533	0.452287	-0.563533	5344
0.453107	-0.573133	0.453107	-0.573133	5376
0.453907	-0.582933	0.453907	-0.582933	5408
0.4547	-0.592733	0.4547	-0.592733	5440
0.455473	-0.602733	0.455473	-0.602733	5472
0.45624	-0.612867	0.45624	-0.612867	5504
0.456987	-0.623067	0.456987	-0.623067	5536
0.457713	-0.6334	0.457713	-0.6334	5568
0.458427	-0.643867	0.458427	-0.643867	5600
0.459127	-0.6544	0.459127	-0.6544	5632
0.459807	-0.665133	0.459807	-0.665133	5664
0.460473	-0.675933	0.460473	-0.675933	5696
0.46112	-0.686933	0.46112	-0.686933	5728
0.461747	-0.698	0.461747	-0.698	5760
0.462353	-0.709267	0.462353	-0.709267	5792
0.46294	-0.7206	0.46294	-0.7206	5824
0.463507	-0.732133	0.463507	-0.732133	5856
0.464053	-0.743733	0.464053	-0.743733	5888
0.46458	-0.755533	0.46458	-0.755533	5920
0.465087	-0.767467	0.465087	-0.767467	5952
0.465567	-0.779533	0.465567	-0.779533	5984
0.46602	-0.7918	0.46602	-0.7918	6016
0.466453	-0.804133	0.466453	-0.804133	6048
0.46686	-0.816667	0.46686	-0.816667	6080
0.467247	-0.829333	0.467247	-0.829333	6112
0.4676	-0.8422	0.4676	-0.8422	6144
0.467933	-0.855133	0.467933	-0.855133	6176
0.468233	-0.868333	0.468233	-0.868333	6208
0.468507	-0.8816	0.468507	-0.8816	6240
0.468753	-0.895133	0.468753	-0.895133	6272
0.468967	-0.908733	0.468967	-0.908733	6304
0.469147	-0.9226	0.469147	-0.9226	6336
0.4693	-0.936533	0.4693	-0.936533	6368
0.46942	-0.950733	0.46942	-0.950733	6400
0.469507	-0.965067	0.469507	-0.965067	6432
0.46956	-0.9796	0.46956	-0.9796	6464
0.469573	-0.994333	0.469573	-0.994333	6496
0.46956	-1.0092	0.46956	-1.0092	6528
0.4695	-1.02427	0.4695	-1.02427	6560
0.469407	-1.03953	0.469407	-1.03953	6592
0.469273	-1.055	0.469273	-1.055	6624
0.4691	-1.07067	0.4691	-1.07067	6656
0.468887	-1.08653	0.468887	-1.08653	6688
0.468633	-1.1026	0.468633	-1.1026	6720
0.468333	-1.11893	0.468333	-1.11893	6752
0.467993	-1.1354	0.467993	-1.1354	6784
0.467607	-1.15207	0.467607	-1.15207	6816
0.467173	-1.169	0.467173	-1.169	6848
0.466693	-1.18613	0.466693	-1.18613	6880
0.46616	-1.20347	0.46616	-1.20347	6912
0.46558	-1.22107	0.46558	-1.22107	6944
0.464953	-1.23887	0.464953	-1.23887	6976
0.464273	-1.25693	0.464273	-1.25693	7008
0.463533	-1.2752	0.463533	-1.2752	7040
0.462747	-1.29373	0.462747	-1.29373	7072
0.4619	-1.31247	0.4619	-1.31247	7104
0.460993	-1.33147	0.460993	-1.33147	7136
0.460033	-1.35073	0.460033	-1.35073	7168
0.459013	-1.37027	0.459013	-1.37027	7200

10mm EAR foam earplug, 30% radial strain

- E = 100 kPa
- $\nu = 0.1$
- $\rho = 220\ kg/m^3$
- Viscoelastic material properties

G_{imag}/G_∞	$1-G_{real}/G_\infty$	K_{imag}/K_∞	$1-K_{real}/K_\infty$	Frequency, (Hz)
0.255189	-0.0146667	0.255189	-0.0146667	1024
0.274903	-0.051	0.274903	-0.051	1056
0.298262	-0.0866667	0.298262	-0.0866667	1088
0.321576	-0.121667	0.321576	-0.121667	1120
0.344764	-0.155667	0.344764	-0.155667	1152
0.367935	-0.189333	0.367935	-0.189333	1184
0.39102	-0.222667	0.39102	-0.222667	1216
0.413839	-0.255333	0.413839	-0.255333	1248
0.436442	-0.287333	0.436442	-0.287333	1280
0.458631	-0.318667	0.458631	-0.318667	1312
0.480705	-0.35	0.480705	-0.35	1344
0.50251	-0.380667	0.50251	-0.380667	1376
0.523856	-0.410667	0.523856	-0.410667	1408
0.545077	-0.440667	0.545077	-0.440667	1440
0.565738	-0.47	0.565738	-0.47	1472
0.586336	-0.499333	0.586336	-0.499333	1504
0.606431	-0.528	0.606431	-0.528	1536
0.626246	-0.556667	0.626246	-0.556667	1568
0.645476	-0.584667	0.645476	-0.584667	1600
0.664669	-0.612667	0.664669	-0.612667	1632
0.683346	-0.640333	0.683346	-0.640333	1664
0.701776	-0.668	0.701776	-0.668	1696
0.719651	-0.695	0.719651	-0.695	1728
0.737394	-0.722	0.737394	-0.722	1760
0.754673	-0.748667	0.754673	-0.748667	1792
0.77178	-0.775333	0.77178	-0.775333	1824
0.788377	-0.801667	0.788377	-0.801667	1856
0.804945	-0.828	0.804945	-0.828	1888
0.820961	-0.854	0.820961	-0.854	1920
0.836736	-0.88	0.836736	-0.88	1952
0.852103	-0.905667	0.852103	-0.905667	1984
0.867197	-0.931333	0.867197	-0.931333	2016
0.882043	-0.956667	0.882043	-0.956667	2048
0.896588	-0.982	0.896588	-0.982	2080
0.910818	-1.00733	0.910818	-1.00733	2112
0.924765	-1.03233	0.924765	-1.03233	2144
0.938574	-1.05733	0.938574	-1.05733	2176
0.952031	-1.08233	0.952031	-1.08233	2208
0.965178	-1.107	0.965178	-1.107	2240
0.978158	-1.13167	0.978158	-1.13167	2272
0.990964	-1.15633	0.990964	-1.15633	2304
1.00359	-1.181	1.00359	-1.181	2336
1.01566	-1.20533	1.01566	-1.20533	2368
1.02774	-1.22967	1.02774	-1.22967	2400
1.03962	-1.254	1.03962	-1.254	2432
1.0513	-1.27833	1.0513	-1.27833	2464
1.0626	-1.30233	1.0626	-1.30233	2496
1.07383	-1.32667	1.07383	-1.32667	2528
1.08491	-1.35067	1.08491	-1.35067	2560

10mm EAR foam earplug, 30% radial strain continued…

1.09551	-1.37467	1.09551	-1.37467	2592
1.10635	-1.39867	1.10635	-1.39867	2624
1.1167	-1.42267	1.1167	-1.42267	2656
1.12689	-1.44633	1.12689	-1.44633	2688
1.13697	-1.47033	1.13697	-1.47033	2720
1.14688	-1.494	1.14688	-1.494	2752
1.15692	-1.518	1.15692	-1.518	2784
1.16654	-1.54167	1.16654	-1.54167	2816
1.17589	-1.56533	1.17589	-1.56533	2848
1.18521	-1.589	1.18521	-1.589	2880
1.19424	-1.61267	1.19424	-1.61267	2912
1.2035	-1.63633	1.2035	-1.63633	2944
1.21247	-1.66	1.21247	-1.66	2976
1.22114	-1.68367	1.22114	-1.68367	3008
1.22977	-1.70733	1.22977	-1.70733	3040
1.23837	-1.731	1.23837	-1.731	3072
1.24678	-1.75433	1.24678	-1.75433	3104
1.25503	-1.778	1.25503	-1.778	3136
1.26324	-1.80167	1.26324	-1.80167	3168
1.2714	-1.82533	1.2714	-1.82533	3200
1.27924	-1.849	1.27924	-1.849	3232
1.28704	-1.87267	1.28704	-1.87267	3264
1.29479	-1.89633	1.29479	-1.89633	3296
1.30249	-1.92	1.30249	-1.92	3328
1.31014	-1.94367	1.31014	-1.94367	3360
1.31775	-1.96733	1.31775	-1.96733	3392
1.32517	-1.99133	1.32517	-1.99133	3424
1.33238	-2.015	1.33238	-2.015	3456
1.3397	-2.039	1.3397	-2.039	3488
1.34681	-2.06267	1.34681	-2.06267	3520
1.35402	-2.08667	1.35402	-2.08667	3552
1.36117	-2.11067	1.36117	-2.11067	3584
1.36797	-2.13467	1.36797	-2.13467	3616
1.37502	-2.15867	1.37502	-2.15867	3648
1.3817	-2.18267	1.3817	-2.18267	3680
1.38879	-2.207	1.38879	-2.207	3712
1.39536	-2.231	1.39536	-2.231	3744
1.40202	-2.25533	1.40202	-2.25533	3776
1.40862	-2.27967	1.40862	-2.27967	3808
1.41531	-2.30433	1.41531	-2.30433	3840
1.42179	-2.32867	1.42179	-2.32867	3872
1.42803	-2.35333	1.42803	-2.35333	3904
1.43454	-2.378	1.43454	-2.378	3936
1.44099	-2.40267	1.44099	-2.40267	3968
1.44738	-2.42733	1.44738	-2.42733	4000
1.45352	-2.45233	1.45352	-2.45233	4032
1.45993	-2.47733	1.45993	-2.47733	4064
1.46594	-2.50233	1.46594	-2.50233	4096
1.47237	-2.52767	1.47237	-2.52767	4128
1.47839	-2.553	1.47839	-2.553	4160
1.48435	-2.57833	1.48435	-2.57833	4192
1.49073	-2.604	1.49073	-2.604	4224
1.4967	-2.62967	1.4967	-2.62967	4256
1.5026	-2.65533	1.5026	-2.65533	4288
1.50857	-2.68133	1.50857	-2.68133	4320
1.51484	-2.70733	1.51484	-2.70733	4352

10mm EAR foam earplug, 30% radial strain continued…

1.52082	-2.73367	1.52082	-2.73367	4384
1.52673	-2.76	1.52673	-2.76	4416
1.53257	-2.78633	1.53257	-2.78633	4448
1.53848	-2.813	1.53848	-2.813	4480
1.54432	-2.83967	1.54432	-2.83967	4512
1.55022	-2.86667	1.55022	-2.86667	4544
1.55606	-2.89367	1.55606	-2.89367	4576
1.56196	-2.921	1.56196	-2.921	4608
1.56779	-2.94833	1.56779	-2.94833	4640
1.57368	-2.976	1.57368	-2.976	4672
1.5795	-3.00367	1.5795	-3.00367	4704
1.58538	-3.03167	1.58538	-3.03167	4736
1.59132	-3.06	1.59132	-3.06	4768
1.59679	-3.08833	1.59679	-3.08833	4800
1.60258	-3.11667	1.60258	-3.11667	4832
1.60856	-3.14567	1.60856	-3.14567	4864
1.61446	-3.17467	1.61446	-3.17467	4896
1.62029	-3.20367	1.62029	-3.20367	4928
1.62576	-3.233	1.62576	-3.233	4960
1.63169	-3.26267	1.63169	-3.26267	4992
1.63767	-3.29267	1.63767	-3.29267	5024
1.64315	-3.32267	1.64315	-3.32267	5056
1.64923	-3.35333	1.64923	-3.35333	5088
1.65468	-3.38367	1.65468	-3.38367	5120
1.66072	-3.41467	1.66072	-3.41467	5152
1.66681	-3.446	1.66681	-3.446	5184
1.67238	-3.47733	1.67238	-3.47733	5216
1.67799	-3.509	1.67799	-3.509	5248
1.68408	-3.541	1.68408	-3.541	5280
1.68976	-3.57333	1.68976	-3.57333	5312
1.69593	-3.606	1.69593	-3.606	5344
1.70168	-3.639	1.70168	-3.639	5376
1.70734	-3.672	1.70734	-3.672	5408
1.71315	-3.70567	1.71315	-3.70567	5440
1.71945	-3.73967	1.71945	-3.73967	5472
1.7252	-3.77367	1.7252	-3.77367	5504
1.73109	-3.80833	1.73109	-3.80833	5536
1.73701	-3.84333	1.73701	-3.84333	5568
1.74295	-3.87867	1.74295	-3.87867	5600
1.74892	-3.91433	1.74892	-3.91433	5632
1.7549	-3.95033	1.7549	-3.95033	5664
1.7609	-3.98667	1.7609	-3.98667	5696
1.76654	-4.02367	1.76654	-4.02367	5728
1.77268	-4.061	1.77268	-4.061	5760
1.77884	-4.09867	1.77884	-4.09867	5792
1.78501	-4.13667	1.78501	-4.13667	5824
1.79079	-4.17533	1.79079	-4.17533	5856
1.79709	-4.21433	1.79709	-4.21433	5888
1.80288	-4.25367	1.80288	-4.25367	5920

10mm EAR foam earplug, 30% radial strain continued…

1.80931	-4.29367	1.80931	-4.29367	5952
1.81532	-4.33433	1.81532	-4.33433	5984
1.82121	-4.375	1.82121	-4.375	6016
1.82732	-4.41667	1.82732	-4.41667	6048
1.83342	-4.45867	1.83342	-4.45867	6080
1.83951	-4.501	1.83951	-4.501	6112
1.84569	-4.544	1.84569	-4.544	6144
1.85197	-4.58767	1.85197	-4.58767	6176
1.85834	-4.632	1.85834	-4.632	6208
1.86468	-4.67667	1.86468	-4.67667	6240
1.87055	-4.722	1.87055	-4.722	6272
1.87706	-4.768	1.87706	-4.768	6304
1.88308	-4.81467	1.88308	-4.81467	6336
1.88974	-4.862	1.88974	-4.862	6368
1.8959	-4.91	1.8959	-4.91	6400
1.90201	-4.95833	1.90201	-4.95833	6432
1.90828	-5.00767	1.90828	-5.00767	6464
1.91461	-5.05767	1.91461	-5.05767	6496
1.9211	-5.10867	1.9211	-5.10867	6528
1.92753	-5.16	1.92753	-5.16	6560
1.93411	-5.21233	1.93411	-5.21233	6592
1.94011	-5.26533	1.94011	-5.26533	6624
1.94614	-5.319	1.94614	-5.319	6656
1.95293	-5.37367	1.95293	-5.37367	6688
1.95921	-5.42933	1.95921	-5.42933	6720
1.96551	-5.48567	1.96551	-5.48567	6752
1.97193	-5.543	1.97193	-5.543	6784
1.97835	-5.601	1.97835	-5.601	6816
1.98497	-5.66033	1.98497	-5.66033	6848
1.99093	-5.72033	1.99093	-5.72033	6880
1.99764	-5.78133	1.99764	-5.78133	6912
2.00377	-5.84333	2.00377	-5.84333	6944
2.00996	-5.90633	2.00996	-5.90633	6976
2.01632	-5.97067	2.01632	-5.97067	7008
2.02264	-6.03567	2.02264	-6.03567	7040
2.02911	-6.102	2.02911	-6.102	7072
2.03502	-6.16967	2.03502	-6.16967	7104
2.04095	-6.23833	2.04095	-6.23833	7136
2.04763	-6.308	2.04763	-6.308	7168
2.0538	-6.37933	2.0538	-6.37933	7200
2.05998	-6.45167	2.05998	-6.45167	7232
2.06551	-6.52533	2.06551	-6.52533	7264
2.07186	-6.60033	2.07186	-6.60033	7296
2.07754	-6.67667	2.07754	-6.67667	7328
2.08413	-6.75467	2.08413	-6.75467	7360
2.09001	-6.834	2.09001	-6.834	7392
2.09515	-6.91467	2.09515	-6.91467	7424
2.10118	-6.997	2.10118	-6.997	7456

Vita

Christian James was born in Savannah, Georgia to Bradley and Patricia James. After several years in Georgia and New York the family settled in Springfield, Virginia. He held various jobs in the automotive parts distribution industry. Christian graduated from West Springfield High School in 2000, and continued onto an engineering curriculum at Virginia Tech, where he led the drive-train group for the 2004 S.A.E. Mini Baja team. Christian received a B.S. degree in Mechanical Engineering in 2004, and continued onto a graduate degree in M.E. at Virginia Tech. Christian worked on modeling acoustic hearing protection devices for Dr. Robert West, and graduated with an M.S.M.E. degree in 2006. He then moved on to a career in automotive engine analysis at Southwest Research Institute in San Antonio, Texas.